T.C.
YEDİTEPE UNIVERSITY
INSTITUTE OF HEALTH SCIENCES
DEPARTMENT OF HISTOLOGY AND EMBRYOLOGY

DETERMINATION OF THE RELATIONSHIP BETWEEN c-ABL PROTEIN TYROSINE KINASE AND YAP IN CELL FATE DETERMINATION DURING MOUSE PREIMPLANTATION EMBRYONIC DEVELOPMENT

THE DOCTOR OF HISTOLOGY AND EMBRYOLOGY THESIS

ECEM YILDIRIM

İSTANBUL-2023

T.C.
YEDİTEPE UNIVERSITY
INSTITUTE OF HEALTH SCIENCES
DEPARTMENT OF HISTOLOGY AND EMBRYOLOGY

DETERMINATION OF THE RELATIONSHIP BETWEEN c-ABL PROTEIN TYROSINE KINASE AND YAP IN CELL FATE DETERMINATION DURING MOUSE PREIMPLANTATION EMBRYONIC DEVELOPMENT

THE DOCTOR OF HISTOLOGY AND EMBRYOLOGY THESIS

ECEM YILDIRIM

SUPERVISOR
PROF. DR. AYLİN YABA UÇAR

İSTANBUL-2023

APPROVAL

Institute : Yeditepe University Institute of Health Sciences

Programme : Doctoral Program in Histology and Embryology

Title of the Thesis : Determination of the Relationship Between c-Abl Protein Tyrosine Kinase and YAP in Cell Fate Determination during Mouse Preimplantation Embryonic Development

Owner of the Thesis : Ecem Yıldırım

Examination Date : 25/07/2023

This study have approved as a Doctorate Thesis in regard to content and quality by the Jury.

Supervisor:	Prof. Aylin Yaba Uçar (Yeditepe University, Faculty of Medicine, Department of Histology and Embryology)
Member/Examiner:	Prof. Rukset Attar (Yeditepe University, Faculty of Medicine, Department of Obstetrics and Gynecology)
Member/Examiner:	Assoc. Prof. Yasemin Seval Çelik (İzmir Ekonomi University, Faculty of Medicine, Department of Histology and Embryology)
Member/Examiner:	Assist. Prof. Murat Basar (Yale School of Medicine, Department of Obstetrics, Gynecology and Reproductive Sciences)
Member/Examiner:	Assoc. Prof. Alev Cumbul (Yeditepe University, Faculty of Medicine, Department of Histology and Embryology)

APPROVAL

This thesis has been deemed by the jury in accordance with the relevant articles of Yeditepe University Graduate Education and Examinations Regulation and has been approved by Administrative Board of Institute with decision dated ..... and numbered .....

Prof. Bayram Yılmaz
Director of Institute of Health Sciences

DECLARATION

I hereby declare that this thesis is my own work and that, to the best of my knowledge and belief, it contains no material previously published or written by another person nor material which has been accepted for the award of any other degree except where due acknowledgment has been made in the text.

Ecem Yıldırım

DEDICATION

To my family and Prof. Dr. Necdet Demir…

ACKNOWLEDGEMENTS

I would like to thank my supervisor Prof. Dr. Aylin Yaba Uçar, who has always been by my side, inspiring me, and illuminating my path with her light. She has been a wonderful academic advisor, a family, and a strong woman who has always been there for me. Thanks to her support, I am the person I am today.

I would like to thanks Dr. Tuğçe Önel for her supportive partnership within the team and sincere friendship. I am more than happy to share my days with you.

I would like to thanks to the all team members at Department of Histology and Embryology at Yeditepe University for their contributions to my education.

I would like to thank Prof. Dr. Bayram Yılmaz and YUDETAM team for all their support.

I am grateful to my dear friend Dr. Mehmet Şerif Aydın, for generously sharing his knowledge in imaging techniques with me. I would also like to thank my friends Dr. Cihan Süleyman Erdoğan and Yunus Kosif for all their support and efforts.

I would like to thank my family, who have always been by my side and supported me in all my decisions. Without your support, I could not have achieved any success.

Ecem Yıldırım

TABLE OF CONTENTS

APPROVAL i

DECLARATION ii

DEDICATION iii

ACKNOWLEDGEMENTS iv

TABLE OF CONTENTS v

LIST OF TABLES viii

LIST OF FIGURES ix

LIST OF SYMBOLS AND ABBREVIATIONS xviii

ABSTRACT xxi

ÖZET xxii

1. INTRODUCTION and PURPOSE 1

2. LITERATURE REVIEW 2

2.1. Preimplantation Embryonic Development in The Mouse 2

2.1.2. Fertilization 3

2.1.3. Embryonic Genome Activation 4

2.1.4. Compaction 6

2.1.5. Polarization 11

2.1.6. Cell Fate Determination 14

2.2. Hippo Signaling Pathway in Preimplantation Mouse Embryo Development 17

2.3. c-Abl Protein Tyrosine Kinase 21

2.3.1. Structure and Regulation of c-Abl Protein Tyrosine Kinase 21

2.3.2. Imatinib-mediated Inhibition of c-Abl 23

2.3.3. PDGF-AA-mediated Activation of c-Abl 26

2.3.4. YAP Phosphorylation by c-Abl and Association with p73 28

2.3.5. The Role of c-Abl Tyrosine Kinase: A Journey Across Germ Cells to the Fertilization 32
3. MATERIALS and METHODS 35
3.1. Experimental Animal Ethics Statements 35
3.2. Superovulation 35
3.3. Collection and Culture of Mouse Preimplantation Embryos 36
3.4. Treatment with PDGF-AA and imatinib 36
3.5. siRNA microinjection 37
3.6. Morphological Evaluation at Different Preimplantation Embryo Stages 39
3.6.1. ZP thickness measurement 40
3.6.2. Measurement of Angle between two blastomeres at the 2-cell embryo 40
3.6.3. Measurement the angle of compaction between blastomeres at the morula 40
3.6.4. Measurement of the blastocoel cavity area 40
3.7. Measuring Individual Blastomeres Areas of Blastocyst. 41
3.8. Calculate the Number of Nucleus and Area of Nucleus in Blastocyst 42
3.9. Analysis of Apoptotic Bodies in the Preimplantation Embryo 42
3.10. Immunofluorescence staining and analysis 42
3.11. Quantitative Real-Time Polymerase Chain Reaction (qRT-PCR) and Analysis 45
3.12. Statistical analysis 49
4. RESULTS 50
4.1. Development and morphological evaluation of embryos from zygote to the blastocyst 50
4.2. The development of mice preimplantation embryos after PDGF-AA treatment 52
4.3. Comparison of immunofluorescent staining and intensities in groups after PDGF-AA treatment 55
4.4. Comparison of *c-Abl, Yap, Tead4, Cdx2, Nanog* and *Oct4* mRNA levels in groups after PDGF-AA treatment 71

4.5. The development of preimplantation embryos after imatinib treatment 72

4.6. Comparison of immunofluorescent staining patterns and intensities in groups after imatinib treatment 75

4.7. Comparison of *c-Abl, Yap, Tead4, Cdx2, Nanog* and *Oct4* mRNA levels in groups after imatinib treatment 84

4.8. c-Abl siRNA microinjection results 85

4.9. Evaluation of qRT-PCR results after *c-Abl* siRNA microinjection 87

4.10. Analysis of area and apoptosis of PDGF-AA and imatinib treated groups 88

4.10.1. Analysis of cell area measurements of blastomers 88

4.10.2. Counting the Number of Cell Nucleus in the Blastocyst 89

4.10.3. Analysis of Apoptotic Bodies in Embryos 90

5. DISCUSSION 92

6. REFERENCES 111

7. APPENDICES 135

7.1. Ethical Approval 135

7.2. Curriculum Vitae 136

LIST OF TABLES

Table 1: Experimental groups design, used PDGF-AA, imatinib and siRNA microinjection are shown in the table. 39

Table 2: Primary and secondary antibodies used in the study 43

Table 3: *c-Abl* and *Yap* RT-PCR program. 48

Table 4: Tead4 and Nanog RT-PCR program. 48

Table 5: Cdx2 RT-PCR program. 48

Table 6: Oct4 RT-PCR program. 48

Table 7: The list of primers used for qRT-PCR 49

LIST OF FIGURES

Figure 1: Changes in expression levels of genes involved in mouse preimplantation embryonic development and their roles in cell fate determination. The genes that are effective in the process from fertilization to the blastocyst stage are indicated in the figure. 5

Figure 2: Molecular and mechanical properyies of compaction in Mouse embryo. During the development of preimplantation stage mouse embryos, the localization of intercellular adhesion proteins between blastomeres has been schematized. Intercellular connections are observed from the 4-cell stage to the blastocyst stage [44]. 8

Figure 3: Microtubule organization in the mouse embryo from the zygote to the early post-implantation stage. In embryonic development, the interstage bridge appears as a non-centrosomal microtubule editing center (ncMTOC) during preimplantation development. Centrosomes first appear at the 16 to 32 cell, but they do not spread microtubules or affect the interphase microtubule network. Centriole-containing centrosomes may be required around gastrulation, suggesting the presence of a dual microtubule network [50]. 10

Figure 4: Asymmetric cell division. First lineage and inside-out pattern differentiation by polarity pattern during mouse preimplantation embryonic development [91]. 17

Figure 5: The Hippo signaling pathway in cell fate determination. When the Hippo signaling pathway is active, the localization of phosphorylated YAP is in the cytoplasm. When the Hippo signal is inactive, non-phosphorylated YAP is translocated to the nucleus [103]. 18

Figure 6: Schematic representation of c-Abl tyrosine kinase, its structure and regulation. (SH3) are denoted as SH1, SH2, and SH3, respectively. The presence of nuclear localization signals (NLS) and DNA binding domain (DBD) is indicated. Additionally, the nuclear export signal (NES) and actin binding sites are mentioned. The interaction between the c-Abl inhibitor and the c-Abl kinase domain is demonstrated by the construct STI-571. Furthermore, the translocation of BCR on chromosome 22, ABL on chromosome 9, and the resulting Philadelphia chromosome, which leads to chronic myeloid leukemia (CML), has been depicted [123]. 22

Figure 7: Roles of c-Abl Protein Tyrosine Kinase in cellular processes. c-Abl Protein Tyrosine Kinase plays a role in many processes such as gonadal development, cell

proliferation, cell apoptosis, regulation and protection of the cytoskeletal structure of the cell, polarization and DNA repair mechanism..... 23

Figure 8: Demonstration of ABL structure and regions and regulation of ABL kinase activity. A. The figure shows the structural isoforms of ABL1 and ABL2. B. Inactive and active forms of ABL kinases and the mechanism that modulates ABL kinase activity are schematized [135]..... 24

Figure 9: In the presence of DNA damage, YAP triggers p73-mediated apoptosis through the involvement of c-Abl. Activation of c-Abl occurs in response to DNA damage, causing p73 and YAP to be phosphorylated. These formations lead to transcription of proapoptotic genes induced by YAP-p73. In addition, phosphorylation of YAP by c-Abl inhibits the activation of the YAP-TEAD' complex, suppressing the expression of anti-apoptotic genes and promoting apoptosis [148]..... 31

Figure 10: Superovulation of C57BL6 female mice at 6 weeks..... 35

Figure 11: Collection and culture of mouse preimplantation embryos. 36

Figure 12: c-Abl siRNA schematic representation and Axio microscope images of the microinjection into the zygote. 38

Figure 13: Schematic diagram of the parameters measured during embryo morphokinetic evaluation. A. ZP thickness measurement for zygote. B. ZP thickness measurement and angle between two blastomeres for 2-cell embryo. C. ZP thickness measurement and angle between two blastomeres for morula. D. blastocoel cavity distance for blastocyst. 41

Figure 14: The graphic shows the measurement of the cell area in the blastomeres at the blastocyst. 41

Figure 15: Detection of apoptotic bodies in mouse preimplantation embryos. 42

Figure 16: Immunofluorescence staining and imaging were schematized. 44

Figure 17: The Real Time Polymerase Chain Reaction schematized..... 49

Figure 18: After superovulation, zygotes were cultured in vitro until they developed to the blastocyst. A.1. day zygote, B. Day 2 of culture 2-cell embryo, C. Day 3 of culture 4-cell embryo, D. Day 3 of culture 8-cell embryo, E. Day 4 of culture embryo at morula, 1F. Embryo at the blastocyst on day 4 of culture. 52

Figure 19: Morphological comparison of the developmental potentials of PDGF-AA groups. A. Morphological comparison of the control, 20 ng/mL and 50 ng/mL PDGF-AA groups of mouse embryos obtained by superovulation and cultured from zygote to blastocyst. B. and C. Comparison of groups by statistically evaluating the developmental potential of PDGF-AA treatment group on embryonic development. (8 different cultures were assessed for their average developmental potential). 53

Figure 20: Statistical evaluation of the morphology of PDGF-AA groups. Control, 20 ng/mL PDGF-AA and 50 ng/mL PDGF-AA groups; the thickness of the ZP (A), the measurement of the angle between the 2 blastomeres in the 2-cell (B), the measurement of the angle between the 2 blastomeres in the morula (C), and the blastocoele cavity formed in the blastocyst (D) embryos were evaluated (n=10) (**p< 0.01)..... 54

Figure 21: Evaluation of c-Abl and YAP localizations by immunofluorescence staining in control, 20 ng/mL and 50 ng/mL PDGF-AA groups. A. Evaluation of cellular localizations of c-Abl and YAP would change with PDGF-AA treatment. After PDGF-AA treatment, YAP localization was determined in the cytoplasm in addition to the nucleus in TE cells in PDGF-AA groups. B. Comparison of immunofluorescence intensities between groups (*p<0.05, **p <0.01, ****p <0.0001). Dotted area: ICM, Arrowhead: TE nucleus, White arrow: Interblastomere bridge-like structure. (C (control), n=8; 20 ng/mL, n=5; 50 ng/mL, n=6)..... 56

Figure 22: Evaluation of p-c-Abl localizations by immunofluorescence staining in control, 20 ng/mL and 50 ng/mL PDGF-AA groups. A. Localization of p-c-Abl in cells was determined after PDGF-AA treatment. p-c-Abl localization was determined around the nucleus and in the cytoplasm in all groups. B. There was no statistically significant difference between the groups when comparing the immunofluorescence intensity. (C (control), n=4; 20 ng/mL, n=4; 50 ng/mL, n=4)..... 58

Figure 23: Evaluation of p-YAP localizations by immunofluorescence staining in control, 20 ng/mL and 50 ng/mL PDGF-AA groups. A. Cellular localization of p-YAP after PDGF-AA treatment. p-YAP localization was determined around the nucleus and cytoplasm in all groups B. When immunofluorescence intensity was compared between the groups, it was observed that the p-YAP level was significantly decreased in the 20 ng/mL and 50 ng/mL PDGF-AA groups (*p<0.05, **p<0.01). (C (control), n=5; 20 ng/mL, n=5; 50 ng/mL, n=5)..... 60

Figure 24: Evaluation of p73 localization by immunofluorescence staining in control, 20 ng/mL and 50 ng/mL PDGF-AA groups. A. Cellular localizations of p73 and YAP would change with the 20 ng/mL and 50 ng/mL PDGF-AA treatment compared to the control group. After PDGF-AA treatment, YAP was gradually expressed in the cytoplasm in TE cells. B. Comparison of c-Abl and PARD6 immunofluorescence intensities between groups (**p <0.01, ****p <0.0001). (C (control), n=4; 20 ng/mL, n=4; 50 ng/mL, n=4) 62

Figure 25: Evaluation of TEAD4 localization by immunofluorescence staining in control, 20 ng/mL and 50 ng/mL PDGF-AA groups. A. Cellular localizations of TEAD4 would change with the 20 ng/mL and 50 ng/mL PDGF-AA treatment compared to the control group. After PDGF-AA treatment, TEAD4 was gradually expressed in the cytoplasm in TE cells. Expression of TEAD4 in the nucleus of TE cells were seen in the control group. B. Comparison of TEAD4 immunofluorescence intensities between groups (**p <0.01, ****p <0.0001). Arrowhead: TE nucleus. (C (control), n=4; 20 ng/mL, n=5; 50 ng/mL, n=6) 64

Figure 26: Evaluation of c-Abl and PARD6 localization by immunofluorescence staining in control, 20 ng/mL and 50 ng/mL PDGF-AA groups. A. Cellular localizations of c-Abl and PARD6 change with the PDGF-AA treatment compared to the control group. After PDGF-AA treatment, no significant changes were seen in the PARD6 pattern. B. Comparison of immunofluorescence intensities between groups (*p<0.05, ***p <0.001). White Arrow: Polarization regions. (C (control), n=4; 20 ng/mL, n=5; 50 ng/mL, n=5) 66

Figure 27: Evaluation of CDX2 and E-cadherin localization by immunofluorescence staining in control, 20 ng/mL and 50 ng/mL PDGF-AA groups. A. Cellular localizations of CDX2 and E-cadherin would change with the PDGF-AA treatment. There are no significant changes were seen in the CDX2 and E-cadherin patterns. B. E-cadherin and filopodia structures formed between blastomeres were determined. Especially in the 50 ng/mL PDGF-AA group, the filopodia were increased and exhibited a longer pattern compared to the control and 20 ng/mL PDGF-AA group. C. Comparison CDX2 and E-cadherin of immunofluorescence intensities between groups (*p<0.05, **p<0.01, ***p <0.001, ****p <0.0001). Dotted area: ICM. (C (control), n=4; 20 ng/mL, n=4; 50 ng/mL, n=5) 68

Figure 28: Evaluation of NANOG localization by immunofluorescence staining in contro 20 ng/mL and 50 ng/mL PDGF-AA groups. A. Cellular localizations of Nanog would change with the PDGF-AA treatment compared to the control group. In control group NANOG expression was determined in ICM. In 20 ng/mL and 50 ng/mL PDGF-AA groups Nanog expression determined in ICM, but we determined weak expression in TE cells. B. Comparison NANOG of immunofluorescence intensities between groups (*p<0.05, **p <0.01, ****p <0.0001). (C (control), n=4; 20 ng/mL, n=5; 50 ng/mL, n=5) 70

Figure 29: Determination of mRNA levels between groups following PDGF-AA treatment. A. After PDGF-AA treatment, c-Abl, Yap, Tead4 mRNA levels were compared between control, 20ng/mL PDGF-AA and 50ng/mL PDGF-AA groups. While c-Abl mRNA level increased significantly in PDGF-AA groups, Tead4 mRNA level decreased significantly in PDGF-AA groups. B. TE and ICM markers were compared between the control, 20ng/mL PDGF-AA and 50ng/mL PDGF-AA groups. While the TE marker Cdx2 mRNA level decreased in the groups treated with PDGF-AA, the ICM markers Nanog and Oct4 did not differ significantly. 71

Figure 30: Morphological comparison of the developmental potentials of imatinib groups. A. Morphological comparison of the control, DMSO, 1 µM, 5 µM and 10 µM Imatinib groups of mouse embryos obtained by superovulation and cultured from zygote to blastocyst. B. and C. Statistical evaluation of the developmental potential of imatinib treatment on embryonic development (*p<0.05, **p<0.01, ***p<0.001). (8 different cultures were assessed for their average developmental potential). 73

Figure 31: Statistical evaluation of the morphology of imatinib groups. Control, DMSO, 1 µM, 5 µM and 10 µM imatinib groups; The thickness of the ZP (A), the measurement of the angle between the 2 blastomeres in the 2-cell (B), the measurement of the angle between the 2 blastomeres in the Morula (C), and the blastocoele cavity formed in the blastocyst (D) embryos were evaluated (n=10) (*p <0.05, ****p<0.0001). 74

Figure 32: Evaluation of c-Abl and YAP localization by immunofluorescence staining in control, 1 µM and 5 µM imatinib groups. A. Cellular localizations of c-Abl and YAP would change with the imatinib treatment. In the control, 1 µM and 5 µM imatinib groups, c-Abl expression was seen in the cytoplasm. In addition to the cytoplasm, it was seen intensely in the nuclei of mitotic cells. YAP expression was determined in the nuclei of TE cells and in the cytoplasm of ICM cells. B. Although the c-Abl and YAP

localization patterns did not change, when the immunofluorescence intensities were examined; It was determined that c-Abl and YAP intensity levels decreased in imatinib treatment (*p<0.05, **p <0.01, ***p <0.001, ****p <0.0001). (C (control), n=5; 1 μM, n=5; 5 μM, n=5)..... 76

Figure 33: Evaluation of p-c-Abl localization by immunofluorescence staining in control, 1 μM and 5 μM imatinib groups. A. Cellular localizations of p-c-Abl would change with the imatinib treatment in the control, 1 μM and 5 μM imatinib groups with the immunofluorescence staining. In the control group p-c-Abl expression pattern was seen in the cytoplasm and cell boundries. In the 1 μM and 5 μM imatinib groups, p-c-Abl cumulative expression pattern was seen in the cytoplasm. B. When the immunofluorescence intensities were examined; It was determined that p-c-Abl intensity levels decreased in 5 μM imatinib treatment group (*p <0.05). (C (control), n=4; 1 μM, n=5; 5 μM, n=5)..... 77

Figure 34: Evaluation of p-YAP localization by immunofluorescence staining in control 1 μM and 5 μM imatinib groups. A. Cellular localizations of p-YAP change with the imatinib treatment. In the control group p-YAP expression pattern was seen in the cytoplasm. In the 1 μM and 5 μM imatinib groups, p-YAP expression pattern was seen in the cytoplasm and peri-nuclear area. B. When the immunofluorescence intensities were examined; It was determined that p-YAP intensity levels increased in imatinib treatments (*p<0.05, ****p <0.0001). (C (control), n=4; 1 μM, n=4; 5 μM, n=4) 78

Figure 35: Evaluation of p73 localization by immunofluorescence staining in control, 1 μM and 5 μM imatinib groups. A. Cellular localizations of p73 would change with the imatinib treatment. In the control, 1 μM and 5 μM imatinib groups, p73 cumulative expression pattern was seen in the cytoplasm. B. When the immunofluorescence intensities were examined, it was determined that p73 intensity levels decreased in imatinib treatment groups (****p <0.0001). (C (control), n=5; 1 μM, n=6; 5 μM, n=8) 79

Figure 36: Evaluation of TEAD4 localization by immunofluorescence staining in control, 1 μM and 5 μM imatinib groups. A. Cellular localizations of TEAD4 would change with the imatinib treatment. In the control, 1 μM and 5 μM imatinib groups, TEAD4 expression pattern was seen in the cytoplasm. B. When the immunofluorescence intensities were examined, it was determined that TEAD4 intensity levels decreased in

imatinib treatment groups (*p<0.05, ***p <0.001, ****p <0.0001). (C (control), n=4; 1 μM, n=6; 5 μM, n=6)..... 80

Figure 37: Evaluation of c-Abl and PARD6 localization by immunofluorescence staining in control 1 μM and 5 μM imatinib groups. A. Cell localizations of c-Abl and PARD6 were determined after imatinib treatment. In the control group, PARD6 localization showed intense localization at the borders of the cells, while it was determined that it spread towards the cytoplasm of the cells in the 1 μM and 5 μM imatinib groups. B. PARD6 expression level was significantly increased in the 1 μM and 5 μM imatinib groups (*p<0.05, ***p<0.001, ****p<0.0001). (C (control), n=5; 1 μM, n=5; 5 μM, n=5) 81

Figure 38: Evaluation of CDX2 and E-cadherin localization by immunofluorescence staining in control 1 μM and 5 μM imatinib groups. A. Cellular localizations of CDX2 and E-cadherin were determined in control, 1 μM and 5 μM imatinib groups. In the control group, CDX2 localization seen in nuclei, while it was determined that it cytoplasm of the cells in the 1 μM and 5 μM imatinib groups. E-cadherin expression was determined at cell borders in all groups. B. E-cadherin and filopodia structures formed between blastomeres were determined. While filopodia structures were visible in the control group, it was seen that it decreased in the 1 μM group, and the structures took a chain-like shape in the 5 μM group. C. CDX2 expression level was significantly increased in the 5 μM imatinib groups and E-cadherin level was significantly increased in 1μM and 5 μM imatinib groups (***p<0.001, ****p<0.0001). (C (control), n=4; 1 μM, n=4; 5 μM, n=5)..... 82

Figure 39:Evaluation of NANOG localization by immunofluorescence staining in control 1 μM and 5 μM imatinib groups. Cellular localizations of NANOG would change with the imatinib treatment. In control group Nanog expression was determined in ICM. In 1 μM and 5 μM imatinib groups NANOGg expression determined in TE, but we determined weak expression in TE cells. B. Comparison NANOG of immunofluorescence intensities between groups (*p<0.05, ****p <0.0001). (C (control), n=3; 1 μM, n=4; 5 μM, n=4) 83

Figure 40: Comparison of c-Abl, Yap, Tead4, Cdx2, Nanog and Oct4 mRNA levels after imatinib treatment (*p<0.05, **p<0.01, ***p<0.001, ****p<0.0001). 84

Figure 41: Morphological comparison of developmental potentials of embryos in control, scrambled, c-Abl siRNA groups. (3 different siRNA injection were assessed for evaliation of average developmental potential). 86

Figure 42: Morphokinetic evaluation of embryonal development following c-Abl siRNA microinjection. A. Comparison of ZP thickness of embryos between control, scrambled and c-Abl siRNA groups. B. Comparison of the interblastomere angle in 2-cell embryos between control, scrambled and c-Abl siRNA groups. 86

Figure 43: Comparison of c-Abl, Yap, Tead4, Cdx2, Nanog and Oct4 mRNA levels in embryonal development following c-Abl siRNA microinjection. A. Comparison of c-Abl, Yap and Tead4 mRNA levels in experimental groups. B. Comparison of Nanog, Cdx2 and Oct4 mRNA levels in experimental groups. 87

Figure 44: The figure shows the areas of blastomeres measured in embryos developing the blastocyst in the PDGF-AA and imatinib groups. 88

Figure 45: Comparison of area measurements of blastomeres in embryos developing blastocyst in PDGF-AA and imatinib groups. A. After PDGF-AA treatment, blastomere areas were significantly reduced in the 20 ng/mL and 50 ng/mL PDGF-AA groups. B. After imatinib treatment, blastomere areas were found to be significantly reduced in the 1 μM and 5 μM imatinib groups (n=44) (**p<0.01, ****p<0.0001). 88

Figure 46: Comparison of the number of nuclei and area measurements of nuclei in embryos that can reach the blastocyst in the PDGF-AA and imatinib groups. The number of nucleus and the area of nucleus did not differ significantly in the 20 ng/mL and 50 ng/mL PDGF-AA groups. After imatinib treatment, the number of nuclei in the 1 μM and 5 μM imatinib groups was significantly reduced in the 5 μM imatinib group, while the core areas did not show a significant change (*p<0.05). 89

Figure 47: Apoptotic bodies identified in preimplantation embryos developing through the blastocyst. 90

Figure 48: Image of apoptotic bodies formed in embryos reaching blastocyst in PDGF-AA and imatinib groups and comparison between groups. A. PDGF-AA treatment and B. imatinib treatment followed by apoptotic bodies in groups. C. Apoptotic bodies were significantly increased in the 20 ng/mL PDGF-AA group and the 5 μM imatinib group (**p<0.01, ****p<0.0001). 91

Figure 49: Cellular distribution of PARD6 following PDGF-AA treatment and imatinib treatment in mouse blastocyst. Following PDGF-AA treatment and imatinib treatment, the localization of PARD6 in the blastomeres shifts from the apical region to the cytoplasm. 100

Figure 50: PDGF-AA treatment and imatinib treatment affect the localization of E-cadherin, which is crucial for compaction, as well as the length and number of filopodia during preimplantation embryo development. 103

Figure 51: c-Abl participates in the determination of YAP location during the preimplantation stage of mouse embryonic development, which in effect determines cell fate. 109

LIST OF SYMBOLS AND ABBREVIATIONS

ICM: Inner cell mass

TE: Trophectoderm

ZP: Zona pellucida

YAP: YES-associated protein

TEAD: TEA domain family member

PrE: Primitive endoderm

EPI: Epiblast

MZT: Maternal zygotic transition

EGA: Embryonic genome activation

ZGA: Zygotic genome activation

E-cad: E- cadherin

Myo-1: Myosin 1

ERM: Ezrin/Radixin/Moesin

NM2: Non-muscular myosin 2

MTOC: Microtubule Organizing Centers

IB: Interphase bridge

C. elegans: *Caenorhabditis elegans*

aPKC: Atypical Protein Kinase C

MDCK: Madin-Darby canine kidney

SOX2: SRY-box transcription factor 2

AMOT: Junction-Associated Scaffold Protein Angiomotin

CDX2: Caudal type homeobox 2

GATA-3: GATA-binding protein 3

POU5F1: POU class 5 homeobox 1

SH1: Src homology 1

SH2: Src homology 2

SH3: Src homology 3

PDGF: Platelet-Derived Growth Factor

TCR: T cell receptor

EGF: Epidermal Growth Factor

hCG: Human Chorionic Gonadotropin

Ras–GAP: GTPase activating protein

PI-3: Phosphatidylinositol-3'

FAK: Focal Adhesion Kinase

KO: Knockout

KD: Knockdown

DSB: Double-strand break

PMSG: Pregnant Mare Serum Gonadotropin

BSA: Bovine Serum Albumin

PBS: Phosphate buffered saline

dsRNA: double-stranded RNA

CML: chronic myeloid leukemia

ECM: Extracellular matrix

HEK293A: Human embryonic kidney 293 cells

LMB: leptomycin B

NBT-II: Nara Bladder Tumor II

TEM: Transmission Electron Microscopy

ABSTRACT

Yıldırım, E. (2023). Determination of the Relationship Between c-Abl Protein Tyrosine Kinase and YAP in Cell Fate Determination during Mouse Preimplantation Embryonic Development, Yeditepe University, Institute of Health Sciences, Department of Histology and Embryology, PhD Thesis, İstanbul.

The successful completion of polarization, compaction and lineage specification is required for the development of embryo from the zygote to the blastocyst during preimplantation embryonic development. c-Abl (Abelson Tyrosine Kinase) is a non-receptor tyrosine kinase localized in cell nucleus and cytoplasm and also capable of nuclear-cytoplasmic shuttling. Despite the established knowledge regarding the YAP1 phosphorylation by c-Abl is very important for selective activation of p73, the involvement of the c-Abl/YAP/p73 mechanism in embryonic development remains unexplored. The aim of thesis is investigate the functional role of c-Abl tyrosine kinase in polarization, compaction and cell fate determination through c-Abl/YAP/p73 cascade during early mouse embryonic development. C57BL6 female mice at 6-8-wk old were superovulated with 7,5 IU PMSG and after 48 hr 7,5 IU hCG, then mated. 20 hours after hCG enjection, zygotes were collected and cultured. We designed mainly 4 groups: Control group, PDGF-AA treatment group, imatinib treatment group, and *c-Abl* siRNA microinjection group. Morphological and morphokinetic parameters, blastomere area measurements, and apoptotic bodies were evaluated in embryos obtained from all experimental groups. We used immunofluorescence staining to determine localization of c-Abl, YAP, p-c-Abl, p-YAP, p73, TEAD4, Pard6, E-cadherin, CDX2 and NANOG by using confocal microscope. We detected *c-Abl, Yap,* trophoectodermal cell markers *Tead* and *Cdx2 and* inner cell markers *Oct4* and *Nanog* expression at the mRNA levels using the qRT-PCR. In this thesis, we suggested for the first time c-Abl/YAP/p73 pathway served as a mechanism during mouse early embryonic development. The results contributes with new knowledge concerning the c-Abl tyrosine kinase may have regulative function in morphokinetic and morphodynamic features of mouse embryo in polarization, compaction, and cell fate specification during preimplantation embryonic development.

This study was supported by Yeditepe University Research Projects and Scientific Activities Support Commission (Project No: YAP-AP-SAB-21019).

Keywords: c-Abl, Yap, p73, preimplantation embryonic development, compaction, cell fate determination.

ÖZET

Yıldırım, E. (2023). Farede Preimplantasyon Dönemi Embriyonal Gelişiminde Hücre Kaderinin Belirlenmesinde c-Abl Protein Tirozin Kinaz ile YAP Arasındaki İlişkinin Belirlenmesi, Yeditepe Üniversitesi, Sağlık Bilimleri Enstitüsü, Histoloji ve Embryoloji Anabilim Dalı, Doktora Tezi, İstanbul.

Zigot aşamasındaki embriyonun blastokiste gelişim sürecinde polarizasyon, kompaktlaşma ve hücre kaderinin belirlenmesi olaylarının başarıyla tamamlanması gerekmektedir. c-Abl, hücrede çekirdek ve sitoplazmada lokalize olan ve ayrıca çekirdek ile sitoplazma arasında taşınabilen bir tirozin kinazdır. c-Abl aracılı YAP1 fosforilasyonunun p73'ün aktivasyonundaki önemi belirlenmiş olmasına rağmen, c-Abl/YAP/p73 mekanizmasının preimplantasyon dönemi embriyo gelişimindeki rolü belirsizliğini korumaktadır.Tez çalışmamızda c-Abl tirozin kinazın, fare preimplantasyon dönemi embriyo gelişiminde c-Abl/YAP/p73 kaskadının polarizasyon, kompaktlaşma ve hücre kaderinin belirlenmesindeki fonksiyonel rolünü araştırmayı amaçladık. 6-8 haftalık C57BL6 dişi fareler, 7,5 IU PMSG ve 48 saat sonra 7,5 IU hCG hormonu verilerek süperovulasyon yapıldı ve ardından erkek fareler ile çiftleştirildi. hCG enjeksiyonundan 20 saat sonra zigot aşamasındaki embriyolar toplanarak kültüre edildi. Tez çalışmamızda temel olarak 4 grup tasarladık: Kontrol, PDGF-AA uygulaması yapılan, imatinib uygulaması yapılan ve c-Abl siRNA mikroenjeksiyonu gerçekleştirilen gruplar. Tüm deney gruplarından elde edilen embriyolarda morfolojik ve morfokinetik parametreler, blastomer alan ölçümleri ve apoptotik cisimler değerlendirildi. c-Abl, YAP, p-c-Abl, p-YAP, p73, TEAD4, Pard6, E-cadherin, CDX2 ve NANOG lokalizasyonu immünofloresan yötemi ile belirlendi ve konfokal mikroskopta görüntülendi. qRT-PCR yöntemi kullanarak c-Abl, Yap, trofoektodermal hücre belirteçleri Tead ve Cdx2, iç hücre belirteçleri Oct4 ve Nanog ekspresyonunu mRNA düzeyinde belirledik. Tez çalışmamızda ilk kez, preimplantasyon dönemi embriyo gelişim sürecinde c-Abl/YAP/p73 sinyal yolağı mekanizması gösterildi. Sonuçlarımız; c-Abl tirozin kinazın, fare preimplantasyon dönemi embriyo gelişiminde polarizasyon, kompaktlaşma ve hücre kaderinin belirlenmesinde morfokinetik ve morfodinamik özellikler üzerinde düzenleyici bir role sahip olabileceğine dair yeni bilgiler sunmaktadır.

Bu çalışma Yeditepe Üniversitesi Araştırma Projeleri ve Bilimsel Faaliyetleri Destekleme Komisyonu tarafından desteklenmiştir (Proje No: YAP-AP-SAB-21019).

Anahtar kelimeler: c-Abl, Yap, p73, preimplantasyon dönemi embriyonal gelişim, kompaktlaşma, hücre kaderinin belirlenmesi.

1. INTRODUCTION and PURPOSE

Determination of cell fate in the preimplantation period embryonal development involves different processes. Apico-basal cell polarity begins to appear in the blastomeres at the 8-cell stage embryo and this polarization is very important for cell differentiation in the later stages of development. In the transition from the 8-cell stage to the 16-cell stage, intercellular adhesion increases and compaction is observed. After compaction, cell differentiation begins and two separate cell lines are formed, the inner cell mass (ICM) and the trophectoderm (TE) [1]. However, the determining factors in the polarization and compaction of cell polarity still remain unclear. The Hippo signaling pathway has been shown to be regulation of cancer development in mammals and involved in cell-cell contact inhibition, control of organ size [2,3]. YES-associated protein (YAP) is a transcription coactivator that acts as an oncogene and is downstream effector of the Hippo signaling pathway [4]. The Hippo signaling pathway plays an important role during fate determination and cell polarity in blastomeres.

In polar cells, the Hippo signal allows YAP to be present in the nucleus and interact with the TEA domain family member (TEAD4). In nonpolar cells, the Hippo signal causes the transcriptional coactivator YAP to translocate to the cytoplasm [5]. c-Abl tyrosine kinase is an important oncogene that plays a crucial role in intracellular signaling mechanisms by localizing in the nucleus and cytoplasm. c-Abl, which plays a role in the DNA repair mechanism, is activated when DNA damage occurs [6,7]. In previous studies, YAP has been shown to act as a substrate for c-Abl [8]. It has also been shown that c-Abl phosphorylates YAP from the Y357 region (Tyrosine 357) and translocates it to the nucleus, and YAP binds to p73 with high affinity and induces p73-mediated apoptosis [9]. With all this literature information, we hypothesized that c-Abl may be involved in the regulation of YAP during preimplantation embryonal development in the proposed thesis project. To demonstrate our hypothesis, we aim to reveal the interrelationships of c-Abl and YAP in the processes of compaction and cell differentiation (specification of cells as ICM and TE in the blastocyst) during preimplantation embryos.

2. LITERATURE REVIEW

2.1. Preimplantation Embryonic Development in The Mouse

Embryo development in mammals spend the first few days after fertilization swimming freely in the oviduct. This process results in the embryo implantation in the uterus. This early stage of mammalian development is commonly referred to as the pre-implantation period. The success of embryo implantation is contingent upon the healthy development of the embryo throughout the pre-implantation stage until it reaches the implantation stage. Therefore, determining the molecular mechanisms underlying preimplantation embryo development and knowing what roles these mechanisms play at which stage of development is very important to understand the structure necessary for a healthy embryonic development.

The preimplantation period includes the development of the mouse embryo from fertilization to implantation. This period starts with fertilization and ends on the 4th-5th day. The is pluripotent zygote stage embryo formed after the fusion of oocyte and sperm [10,11]. Following fertilization, the male and female genomes form pronuclei in the zygote, which initiates mitotic divisions [12]. During mitotic divisions, the embryo increases the number of cells and divides into blastomeres without cell growth [11].

Morphogenetic and epigenetic events lead to the formation of two different cell types that form the first two progenitor cell lines at the 16-cell stage [10]. Polarization and compaction occur at the 8-cell stage, followed by asymmetric divisions forming two different cell types: TE and ICM cells. Afterwards, the embryos transforms into a fluid-filled cell sphere known as the blastocyst, while the ICM differentiates into the epiblast (EPI), which forms all fetal cells, and Primitive endoderm (PE), which will often join the extra-embryonic yolk sac [13].

The advent of novel imaging techniques that facilitate quantitative analysis at various levels, ranging from cell-cell interactions to the dynamics of cellular regulatory molecules, has shed new light on the intricate processes involved in shaping the embryo from fertilization to implantation stages. These studies have greatly contributed to enhancing our understanding of the complex and intricate developmental events occurring during this critical period.

2.1.2. Fertilization

Fertilization marks the initiation of embryonic development, wherein the successful penetration of the sperm into the egg and the subsequent block against polyspermia are crucial. In mammals, the zona pellucida (ZP), which surrounds the oocytes and preimplantation embryo, plays a vital role in the multi-step process of successful fertilization and preimplantation development. The ZP serves as an important determinant for facilitating these processes and ensuring the progression of embryonic development. The ZP encoded by maternal genes, not only provides species-specific gamete recognition and blocks polyspermy, but also allows the early embryo to migrate through the female genital tract prior to implantation in the uterus [14].

After the sperm enters the female genital tract, it undergoes physiological and molecular changes called capacitation in order to have the ability to fertilized. Capacitated sperm travels to the ampulla part of the oviduct [15,16]. A single capacitated sperm capable of fertilization passes through the cumulus cells around the oocyte and successfully penetrates the oocyte. Sperm penetrates the ZP and passes through the ZP to the perivitelline area. Thereby, the sperm plasma membrane and the oolemma interacting with the acrosome become direct contact. Finally, following sperm fusion, the sperm membrane and oolemma fuse to form the zygote, called "gamete fusion" [17]. Exocytosis of cortical granules occurs following gamete fusion. Cortical granules are formed in the Golgi apparatus and are membrane-bound vesicles containing the biochemical matrix-remodelling apparatus [18]. The resulting molecular changes prevent polyspermia, which is fatal for the embryo [17].

2.1.3. Embryonic Genome Activation

Maternal mRNAs and proteins that are synthesized and accumulated within the cytoplasm of the oocyte during oocyte maturation play crucial roles in the initial stages of embryonic development. The mechanisms underlying embryo development are genetically controlled coordinated steps, demethylation of maternal and paternal genomes, including embryonic genome activation, Zygotic genome activation (ZGA) [19]. It is based on post-transcriptional gene regulation in the transitional phase between embryonic and maternal genome activation Maternal zygotic transition (MZT). MZT mainly involves the elimination of maternal mRNA accompanied by initially maternally encoded factors. At the same time, as zygotic/embryonic transcription intensifies, formation of new proteins and miRNAs increases the effect of maternal mRNA degradation. In mice, ZGA occurs towards the end of the 1-cell stage and peaks at the 2-cell stage [20,21]. In non-rodent mammals, this process is divided into 2-cell, minor embryonic genome activation (EGA) and major EGA. It has been seen in studies conducted with cattle and sheep embryos that; major EGA occurs in the 8-16 cell stage [22,23]. In in vivo studies with porcine embryos, major EGA occurs similarly to human embryos at the 4-5 cell stage, during the 3rd cell cycle following fertilization [24].

ZGA emerges as a result of transcriptional changes, and following these changes, fluctuations occur in gene expression [25]. These changes also involve different proteins produced at different times during each division [26]. While low level gene transcription is detected in the late stage of the mouse 1-cell embryo, a transcriptional burst occurs in wave 1 of embryonic genome activation (EGA1), with over 800 genes detected. Following the termination of EGA1, thousands of more genes are activated in the final stages of the 2-cell embryo, which is Wave 2 of embryonic genome activation. Following embryonic development, activation continues in 8-cell, morula and blastocyst stages [14,27] **(Figure 1).**

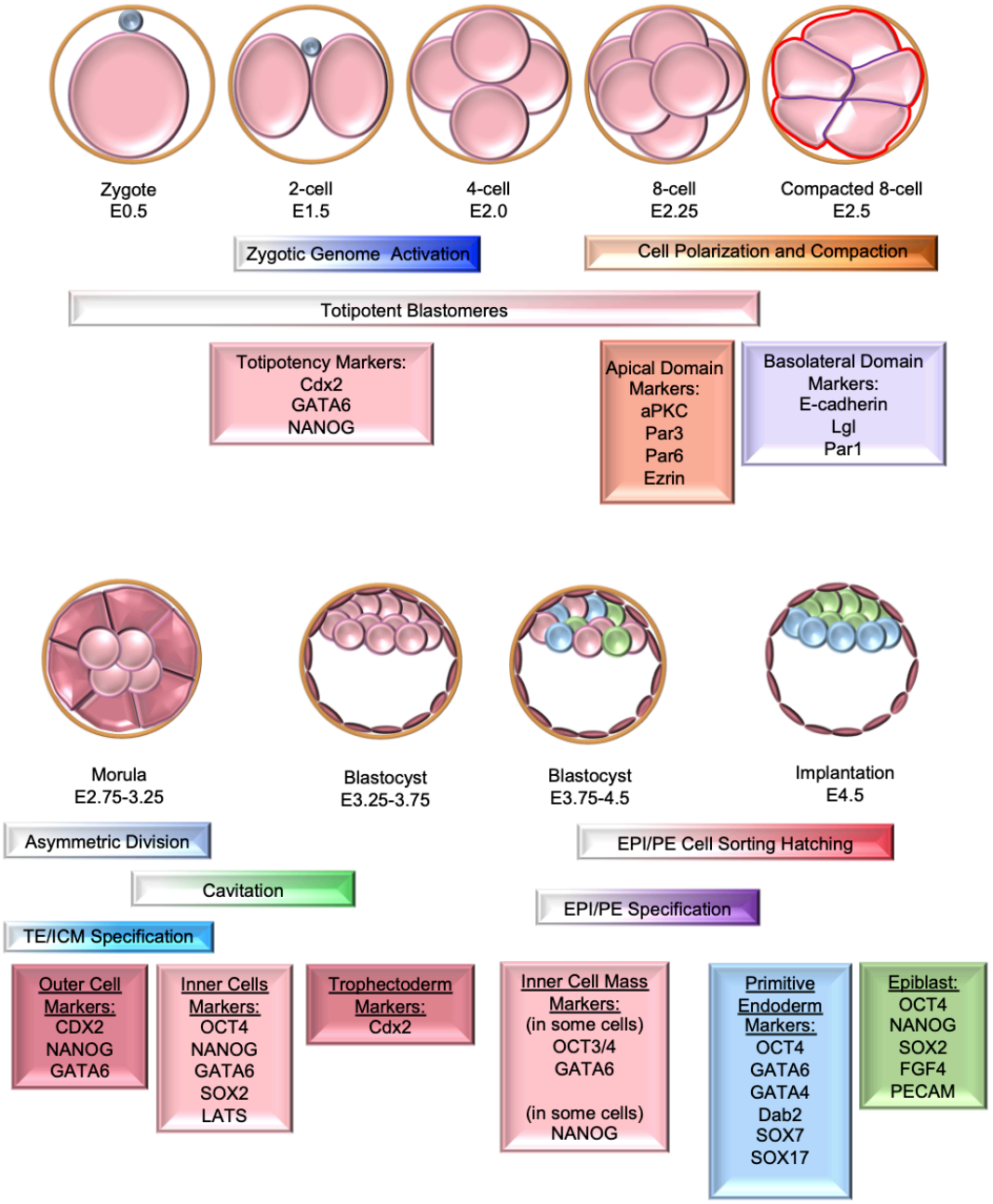

Figure 1: Changes in expression levels of genes involved in mouse preimplantation embryonic development and their roles in cell fate determination. The genes that are effective in the process from fertilization to the blastocyst stage are indicated in the figure.

2.1.4. Compaction

Compaction is a crucial process for the formation and development of blastocysts. During the preimplantation embryo development stage, blastomeres assemble with adherens and tight junctions to form primitive forms of tissue architecture [28]. Ca^{2+} dependent E-cadherin (E-cad) trans-ligation provides mechanical attachment of cell cortices between adjacent cells in regions of adherens juncitons and promotes cell-cell adhesion [29]. In the mouse embryo, E-cadherin is maternally supplied and expressed de novo at the 2-cell stage [30]. Maternal deficiency of E-cadherin in preimplantation embryo development delays compaction in embryos [31]. Deletion of zygotic E-cadherin or β-catenin was tolerated thanks to the maternal reserve present in the embryos, but it was found to be lethal before implantation. It was also determined that it could not form the TE epithelium [32,33]. As a result of deletion of E-cadherin, both maternally and zygotically, embryos cannot achieve compaction. In addition, Ca^{2+} exposure of the culture medium causes the blastomeres of the morula stage embryo to separate, leaving it as an uncompacted, loose cell cluster [34,35].

Adherens junctions are attached to the actin cytoskeleton by catenins and other proteins such as myosin 1 (Myo-1) or ezrin/radixin/moesin (ERM) [36,37]. This interaction is necessary for the cells to change shape after compaction, by causing the forces generated by the cytoskeleton-related motor proteins non-muscular myosin 2 (NM2) to be transmitted towards the cell surface [38]. This cortical tension created by the cell is transmitted to neighboring cells via adhesive filopodia [39].

The tight junctions create a permeability barrier that surrounds the embryo from the outside [40]. The establishment of this barrier enables the accumulation of osmotic hydrostatic pressure within the intercellular space, leading to the expansion of the initial internal cavity of the embryo. As a result, the morula undergoes transformation into a blastocyst. This process allows for the development of distinct cell lineages within the blastocyst and is crucial for further embryonic growth and development [41].

The actin ring typically forms a constriction, directing various morphogenetic processes in the cell [42]. Furthermore, in the mouse embryo, instead of creating a contraction, this mechanism causes actin rings seen in the embryo to expand into cell-cell junctions over the entire apical cortex during the 16 to 32 cell stage [41]. Following this expansion, the ring structures of neighboring cells form an initial point of contact at the common junction. Once these junctions are formed, a zipper-like structure forms, forming a unified linear structure that connects adjacent cells and extends bidirectionally at the point where both cells connect [41]. This zipper pattern of occurring actin rings occurs simultaneously at multiple junctions during the 16 to 32 cell stage, but when blastomeres divide after the 32-cell stage, the nascent cells retain their existing architectural structure before continuing to form the actin ring [41]. Since this actin ring expansion and zipper pattern formation occurs just before the blastocyst stage, it is considered a mechanism involved in the embryo having the necessary architecture for blastocyst formation [41].

In another study, the role of actin rings formed at the end of cytokinesis and microtubules that regulate the cortex differently during cell division were investigated. In dividing somatic cells, microtubules originate from centrosomes [43,44] (Figure 2). During cell division, microtubules attract actomyosin to the cytokinetic region where cells divide, while astral microtubules inhibit cortical F-actin, which is typically known as polar relaxation at the cell poles [45]. Indeed, the early mouse embryo lacks traditional centrosomes, which are known to play a critical role in organizing microtubule dynamics in many other cell types [46].

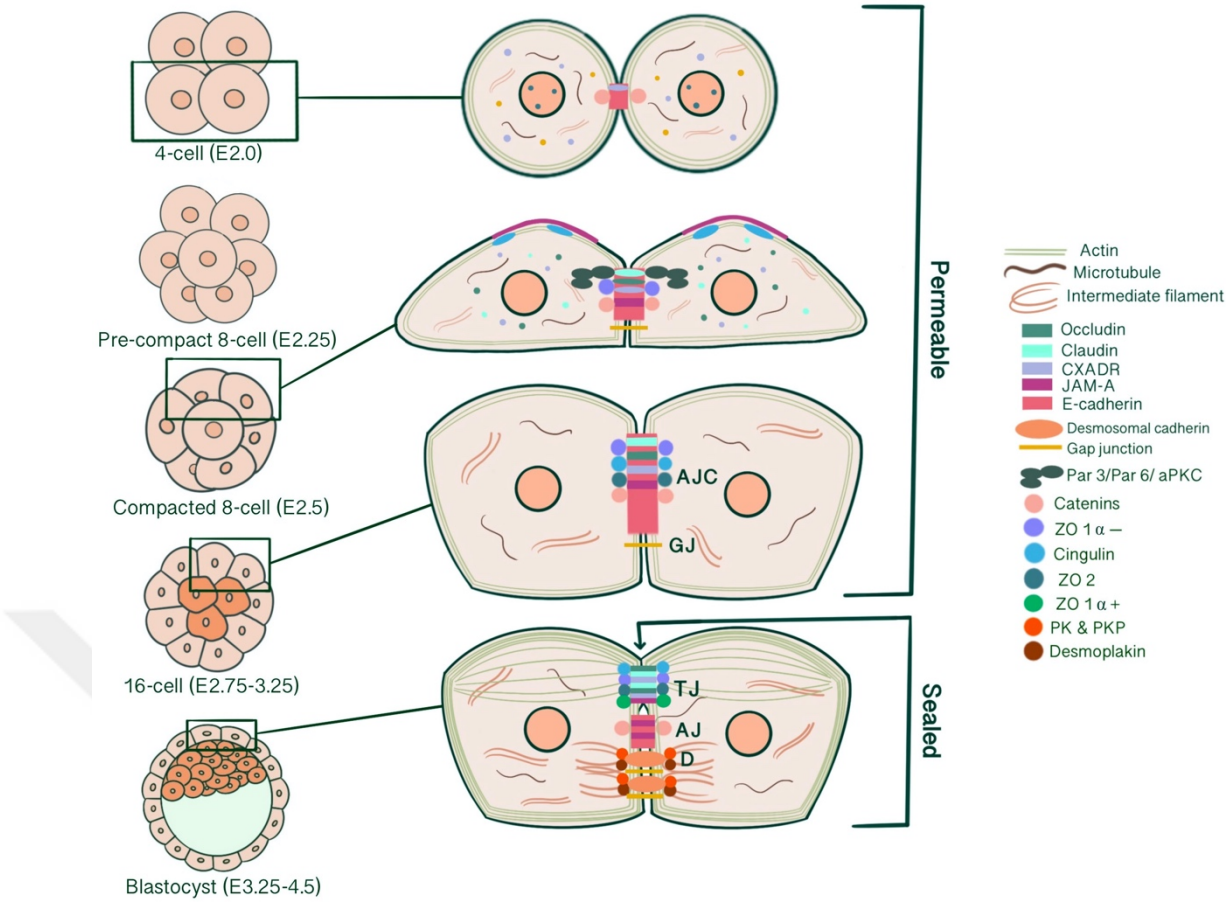

Figure 2: Molecular and mechanical properyies of compaction in Mouse embryo. During the development of preimplantation stage mouse embryos, the localization of intercellular adhesion proteins between blastomeres has been schematized. Intercellular connections are observed from the 4-cell stage to the blastocyst stage [44].

During the studies, it was thought that the microtubule organization in the early mouse embryo was randomly organized [46]. Subsequent studies used immunofluorescence and immunoelectron microscopy and revealed the presence of aligned microtubule arrays along sister blastomeres at the interphase stage [47,48]. Therefore, together with the live imaging methods used in recent studies, functional non-centrosomal Microtubule Organizing Centers (nc-MTOCs) in preimplantation mouse embryos have been revealed [49]. After mitosis, the typical cytokinetic bridge is not abscised (i.e., cells do not separate), but is instead transformed into an interphase bridge (IB), which is maintained from the bicellular stage to at least the blastocyst [50]. In most cells, the centrosome is present as the main MTOC [43]. But preimplantation embryos develop up to the mid-blastocyst (64 cells) before the centrosomes assemble [46]. Indeed, the spatial organization of microtubules (MTs) during early embryonic development is not fully understood yet. One intriguing

phenomenon observed is that when a cell undergoes mitosis and the MT network depolymerizes, this depolymerization can extend to the neighboring interphase sister cell, causing it to enter mitosis as well [49]. When this interphase bridge was disrupted using a laser ablation, their MTs were found to undergo depolymerization within ~60 s [49]. It was shown that as a result of ablation of IBs, the total MT density in both sister cells decreased and the cell took a more spherical cell shape [49]. Based on this study, it was suggested that the interphase bridge could function as an MTOC in the mouse embryo [49]. As a result of laser ablation targeting the interphase bridges, it was shown that not only the cell shape was changed, but also E-cad localization was affected and its expression decreased [49]. These results suggest that E-cadherin is transported to the basolateral membrane along MTOC-regulated MTs at the interphase stage, and this process is a crucial for early mammalian development [49,50] **(Figure 3).** The results show that cellular connections and compaction, which are important for embryonic development, depend on many factors. All the cell-cell connections and bridges seen at this are effective in determining cell fate.

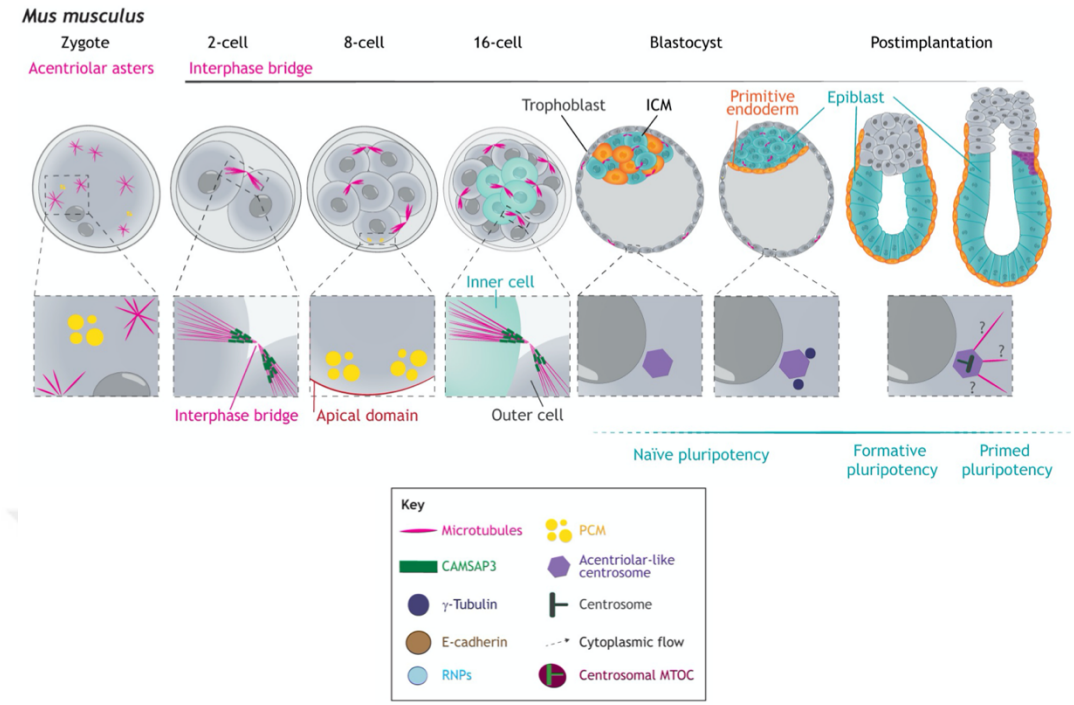

Figure 3: Microtubule organization in the mouse embryo from the zygote to the early post-implantation stage. In embryonic development, the interstage bridge appears as a non-centrosomal microtubule editing center (ncMTOC) during preimplantation development. Centrosomes first appear at the 16 to 32 cell, but they do not spread microtubules or affect the interphase microtubule network. Centriole-containing centrosomes may be required around gastrulation, suggesting the presence of a dual microtubule network [50].

2.1.5. Polarization

The establishment of polarity in mammalian embryos occurs through the rearrangement of various cell fate determinants. In this process, cytoplasmic streaming typically takes place, which is mediated by actomyosin cytoskeleton. This process has been extensively studied in *Caenorhabditis elegans* (*C. Elegans)*, while in mammalian oocytes and embryos, some processes have been described [51,52]. Cell polarization in the mouse embryo begins to occur in the early or middle stage of the 8-cell, which includes the uneven distribution of certain cellular components along the cell's apico-basal axis [12,53]. Until the early 8-cell, each blastomere in the embryo is morphologically similar. Within 1-3 hours of reaching the 8-cell, the blastomeres show the formation of prominent apical and basolateral areas, the first signs of radial polarity [54]. At this stage, the actin cytoskeleton is rearranged to form a microvillus-rich apical pole. In addition, cytoplasmic organelles and cytoskeletal elements adapt to polarization by redistribution [55]. Members of the ERM protein family, with different isoforms such as Par proteins (Par3 and Par6) and atypical protein kinase C (aPKC), regulate the polarization of the cytoskeleton by determining the apical region in the cell [56].

The non-contact surface of each blastomere forms the apical area, which is characterized by aggregation of microvilli and increased localization of the actin-binding protein Ezrin [57] and the Par3-Par6-aPKC complex towards the apical area [58].

Integrin is recruited by a variety of signaling pathways to regulate polarity motility and apico-basal epithelial polarity in cells, including the Par6 protein complex, integrin, TGFβ. Par6 protein complexes are involved in neuronal polarity, apico-basal polarity of epithelial cells, asymmetric cell division, and polarized cell movement [59]. However, Par6 has three distinct isoforms: A, B, and C. Limited information is known about the changes observed in the expression patterns of these three different isoforms. These isoforms exhibit different subcellular localizations in the epithelium. Therefore, it is believed that they may also have different functions. Par6A co-localizes with tight junction markers, while Par6B is localized in the cytosol [59]. Par6C, on the other hand, can localize both at tight junctions like Par6A and in the cytosol like Par6B. Par6 contains different sites that allow it to interact with other isoforms [60,61].

Par6 was originally known as a gene that plays an important role in the regulation of asymmetric division of zygote in the *C. elegans*. Subsequently, its significance in cellular polarity processes has been demonstrated in various organisms, including humans [62-64]. Par proteins localized in cortical clustering in cells and the pattern they create are

highly dynamic compared to other polarity complexes and can rapidly interact with cytoplasmic proteins [65]. For instance, upon activation of Par6/aPKC in epithelial cells, it interacts with Par3, the Crumbs complex, and the Scribble complex to regulate the establishment of apical-basal polarity [66,67]. Par6/aPKC, which is localized in the anterior region of migrating astrocytes and keratinocytes, facilitates the movement of microtubules that are necessary during migration [68,69]. In addition to its cytoplasmic localization, it has been reported that Par6 is also localized in the nucleus [70]. As demonstrated in several studies, Par6 expression has been identified not only at tight junctions but also in the nucleus and cytoplasm of Madin-Darby canine kidney (MDCK) cells. In this case, overexpressed Par6 was reported to localize to the nucleus [59,71]. The specificity and significance of nuclear localization of Par6 have not been clearly elucidated yet. However, it has not been indicated whether Par6 prioritizes localization in the nucleus or the plasma membrane. Such "dual-location" proteins have been increasingly observed in various studies [72,73].

Multiple studies indicate that the polarization process during the 8-cell stage of embryonic development does not depend on transcription or translation. Instead, it is believed to be regulated primarily through post-translational mechanisms [74,75]. However, in a study conducted with human embryos in 2019, individual transcriptome analysis of each blastomere was performed at the 8-cell [76].

Although it has been known in previous studies that blastomeres have different transcriptional and epigenomic identities, their relationships with gene families that play a role in determining cell fate were also defined in the study [76-78]. An analysis of genes involved in the Hippo signaling pathway, pluripotency, and cell polarity, which is effective in determining cell fate, was performed and reported that neither blastomere exhibited similar expression pattern with the other in the same embryo or in blastomeres from other 8-cell embryos [76]. Based on these studies, we can think that much more complex mechanisms play a role in important processes such as determination of polarity, compaction, blastocyst formation and cell fate determination in the embryo. The mechanisms and cell elements involved in the polarization process, which began to be seen in the 8-cell, should be investigated in more detail.

A trigger has been investigated in the polarization of the mouse embryo. However, there is no definitive study on this. However, many signaling pathways involved in this process have been identified. The most well-known among these is the accumulation of actomyosin in the apical cortex. This mechanism is initiated through phospholipase C-

mediated hydrolysis of PIP_2, aPKC. This activates RhoA, causing polarization of actin junctions. The Par3/Par6/aPKC complex is taken to the apical surface by undetermined factors [79]. Polarization of the PAR complex excludes actomyosin, which forms a suggested mature apical area with reduced cortical contraction [80,81].

There are also studies suggesting that the establishment of cell polarity occurs independently of the compaction of the embryo. From these studies, it has been demonstrated that embryos cannot become compacted as a result of maternal and zygotic knockout (KO) of *Cdh1*. However, they can still polarize [34]. It should be noted, however, that intercellular contacts play a role in establishing cell polarity. Cell-cell contact is important in establishing cell polarity. In studies, it has been noted that the apical domain tends to form as far away as possible from the cell-cell contact regions. This suggests that the orientation of the apical-basolateral axis is largely dependent on the asymmetric cell-cell contact patterns observed during compaction [82]. In another study, E-cadherin was shown to play a critical role in guiding the course of the intracellular apical-basolateral axis [83]. Although the acquisition of polarization occurs in blastomeres isolated from cell-cell contact or inhibited from compaction, it is extremely difficult to induce polarity experimentally in blastomeres that are completely surrounded by other cells (i.e. cells whose entire surface is in contact with other cells) [84].

2.1.6. Cell Fate Determination

Following the acquisition of polarization and the realization of asymmetric division, the process of determining the cell fate in the embryo begins. The blastomeres now differentiate into the inner cells ICM and the outer TE [85]. Three different models have been proposed for the mechanisms that occur during cell lineage determination: 1. inside-outside model, 2. cell polarity model, and newly updated 3. polarity model.

The interior-exterior model proposed in a 1967 study still remains acceptable. In their studies, it has been shown that they can form mini-blastocysts with ICM and TE from blastomeres isolated from 2-cell and 4-cell embryos; however, trophoblast vesicles were formed from the blastomeres isolated from the 8-cell embryo, and ICM could not be formed. The logic of this model; In preimplantation mouse embryos, it is based on the external environment on the one hand, and cell-to-cell contact in the morula, that is, the cell position. In this inside-out model, the inner cells that will become the ICM have symmetrical contact, while the outer cells that will become the TE have trilateral contacts and a free apical surface [86].

In another model proposed by the study conducted in 1981, they showed that polarization occurred in each of the blastomeres isolated from the 8-cell embryo and microvilli-like structures were determined in the apical areas of the cells [84]. According to this study, the cell polarity pattern is known as a cell fate-determining expression that is observed at the 8-cell and is formed by asymmetric and symmetric cell divisions. The last model proposed for the polarity model was determined in studies conducted in 2006 and 2017. This model shows cell polarity, which is the stage after cell division. It is thought that gene expressions are important for cell polarity and that cell polarity and cell fate are determined by the presence of certain genes expression [87,88].

Within all these studies, there are still unexplained questions. Whether blastomeres can contribute to lineage differentiation before embryo polarization is established is one of the questions being investigated. When we look at all transcriptome analyzes and gene expression patterns, can the embryo up to the 8-cell be considered a completely equal cell mass in terms of morphology, genetics and morphokinetics? When exactly and depending on what factors do these cells with totipotent character lose their plasticity and become unable to differentiate into one of the two lineages? In TE cell precursors, lineage differentiation occurs mainly in the 16-cell and often simultaneously starting at the early 32-cell. Although ICM precursors are similarly identified at the 32-cell, adherence is not gained until the 64-cell [89]. Determining the ICM and TE lineage can

ensure an adequate TE cell count prior to implantation [89]. Other studies have reported a link between the heterogenity seen in early embryonic development and cell specification. This opens up new discoveries that will determine cell fate in the early stages of development [13,90].

All blastomeres in the pre-compact embryo appear morphologically and morphokinetically similar, but this changes in the 16-cell following compaction [12]. When compaction occurs, lineage separation in blastomeres is driven by apical area formation. Apico-basal cell polarity was showed in blastomeres at the 8-cell, while continued linegae differentiation has been suggested to play a role in specification of ICM and TE cells [84]. TE cells that arise after lineage specilization possess junctional complexes known as Tight Junctions and Adherens Junctions that protect the blastocyst cavity, as well as possess apical-basal polarity [40].

Considering the cell polarity model, cells with polarity undergo "asymmetrical" divisions, while nonpolar cells divide symmetrically and competition for internal positions begins. As a result of this competition, the cells located on the surface turn into TE cells [83,91] **(Figure 4).** Polarized TE cells that remain in the outer part of the embryo acquire characteristics to epithelial cells, and after the initiation of asymmetrical divisions at 8-16 cell, the outer cells express high levels of cytokeratin [92]. In the blastocyst, cytokeratin 8 expression is observed in cells that will differentiate into TE cells [93]. The epithelial polarization seen in TE cells is regulated by molecules located between different protein complexes. These complexes exhibit regional localization in TE cells, allowing the identification of apical and basolateral regions. The polarization seen in cells has been conserved throughout evolution, and the PAR complex is the well-known complex related to apical polarity [93]. The PAR complex discovered in *C. elegans* embryos has major components. These components are; Par6 is Par3 and aPKC [94]. In mouse embryos, towards the end of the 8-cell, during compaction, the expression levels of Par6 and aPKC increase in the apical region of the cell, and these two proteins are localized together [95]. While Par3 is localized in the apical area in the late of 8-cell embryonic development, it co-localizes in TJs in outer cells with blastocyst development [96]. Besides these molecular signals, after the 16-cell, lineage differentiation is regulated by the YAP [97]. YAP activates the transcription of several TE-specific target genes, such as caudal type homeobox 2 (*Cdx2)*, by binding the transcription factor Tead4, which is the main factor in determining the fate of TE [98]. TE lineage differentiation is mainly regulated by *Cdx2* [99]. *Cdx2*$^{-/-}$ embryos were formed and it was determined that OCT4 and NANOG, known

as pluripotency factors, were suppressed in all cells in the embryo, resulting in suppressed expression of TE markers and not preserved blastocyst structure [99]. CDX2 has also been shown to be associated with another TE marker, the cytokeratin intermediate filament Krt8. CDX2 is required for the normal formation of TE cell fate, and Cdx2 is an essential component of this regulatory network [92,100].

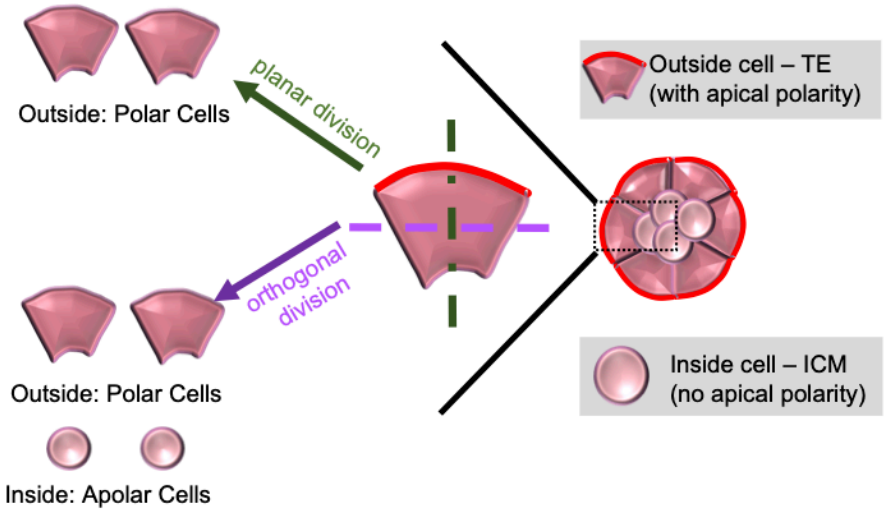

Figure 4: Asymmetric cell division. First lineage and inside-out pattern differentiation by polarity pattern during mouse preimplantation embryonic development [91].

2.2. Hippo Signaling Pathway in Preimplantation Mouse Embryo Development

Recent studies have revealed that Hippo signaling is important in determining cell fate and provides a molecular basis for new studies [97,101]. Activation of the Hippo pathway varies depending on the cellular position in the blastocyst embryo. The Hippo signaling is in an 'OFF' in the outer TE cells, while it is in an 'ON' in the ICM cells located on the inside.

In outer cells, inactive Hippo signaling promotes nuclear localization of YAP and TEAD (here collectively after YAP) by forming a YAP-TEAD4 complex. Activated Tead4 stimulates the TE-specific transcription factor Cdx2, and expression of Cdx2 plays an important role in the development of TE [101,102]. In contrast, in inner cells, activation of the Hippo pathway inhibits YAP accumulation and TEAD4 remains inactive. Since Tead4 does not induce Cdx2, these cells adopt the ICM fate. Based on this cell location, the Hippo signal provides an evidence for the inside-outside model [85,103] (Figure 5).

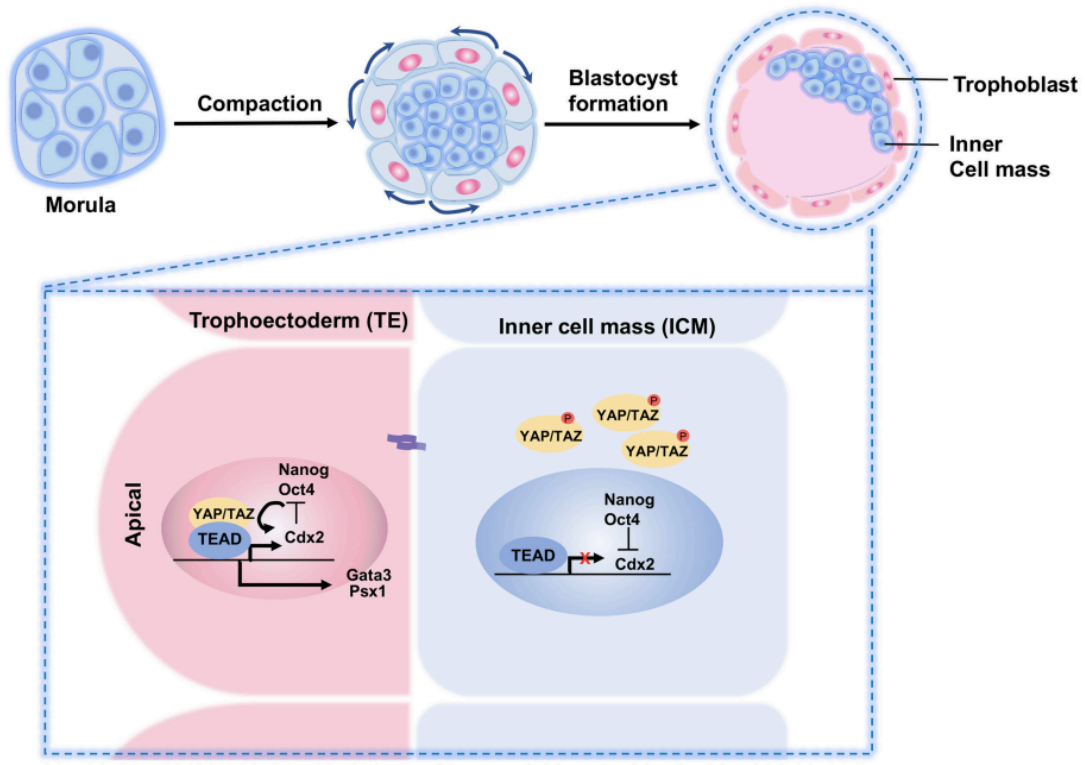

Figure 5: The Hippo signaling pathway in cell fate determination. When the Hippo signaling pathway is active, the localization of phosphorylated YAP is in the cytoplasm. When the Hippo signal is inactive, non-phosphorylated YAP is translocated to the nucleus [103].

During preimplantation development, the totipotent zygote has ability to give rise to embryonic and extra-embryonic structures. YAP/TAZ has also been shown to play a role in determining totipotency. As a result of maternal deletion of YAP/TAZ in the zygote embryo, it was observed that the embryo was arrested before reaching the blastocyst [97]. Maternal YAP/TAZ deletion inhibits the expression of SRY-box transcription factor 2 (SOX2) while the embryo is at the 16-cell, indicating that blastocyst formation is prevented due to abnormalities that may occur during ICM and TE differentiation [104].

During preimplantation embryo development, SOX2 is not expressed in TE cells [105]. In a study conducted in 2018, the YAP1/WWTR1 complex was identified as the key complex that suppresses the expression of Sox2 in the outer cells of the embryo [106]. To demonstrate this hypothesis, they chemically inhibited ROCK and antagonizes YAP1/WWTR1 activity, favoring over-expression of LATS2. As a result of all these manipulations, they found that Sox2 was ectopically expressed in TE cells. They reported

that YAP1/WWTR1 activity is required to inhibit Sox2 expression, especially in outer cells [106].

In addition, intermediate knockdowns (KD) of active Yap1/WWTR1 ($Yap1^{-/-}$/$WWTR1^{+/-}$ or $Yap1^{+/-}$/$WWTR1^{-/-}$) produced cells that co-express both SOX2 and CDX2, so SOX2 expression was relative to CDX2. They showed that it was more sensitive to YAP1/WWTR1 activity [106]. Due to the high LATS activity in the embryo, YAP1/WWTR1 activity is severely reduced, and in this way, the Hippo signaling pathway rapidly pushes the SOX2-expressing cells to their right final position in the embryo, ensuring healthy development [106]. [106]. In support of Frum et al, the timing of Hippo-induced cell internalization is similar to loss of cell fate plasticity around 32 cells [5]. However, the difference in Hippo signaling activity between the inner and outer parts of the embryo is one of the factors suggesting tight junctions between outer cells [107].

Cell polarity is known to cooperate with the junction-associated scaffold protein angiomotin (AMOT) family to regulate the Hippo signaling pathway [108]. In the absence of polarity in cells, AMOT is phosphorylated on serine 176 (S176), interacts with NF2 and LATS kinases to facilitate phosphorylation of YAP/TAZ, and is localized at adhesion junctions (AJs) [109-111]. However, when cells acquire polarity, AMOT is transported from basolateral AJs to apical regions by the cell polarity regulator, the Par-aPKC system; where AMOT interacts with F-actin to inhibit YAP/TAZ activity [107,109].

It has been shown in previous studies that YAP/TAZ has a role in totipotency of cells. When this mechanism was investigated in the zygote with totipotent character, it was shown that zygotes that did not have YAP/TAZ maternally could not develop until the blastocyst [97]. Maternal KO of YAP/TAZ results in early expression of the ICM marker SOX2 before the 16-cell. Thus, trophoblast factor inhibits *Cdx2* expression [106]. It explains that the reason why the zygote embryo does not reach the blastocyst as a result of YAP/TAZ deletion may be due to abnormal ICM and TE differentiation. Following fertilization, transcription of the newly formed embryo genome is inactivated and development continues depending on maternal RNA and proteins in the ovum [112]. This event, termed ZGA is known as the onset of embryonic transcription, and zygotes eliminate maternally supplied mRNA, resulting in elimination of maternal gene products [112]. This event, which includes both ZGA and lack of maternal products, is termed 'maternal to zygotic transition (MZT)'. The developmental process after MZT is controlled by zygote genomes [112].

Because the very early stage of development is controlled by maternal RNA and protein, a true inactivation of YAP cannot be achieved in $Yap^{-/+}$ parents formed by the maternal $Yap^{-/+}$ parents, as this can be tolerated as maternal YAP proteins are delivered by oocytes. However, when an oocyte-specific KO is established, YAP-deficient embryos can be produced because maternal YAP is important in MZT [113]. *Yap1* KO embryos were obtained with Yap KO oocytes fertilized by WT sperm, and it was observed that the duration of the 2-cell was considerably longer in these embryos and the transition to the 4-cell was delayed compared to the WT control [113]. In addition, transcriptome analyzes of 4-cell embryos created from $Yap^{♀-/♂+}$ and $Yap^{♀+/♂+}$were performed, and as a result, significant differences were detected in thousands of genes. When comparing $Yap^{♀-/♂+}$ and $Yap^{♀+/♂+}$embryos, many maternal transcripts were upregulated in $Yap^{♀-/♂+}$ embryos [113]. These obtained data revealed the role of YAP in MZT.

After TE/ICM cell differentiation occurs, the Hippo signaling pathway is suppressed in outer polar cells: YAP/TAZ interacts with TEAD and translocates to the nucleus. As a result, it directly induces the TE-specific transcriptional factors CDX2 and GATA-binding protein 3 (GATA3) and promotes differentiation into TE [97,114]. However, the Hippo signaling pathway is active in apolar cells in the ICM. Thus, LATS1/2 is phosphorylated and supports the localization of YAP/TAZ in the cytoplasm. Localization of YAP/TAZ in the cytoplasm prevents it from inducing target genes [95].

Downregulation of *Cdx2* in all blastomeres and abnormally high expression of ICM-specific transcription factors such as POU class 5 homeobox 1 (POU5F1) and NANOG were seen in TEAD4 KO embryos [97]. The Hippo signaling pathway plays an important role in controlling TE differentiation. Studies have also shown that YAP/TAZ-TEAD4 directly suppresses SOX2 gene expression [106].

In ICM, on the other hand, activation of LATS kinases reduces the effect of SOX2 in the nucleus, induces cytoplasmic translocation of YAP/TAZ, and differentiates cells into ICM [106]. From implantation of the blastocyst, the ICM will differentiate into epiblasts and hypoblasts; epiblast cells will develop into three germ layers and hypoblast cells will differentiate into yolk sac [106]. Epiblast cells are highly pluripotent cells. YAP-TEAD plays an important role in the formation of epiblasts and activates the expression of pluripotent genes [115]. Cells that do not have YAP-TEAD signal activated cannot achieve pluripotency, so these cells are eliminated by cell competition [115].

2.3. c-Abl Protein Tyrosine Kinase

2.3.1. Structure and Regulation of c-Abl Protein Tyrosine Kinase

The proto-oncoprotein c-Abl belongs to the non-receptor tyrosine kinase family, specifically the Src family, and has a molecular weight of approximately 140 kDa [116]. The c-Abl protein tyrosine kinase found in all cells has different sub-cellular localizations [116]. Among them, c-Abl is localized in cytoplasm in primary hematopoietic cells and neurons, while it is predominantly localized in the nucleus in fibroblasts. In contrast, all transformed Abl components are found only in the cytoplasm [116]. Protein tyrosine kinases play important roles in transducing extracellular signals. Most of the protein tyrosine kinases, such as receptor-tyrosine kinases or cytoplasmic tyrosine kinases, are located at or near cell membranes, such as Src, JAK, and FAK. Unlike other tyrosine kinases, c-Abl tyrosine kinase differs from others in that it is also present in the nucleus [117]. These changing subcellular localizations of c-Abl are controlled by NLSs (nuclear localization signals) and an NES (nuclear export signal) [116].

The regulation of Abl kinases activity is governed by intramolecular interactions with specific conformations of the kinase domain. These interactions are also associated with inhibition and activation regions [118]. The tyrosine kinase Src gives rise to two proteins, ABL1 (c-Abl) and ABL2, both of which share a conserved SH3–SH2–SH1 domain with interspecies homology, along with regulatory SH3 and SH2 domains. These domains are preceded by an N-terminal cap region. ABL1 possesses DNA-binding domain, nuclear localization signals (NLS), and a nuclear export signal (NES) at its C-terminus, contributing to its nucleocytoplasmic localization. On the other hand, ABL2 features microtubule and actin-binding domains at its C-terminus, enabling its localization at the cell periphery [119]. These domains located at the C-terminus of Abl tyrosine kinases are conserved regions rich in proline and these regions mediate protein-protein interactions [120] **(Figure 6).**

Alternative splicing of first exons produces a variety of ABL1 and ABL2 isoforms that contain different N-terminal sequences [121]. The 1b isoforms of both Abl kinases contain a myristoylated N-terminal glycine [121]. There are two groups of ATP-competitive inhibitors: type I inhibitors (dasatinib, bosutinib) targeting the active conformation of the kinase domain of Abl kinases, and type II inhibitors (imatinib, nilotinib, ponatinib) targeting the inactive conformation of the kinase domain [122].

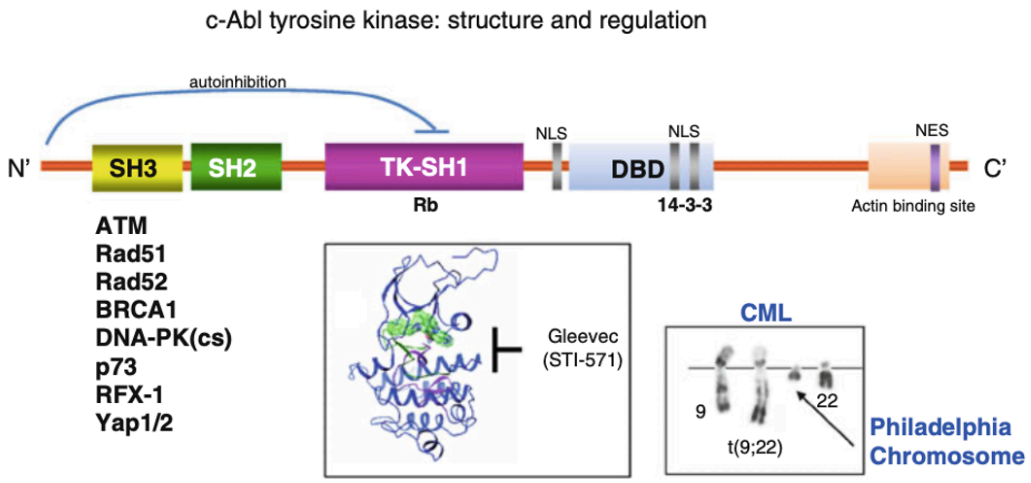

Figure 6: Schematic representation of c-Abl tyrosine kinase, its structure and regulation. (SH3) are denoted as SH1, SH2, and SH3, respectively. The presence of nuclear localization signals (NLS) and DNA binding domain (DBD) is indicated. Additionally, the nuclear export signal (NES) and actin binding sites are mentioned. The interaction between the c-Abl inhibitor and the c-Abl kinase domain is demonstrated by the construct STI-571. Furthermore, the translocation of BCR on chromosome 22, ABL on chromosome 9, and the resulting Philadelphia chromosome, which leads to chronic myeloid leukemia (CML), has been depicted [123].

Another significant evolutionarily conserved feature of the Abl kinase family is their ability to regulate cellular cytoskeletal dynamics [124]. Abl tyrosine kinase is involved in actin cytoskeleton reorganization, cell migration, invasion, and is activated by growth factors that stimulate receptor tyrosine kinases [125]. In the cell, Abl-dependent regulation of cytoskeletal dynamics involves the phosphorylation of nucleation-promoting actin, a crucial component of the cell membrane. Additionally, Abl targets proteins such as cortactin, which are essential for PDGF-induced dorsal membrane folds, and factors like N-WASP and WAVE that mediate protrusion [126]. Furthermore, cell surface receptors including Abl tyrosine kinases, integrins, cadherins, chemokine receptors, and the T cell receptor (TCR) play a significant role in regulating the cytoskeleton. Stimulation of these receptors triggers signaling pathways that modulate the cytoskeleton. Specifically, induced binding of integrins promotes the generation of membrane protrusions and facilitates the reorganization of focal adhesions and F-actin stress fibers, which are essential for the activation of Abl kinases [124]. Abl kinases are also activated in response to E-cadherin and N-cadherin [127,128]. Active Abl kinases play a crucial role in both the maintenance and remodeling of cadherin-dependent adherent junctions. The

simultaneous inactivation of both ABL1 and ABL2 has been shown to disrupt adherent junctions in fibroblasts and epithelial cells [128] **(Figure 7).**

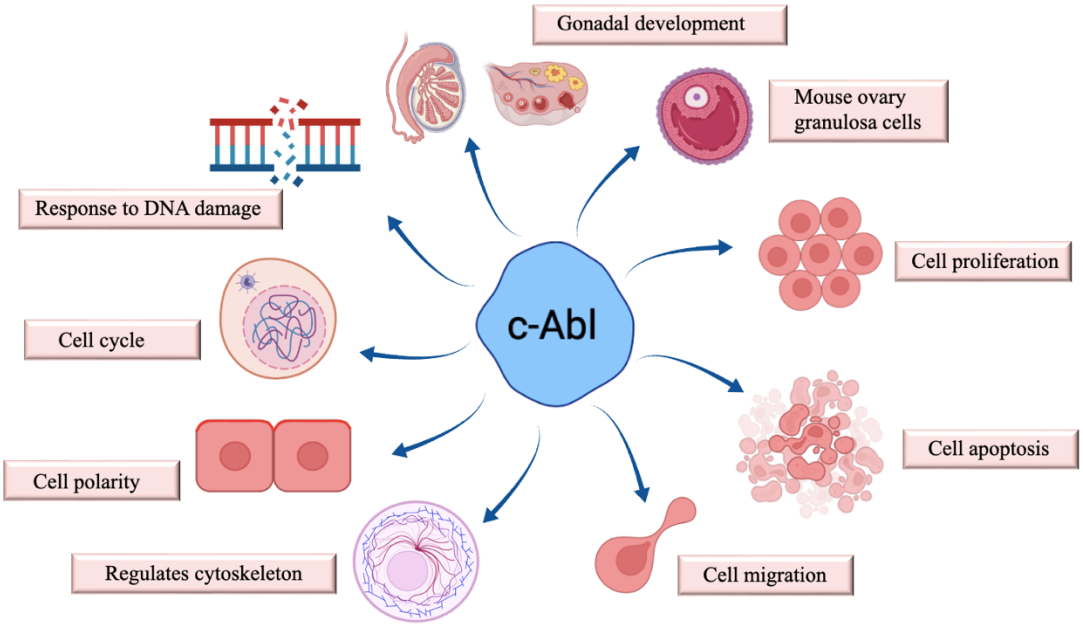

Figure 7: Roles of c-Abl Protein Tyrosine Kinase in cellular processes. c-Abl Protein Tyrosine Kinase plays a role in many processes such as gonadal development, cell proliferation, cell apoptosis, regulation and protection of the cytoskeletal structure of the cell, polarization and DNA repair mechanism.

2.3.2. Imatinib-mediated Inhibition of c-Abl

Imatinib (STI571, Gleevec/Glivec), the first identified inhibitor of c-Abl, is actively used in the treatment of CML [129-131]. In addition to inhibiting BCR-ABL, imatinib has been shown in *in vitro* animal studies to inhibit other tyrosine kinases such as KIT and platelet-derived growth factor receptor (PDGFR)-α/β [132,133]. The terminal elimination half-life of imatinib is 18 hours, and it binds to plasma proteins, primarily albumin and alpha-1 acid glycoprotein, to an extent of 95%. Its elimination from the body occurs predominantly via the biliary route as metabolites [134].

Tyrosine kinases are enzymes that cleave phosphorus from ATP and transfer it to the amino acid tyrosine. Indeed, imatinib, a tyrosine kinase inhibitor, specifically binds to the cleft formed between the N- and C-lobes of the kinase domain in Bcr-Abl. While there are differences between Bcr-Abl and c-Abl upstream of the SH3 domain, imatinib is expected to inhibit c-Abl as well, given that it targets the kinase domain shared by both proteins **(Figure 8)** [135]. The tyrosine kinase domain to which imatinib is specific is present

in the abl, c-kit, and PDGF-R-linked tyrosine kinase domains. There is Asp-Phe-Gly (DFG, D:Aspartate, F:Phenylephrine, G:Glycine) conformation in the activation region of Bcr-Abl-linked tyrosine kinase. This region is very close to the ATP binding site. The active state of tyrosine kinases is in the "DFG-in" conformation, and the inactive state is in the "DFG-out" conformation [136,137]. Imatinib binds to both the ATP binding site and the hydrophobic region formed in the DFG-out conformation, causing the enzyme to remain in the inactive conformation. This process can occur through 2 mechanisms; 1) Phosphorylation of the activation ring is dynamic and temporarily dephosphorylated. Thus, imatinib binds to the enzyme and its kinase activity decreases. 2) Imatinib binds to the newly synthesized bcr-abl kinase and prevents activation if it does not allow for phosphorylation and modification [138].

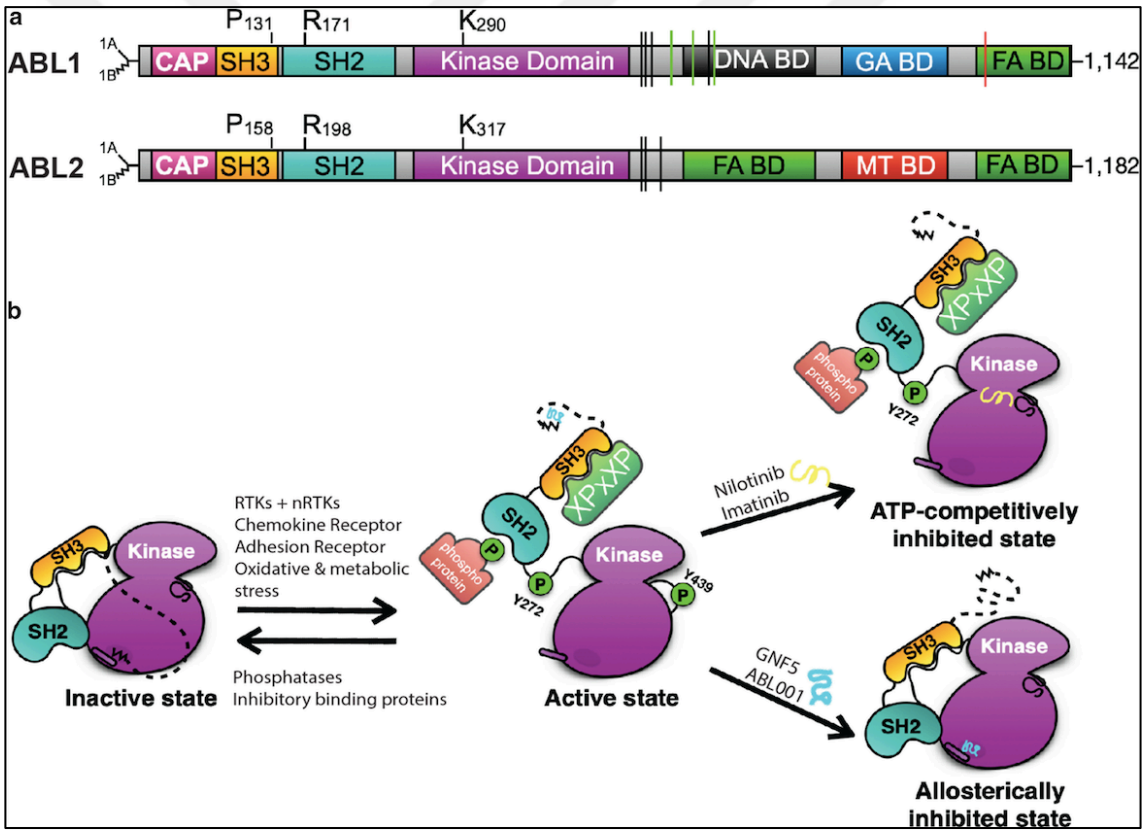

Figure 8: Demonstration of ABL structure and regions and regulation of ABL kinase activity. A. The figure shows the structural isoforms of ABL1 and ABL2. B. Inactive and active forms of ABL kinases and the mechanism that modulates ABL kinase activity are schematized [135].

There is tyrosine kinase activity of c-Abl, which is controlled in an organized manner in the cell, and stimuli that specifically activate cytoplasmic c-Abl are known [139]. While most of these stimuli cause very low to moderate levels of kinase stimulation, it is

also possible that c-Abl is kept in an inactive state due to intramolecular and intermolecular restrictions [140].

Current studies suggest that the SH3 domain, the proline-rich SH2-CAT linker, and its excess N-terminus, including the myristate group, are involved in keeping the kinase domain in a suppressed state. Inhibitory proteins that bind selectively to inactive c-Abl can also cause a repressed kinase conformation [141,142].

In a study with fibroblasts and neurons, it was shown that the number of microspikes and filopodia on cells increased via c-Abl. In addition, when these cells were treated with imatinib, an Abl kinase inhibitor, it was observed that the increase in the number of microspikes and filopodia was largely blocked [143,144]. In another study conducted in 2002, reductions in the number of filopodia were also showed in primary cultured embryonic cortical neurons treated with imatinib or neurons isolated from mice lacking c-Abl [145].

A decrease in primordial follicles and a rise in developing follicles were seen in a study with mice who had intraperitoneal imatinib treatment for 4 weeks [146]. This situation caused a decrease in ovarian reserve. In addition, preimplantation embryos obtained from mice with long-term exposure to imatinib were examined and a decrease in the quality of preimplantation embryos was observed [146]. It was determined that blastocysts obtained from embryos of mice exposed to long-term imatinib had significantly fewer cells compared to the control group [147].

Studies have shown that c-Abl activation induced by DNA damage antagonizes the oncogenic function of YAP by phosphorylating it from the Y357 site [9,148]. BCR/ABL activates the PI3K-AKT and MEK-ERK pathways and regulates YAP in both signaling pathways [149]. In a study with CML cell lines and CML patients, it was seen that pharmacological and genetic inhibition of YAP effectively suppressed cell proliferation. It was suggested that the cells induced cell cycle arrest in the G1 phase and also supported apoptosis in chronic myeloid leukemia (CML) cells. It was determined that after inhibition of BCR/ABL kinase activity with imatinib, the proteic level of YAP decreased [150].

Mechanisms affecting development as a result of imatinib exposure in preimplantation embryo development have not been clarified yet. In addition, its effect on critical stages in preimplantation embryo development was not detected. The effect of imatinib exposure on preimplantation embryo development is also unknown.

2.3.3. PDGF-AA-mediated Activation of c-Abl

Receptor tyrosine kinases (RTKs) comprise a family of cell surface receptors that bind extracellular ligands and initiate diverse signaling pathways, including the MAPK/ERK and PI3K pathways. They are commonly referred to as entry points into the cell, as they facilitate the integration of external signals and govern intracellular responses [151]. Receptor tyrosine kinases consist of several significant receptor subfamilies, such as FGFRs, EGFRs, VEGFRs and PDGFRs. These receptor families play critical roles in various biological processes, including embryonic development, angiogenesis, oncogenesis, and metabolism [152].

Ligand binding to platelet-derived growth factor (PDGF) and epidermal growth factor (EGF) receptors initiates their activation, which is then followed by dimerization and subsequent autophosphorylation [153]. The expression of a kinase-inactive Src or an SH3-domain mutant lacking the phosphorylation site of the PDGFβ receptor can inhibit PDGF-induced DNA synthesis. After stimulation by growth factors, Src kinases translocate to the plasma membrane, specifically to actin-rich regions [153]. Constitutively activated Src kinases exhibit localization to focal adhesions, and it is believed that they contribute to cytoskeletal reorganization, the focal adhesion cycle, and cell motility in this specific region where they are situated [153].

Plattner et al. showed that the membrane-localized pool of c-Abl is activated upon stimulation by growth factors. The activation of c-Abl in response to growth factors is mediated through the activation of Src kinases [154]. Studies have demonstrated that c-Abl activation in response to PDGF is partially reliant on the activity of Src tyrosine kinase. Apart from its role in cytoskeletal reorganization following PDGF stimulation, c-Abl also influences the transition of quiescent cells into the S phase of the cell cycle. Activation of Abl kinases can occur through interactions with cell adhesion molecules and receptor tyrosine kinases in various cell types. These activated Abl kinases initiate signaling cascades that impact membrane-bound receptors, thereby influencing cell morphology and motility [154].

PDGFRα was first detected in cells at the morula, and then it was determined as one of the identifiers of the PrE cell line in blastocysts [155]. While *Pdgfra*-deficient preimplantation embryos did not present a severe phenotype at the developmental stages, Pdgfra mutant blastocysts had significantly fewer PrE cells compared to WT embryos [156,157]. It was also shown that cell specification and sequencing were not affected despite increased cell death [157]. Pdgfra expression has been reported to be necessary for the

survival of PrE (primitive endoderm) cells but is not involved in the determination of PrE fate. The regulation of Pdgfra expression is attributed to the transcription factor GATA6 [157]. Although the presence of PDGF-A among the 4 types of PDGF ligands identified in mammals has been reported, its clear role in preimplantation embryo developmental stages has not been determined.

The catalytic domain of c-Abl encompasses the activation site found in all tyrosine kinases. Interestingly, a conserved tyrosine residue within the catalytic domain, Y412, is phosphorylated in oncogenic forms of Abl, including ΔSH3-Abl, Abl-P131L, Bcr-Abl, and v-Abl [158-160]. This phosphorylation is characterized by an increase in catalytic activity like the phosphorylation seen in tyrosine kinases [161].

Mutation of phenylalanine at the Y412 region regulates the activation of c-Abl by Src kinases. On the other hand, mutation of the Y412F region does not impede the autoactivation of c-Abl, suggesting that phosphorylation of other tyrosine residues might be involved in its autoactivation. Phosphorylation of Y245 or other tyrosine residues is considered to potentially contribute to the autoactivation of c-Abl tyrosine kinase [161]. In this context, it is suggested that phosphorylation of Y245 or other tyrosine residues could potentially contribute to the autoactivation of c-Abl kinase. Interestingly, while phosphotyrosine (pY) is readily detectable *in vivo* in oncogenic Abl kinases, it has not been detected endogenously on the c-Abl protein when its catalytic activity is enhanced [162]. This indicates that other mechanisms or phosphorylation events might be responsible for the activation of c-Abl in such cases. Phosphorylated c-Abl becomes detectable when cells are co-stimulated with PDGF and pervanadate (a phosphatase inhibitor, which itself can increase phosphotyrosine on c-Abl). Although phosphorylation at Y412 is required to achieve maximal c-Abl activity, it is possible to gradually reach levels of kinase activation. Disruption of the Inactive conformation of Abl can be achieved by displacement of the N-terminus, SH3 or SH2 domains [142,162]. Association of substrates with the SH3 or SH2 domain of c-Abl can increase in situ catalytic activity to induce substrate phosphorylation without the need for Y412 phosphorylation [163].

In a study conducted using NIH3T3 cells expressing the c-Abl biosensor, it was demonstrated that PDGF stimulation resulted in the accumulation of substantial c-Abl activity in the membrane ruffles of the cells. These findings are in line with the notion that c-Abl exhibits high dynamics within actin structures and that PDGF-induced stimulation leads to the activation of membrane-localized c-Abl [154,164]. Live imaging studies have revealed that c-Abl activity is particularly high in membrane protrusions,

notably at the tips of lamellipodia and filopodia [145,165]. However, in immunofluorescence staining with fixed cells, c-Abl was determined to be localized within membrane protrusions [166].

2.3.4. YAP Phosphorylation by c-Abl and Association with p73

c-Abl is a shuttle protein that can translocates between the nucleus and cytoplasm, and phosphorylation of c-Abl at T735 by TTK/Mps1 generates a binding site for 14-3-3 proteins [167]. After the formation of this binding site, c-Abl is localized in the cytoplasm [168]. The cytoplasmic localization of c-Abl is regulated by the phosphorylation of T735, which is situated between the second and third nuclear localization signals (NLS) of c-Abl. The binding of 14-3-3 proteins to c-Abl masks the NLSs, potentially preventing the nuclear localization of c-Abl [168]. In the event of DNA damage, activation of JNK triggers the phosphorylation of 14-3-3 proteins, leading to the dissociation of 14-3-3 from c-Abl. This release of 14-3-3 allows for the nuclear localization of c-Abl [168]. While it is known that the binding of YAP and TAZ to 14-3-3 proteins leads to their cytoplasmic localization, it remains unclear whether JNK phosphorylation, triggered by 14-3-3 binding, facilitates the nuclear localization of YAP and TAZ [169].

DNA damage and c-Abl function as negative regulators of TEAD coactivation by YAP. Furthermore, c-Abl is activated in response to DNA damage and phosphorylates YAP at Y357 (pY357) residue [9,148]. YAP pY357 shows a direct correlation with p73 in the process of targeting proapoptotic genes. It is known that YAP-TEAD target genes are expressed at low levels in response to DNA damage, and this inhibitory effect is triggered by c-Abl activation [148]. YAP-p73 complex formation and subsequent transcription are enhanced by c-ABL [170]. In multiple myeloma, *Yap* was deleted or consistently downregulated to avoid apoptosis despite extensive DNA damage [170]. c-Abl is activated in response to DNA damage and then phosphorylates YAP on residue Y357 [9]. The YAP complex, specifically phosphorylated at Y357, localizes to the nucleus. Within the nucleus, YAP interacts with p73 and facilitates the activation of proapoptotic genes (BAX and PIG3, etc.) [9,148]. c-Abl-mediated phosphorylation of YAP triggers the cleavage of other YAP complexes, which potentially aids in the formation of the YAP-p73 complex. Thus, c-Abl determines the complex to which YAP will bind by controlling its phosphorylation state [171] **(Figure 9).** c-Abl plays a pivotal role in mediating the oncogenic and tumor-suppressive functions of YAP [172].

Certain control mechanisms are in place for the proper completion of the cell cycle period and the preservation of genome integrity, and these control mechanisms are called 'cell cycle checkpoints'. Numerous proteins have crucial roles in regulating these checkpoints. Among them, the tumor suppressor p53 stands out as a checkpoint protein that halts the cell cycle upon encountering DNA damage induced by ultraviolet radiation, ionizing radiation (IR), or radiomimetic chemicals [173]. In a study with c-Abl-null fibroblasts, it was shown that Cdk2 is downregulated and their capacity to arrest at G1 phase in response to IR is impaired [174,175]. In contrast, overexpression of an activated form of c-Abl in wild-type cells suppresses cell growth and induces G1 arrest [176]. However, it has been reported that cells assumed to have lower amounts of endogenous c-Abl show a shorter G1/S transition [177]. As a member of the p53 gene family, p73 has been identified to directly interact with c-Abl. However, unlike p53, p73 undergoes phosphorylation by c-Abl [178]. The potential of p73 to induce G1 arrest upon c-Abl activation is yet to be determined. However, the ability of p73 to induce p21 expression aligns with the possibility of p73 contributing to G1 arrest [99].

The p73 genes from the p53 family have domains with a transactivation site (TA) at their amino terminus and a DNA field at their amino terminus, allowing the production of a large number of proteins [179]. p73 can bind promoters and regulate the expression of some of the same genes to elicit results similar to p53 when activated; However, the regulatory mechanisms of this process can vary, particularly in terms of upstream signaling. One of the key differences lies in the binding of YAP to different kinases [180]. p73 plays a role in many processes such as neuronal signaling, immune cell apoptosis and inflammation during development [179]. Furthermore, p73 was found to be activated by the non-receptor tyrosine kinase c-Abl, inducing apoptosis in response to DNA damage [8]. A study of p73 KO mice noted that the epithelial phenotype was affected (histological defects in the oviduct epithelium, middle ear mucosal epithelium, sinus, bronchiole, and ciliation in the trachea [181].

YAP is a critical factor that regulates the functions of p73. YAP regulates transcriptional activity and cell death induction by binding to p73 [180,182]. In addition, YAP stabilizes the p73 protein in a post-translational manner [183].

It is established that in response to DNA damage, YAP activates p73-mediated transcription of pro-apoptotic genes, and this process is facilitated by the involvement of c-Abl [148]. There is also an increased association between YAP p-Y345 and p73 in targeting proapoptotic genes. YAP-TEAD target gene expression weakens following

DNA damage. However, c-Abl can prevent the attenuation of this effect. While it is well-established that c-Abl is activated in response to DNA damage, phosphorylates p73 and YAP, leading to the transcription of pro-apoptotic genes, the involvement of the c-Abl/YAP/p73 mechanism in embryonic development has not yet been addressed or explored. In our study; After determining the role of c-Abl at the preimplantation embryo development, it was aimed to evaluate the c-Abl/YAP/p73 cascade in the case of PDGF-AA and imatinib treatment.

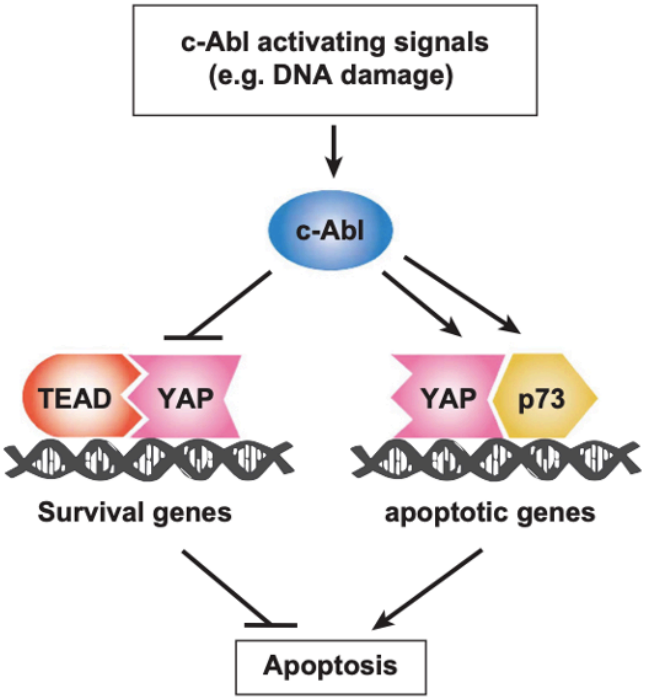

Figure 9: In the presence of DNA damage, YAP triggers p73-mediated apoptosis through the involvement of c-Abl. Activation of c-Abl occurs in response to DNA damage, causing p73 and YAP to be phosphorylated. These formations lead to transcription of proapoptotic genes induced by YAP-p73. In addition, phosphorylation of YAP by c-Abl inhibits the activation of the YAP-TEAD' complex, suppressing the expression of anti-apoptotic genes and promoting apoptosis [148].

2.3.5. The Role of c-Abl Tyrosine Kinase: A Journey Across Germ Cells to the Fertilization

The expression level, localization, and role of c-Abl tyrosine kinase have been demonstrated in various somatic tissues. Abl is also highly important for embryonic development. Deletion of the binding domains, HLB-A and HLB-3, from the C-terminus region of the Abl gene leads to various developmental defects, including morbidity [184]. It has been observed that Abl2 KO mice are healthy and fertile. However, simultaneous deletion of both Abl1 and Abl2 results in prenatal death on embryonic days 8 and 9 [184,185]. It is known that the observed death in cases where Abl1/2 are knocked out together is due to defects in neurulation during early developmental stages. The Abl family of tyrosine kinases is also essential for basal membrane integrity and cortical laminar formation in the cerebellum [186]. Additionally, the role of c-Abl tyrosine kinase has been extensively investigated in many fetal and adult healthy and cancerous somatic tissues. However, somatic cells and germ cells have different signaling mechanisms. Germ cells have developed unique mechanisms compared to somatic cells in order to ensure the transmission of healthy genetic material to the next generation in response to potential DNA damage. Unlike somatic cells, germ cells undergo meiotic division instead of mitotic division, and meiotic division also differs between female and male germ cells. Double-strand break (DSB) formation occurs during meiotic division, and DSBs in meiosis promote various events such as recombination and the formation of the synaptonemal complex [187].

The *Abl* gene has been conserved throughout evolution, and orthologous genes associated with Abl have been identified in the genomes of diverse organisms, including *Drosophila melanogaster*, *C. elegans*, and several others [188-190]. Dash is the c-Abl homolog found in *Drosophila*. It has been detected as a maternal mRNA in the unfertilized eggs of *Drosophila*, but it is not detected in embryonic larvae or adult RNA [191]. In sea urchins, active Abl kinase has been shown to localize in the actin layer of the egg cortex following fertilization [192]. When investigating the role of Abl in Xenopus oocytes, it has been shown to be involved in progesterone-mediated oocyte maturation [193]. In a study conducted by Rawe and colleagues, Abl kinase was identified in close association with actin in the pronuclei of bovine zygotes [194]. In studies, lethality was observed in c-Abl homozygous mutant mice at E 13.5 days. It has also been suggested that subfertility and defects in embryonic development may occurs [195,196].

In a study conducted in 2003, it was shown that c-Abl is expressed in the human ovarian surface epithelium [197]. In another study, it was reported that c-Abl is expressed in the surface epithelium of 4 different ovarian serous carcinoma tissues, while its expression was not observed in the stroma and follicles [198]. In 1993, the presence of c-Abl was demonstrated in the gonads of adult female and male mice. It was reported that c-Abl is expressed in both female and male gonadal cells, but with different expression patterns. In the testes, c-Abl mRNA levels have been found to be high from the round spermatid to the elongated spermatid. These observations suggest that c-Abl may have a significant role in male gonads, particularly during the haploid stages and fertilization following completion of meiotic division [199]. In the same study, c-Abl was detected in oocytes during the meiotic prophase in ovarian tissue [199]. The presence of c-Abl was demonstrated in human sperm cells. It was reported that c-Abl is predominantly found in the acrosomal region and localized in the same region in capacitated and non-capacitated sperm [200]. It has been shown that Abl directly interacts with meiotic chromosomes in the testes of mice and rats [201]. Meiotic crossing-over occurs during the pachytene, which is the stage with the highest expression of Abl. It has been shown that mice lacking Abl exhibit defects in spermatogenesis [202,203]. In our study, we demonstrated that the expression of c-Abl, starting from the ectoplacental cone, plays an important role in vascularization of the fetal portion in the third-trimester placenta in mice [7]. In our previous studies, we demonstrated the expression of c-Abl in mouse granulosa cells. Additionally, we determined that silencing c-Abl through siRNA transfection resulted in a decrease in mTERT expression [204]. We identified the expression of c-Abl tyrosine kinase in various stages of gonadal development, including E10.5, E11.5, E12.5, E13.5, as well as postnatal stages at 1, 3, 5, 7, and adulthood. These findings suggest a potential involvement of c-Abl in gonadal development [205]. DNA-damaging drugs activate the c-Abl/TAP63 pathway in cells. Suppression of Abl kinase activity through imatinib-mediated inhibition exhibits a protective effect on oocyte health following chemotherapy treatment. This indicates the potential role of Abl activity in fertility preservation [206]. Based on observations from c-Abl KO models, it is evident that c-Abl, a tyrosine kinase, serves crucial functions in embryonic development and implantation. All these studies suggest that the c-Abl mechanism may be effective in the growth and differentiation of the embryo, starting from much earlier stages of embryonic development. Although the localization of c-Abl tyrosine kinase in the preimplantation period of embryonic development has been demonstrated [207] there is currently no study in the literature that

specifically elucidates its functional role in early embryonic development. When considering these studies together, it can be said that Abl plays a significant role in preserving genomic integrity by being involved in DNA breaks in both germ cells undergoing meiotic division and somatic cells undergoing mitotic division. However, how the role of c-Abl tyrosine kinase in germ cells is transmitted to preimplantation stage embryos remains unclear.

While previous studies have demonstrated the association between c-Abl and YAP in various cell lines, there is currently a lack of literature regarding the regulatory role of c-Abl on YAP in preimplantation embryonic development in mice and its potential involvement in determining cell fate. What are the mechanisms dictating the control of c-Abl tyrosine kinase during the developmental process of preimplantation embryos? In our proposed study, we hypothesize that c-Abl, whose role in preimplantation embryo development is not yet clearly understood, may be a key factor in determining the fate of TE cells by interacting with YAP. Considering the potential ability of PDGF-AA treatment and imatinib treatment to modify the cellular localization of YAP, it raises the question of whether c-Abl could play a pivotal role in preimplantation embryonal development. Furthermore, could c-Abl tyrosine kinase regulation also play a role in other crucial events that determine cell fate, such as polarization, compaction, and translation of distinct markers in TE and ICM cells? If the c-Abl regulation lead to changes in polarization, compaction, and transcriptional and translational modifications of cell-specific markers, it could shed light on the mechanisms underlying its involvement in preimplantation embryo development and cell fate determination.

3. MATERIALS and METHODS

3.1. Experimental Animal Ethics Statements

The Yeditepe University Faculty of Medicine Experimental Research Center (YUDETAM) provided all of the animals used in the present study and all experimental protocols were conducted in accordance with the approval of the Yeditepe University Ethical Committee, protocol number: 2020/859, 2020/08-6. All procedures were carried out under the supervision of veterinarians. All experiments were performed in accordance with guidelines and regulations of Faculty of Medicine of Yeditepe University. 6 week old C57BL6 female mice were used fort this study.

3.2. Superovulation

6-8 week old C57BL6 female mice were superovulated. 7,5 IU of Pregnant Mare Serum Gonadotropin (PMSG) (BioVender, #RP17827210000) was given intraperitoneally to induce follicular development in the ovaries, and then 7,5 IU of Human Chorionic Gonadotropin (hCG) (Sigma, #CG10-10VL) to induce ovulation 48 hours later, intraperitoneally and hCG injection was administered (Figure 10). Then placed in the same cage with male mice. Animals with vaginal plaque or sperm on the vaginal smear the next day were considered mated.

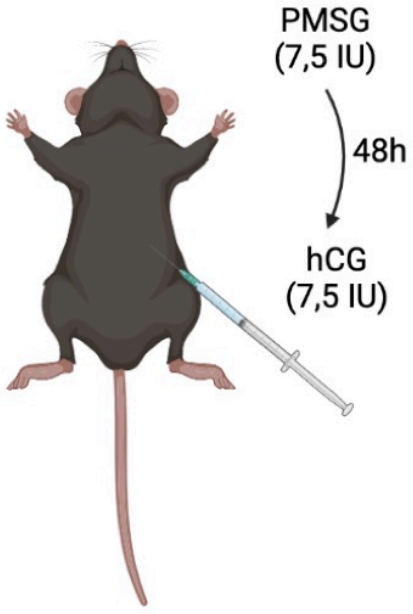

Figure 10: Superovulation of C57BL6 female mice at 6 weeks.

3.3. Collection and Culture of Mouse Preimplantation Embryos

20 hours after hCG injection, zygotes were collected from oviduct and cultured in KSOM+AA (Sigma, #MR-106-D) embryo incubation medium at 5% CO_2, 5% O_2 , 37 ºC (phcbi, #MCO-170M) [208]. The oviduct dissection and the retrieval of embryos from the oviduct were performed in HEPES (Thermo, #12340030) medium previously heated to 37 ºC. We cutted above the oviducts, below the ovaries, placed on a petri dish and covered with HEPES. We used a fine mouth controlled pipette for embryo collection and made microdrops of KSOM on the 35mm dish and cover with mineral oil. Placed embryos in the microdrops. Embryos were developed from the zygote to the blastocyst (Figure 11). The embryo culture medium was changed every 2 days. Morphological evaluation was followed by examination under the microscope (Zeiss, Axio Observer).

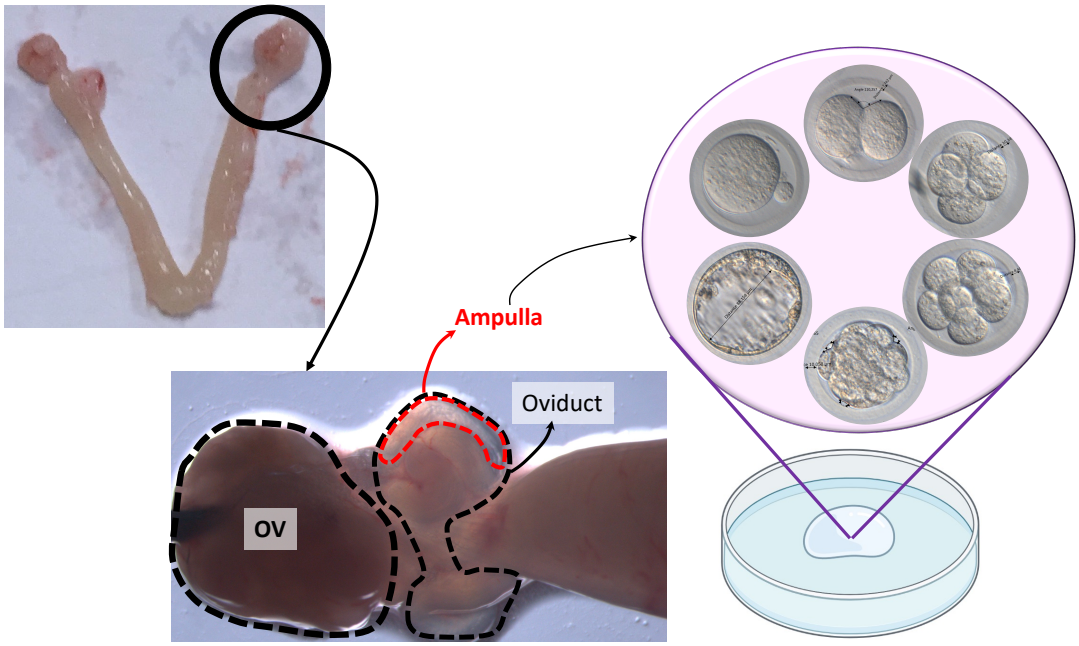

Figure 11: Collection and culture of mouse preimplantation embryos.

3.4. Treatment with PDGF-AA and imatinib

Zygotes were treated with PDGF-AA and imatinib. After the appropriate doses for PDGF-AA Platelet Derived Growth Factor-AA (PDGF-AA) (Sigma, #SRP3228-10UG) (Diluated in 1% BSA + PBS, KSOM+AA,Sigma, #MR-106-D) were determined as 20 ng/ml and 50 ng/ml groups were formed [154]. Treatment groups with PDGF-AA were repeated 14 times for immunofluorescence and qRT-PCR evaluations. Initial trials for

imatinib treatment (BioVision, #1625-1000) (diluated in DMSO+ KSOM+AA, Sigma, #MR-106-D) tested doses of 10 µM, 20 µM, and 50 µM. However, the embryos did not develop to blastocyst. Since the embryos were arrested at high doses, the study was continued with 1 and 5 µM imatinib treatment [9,209]. Treatment groups with imatinib were repeated 18 times for immunofluorescence and qRT-PCR evaluations. Embryos were incubated at 5% CO_2, 5% O_2 at 37ºC until the blastocyst (day 5). The morphological control of the embryos was followed by imaging under the microscope. Embryos were used to perform immunofluorescence staining and qRT-PCR techniques.

3.5. siRNA microinjection

Abl non-receptor tyrosine kinase (Abl1), transcript variant 5, mRNA; 3 unique 27mer siRNA duplexes (Locus-NM_001283047) (ON-TARGETplus Mouse *Abl1* siRNA, mouse, Horizon, #AI32509) were used for c-Abl [210]. This region silences *c-Abl* from the SH3 region. The SH3 domain of c-Abl is small protein modules containing about 50 amino acid residues found in intracellular or membrane-associated proteins. The SH2 domain of c-Abl binds directly to the C-terminal, while SH3-SH2 rigidity is involved in autoinhibition. This rigidity affects the N-terminal via the SH3 domain [137,211].

Microinjection was performed in KSOM medium using a Zeiss Axio Observer inverted microscope equipped with a Narishige (#IM94, #MMO-4, #IM-11-2, #MM94B, #MM-94) micromanipulator. A volume of 200 nl siRNA (10µM/µl) was microinjected into the cytoplasm of zygotes using a ICSI micropipettes, 6-7 um, Spike, 30 angle (Origio, HUM-MIC-SLM-30-B1.0) and holding pipette (Cooper surgical, #HUM-MPH-MED-30). The siRNA used is used with the 10 µM GFP labeled indicator (Dharmacon, siGLO Green Indicator, #D-001630-01-50). The same concentration and volume of Scrambled control pool was injected as control in all experiments (Figure 12). After microinjection, zygotes were washed with KSOM and cultured in KSOM medium at 37 °C in a humidified atmosphere at 5% CO_2, 5% O_2 at 37ºC. siRNA microinjection groups were repeated 3 times for qRT-PCR evaluation.

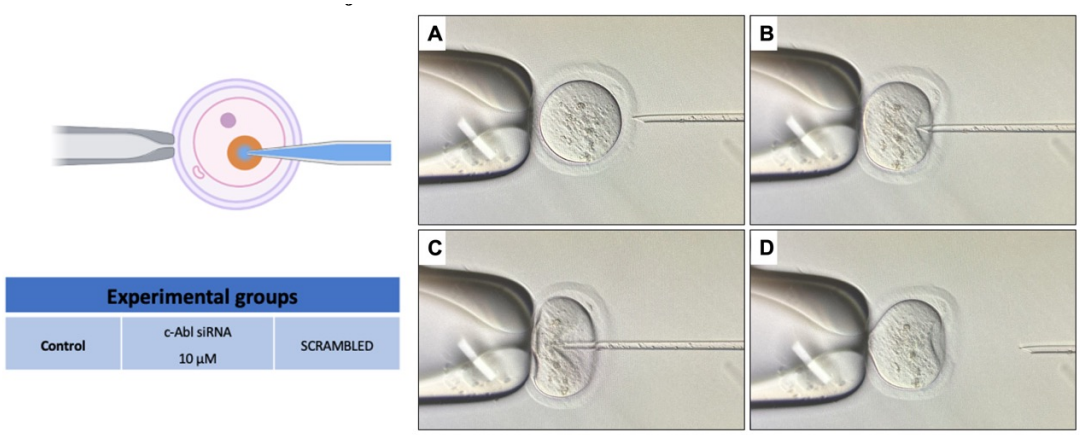

Figure 12: *c-Abl* siRNA schematic representation and Axio microscope images of the microinjection into the zygote.

3.6. Morphological Evaluation at Different Preimplantation Embryo Stages

Morphological evaluation was followed by examination under the microscope (Zeiss, Axio Observer). We conducted morphological evaluation of both the PDGF-AA treatment, imatinib treatment and siRNA microinjection targeting *c-Abl* groups. Experimental groups are given in the table below.

Table 1: Experimental groups design, used PDGF-AA, imatinib and siRNA microinjection are shown in the table.

Experimental groups			
PDGF-AA Groups	Control	20 ng/mL PDGF-AA	50 ng/mL PDGF-AA
Imatinib Groups	Control	1 µM imatinib	5 µM imatinib
c-Abl siRNA Microinjection Group	Control	SCRAMBLED	c-Abl siRNA

Morphological and morphokinetic assessments were performed considering specific criteria based on the literature, including studies by Weinerman et al. and Desai et. al. [212,213]. The evaluated criteria were as follows:

- Time of appearance of both pronuclei
- Perivitelline space and ZP characteristics
- Duration of the first embryonic cell cycle (transition to the 2-cell)
- Duration of the second embryonic cell cycle (transition to the 4-cell)
- Duration of the third embryonic cell cycle (transition to the 8-cell)
- Number of blastomeres
- Cytoplasmic effects
- Multinucleation

In addition to these criteria, some evaluations were conducted to enable quantitative comparisons between the groups using with ZEN Blue. These evaluations included: Measurement of ZP thickness in zygote, 2-cell, 4-cell, 8-cell embryo and morula.

- Measurement of the angle between two blastomeres at the 2-cell embryo.
- Assessment of compactness level by measuring the angle of compaction between blastomeres at the morula.
- Measurement of the blastocoel cavity at the blastocyst.

3.6.1. ZP thickness measurement

The ZP of each embryo was subjected to measurements made at usually made at the average looking site **(Figure 13A)**. The data collection was performed prospectively and independently of embryo selection. ZP thickness measurement was made with Zeiss ZEN Blue software and measured in micrometers [214].

3.6.2. Measurement of Angle between two blastomeres at the 2-cell embryo

Vector angle was used to evaluate the angle between the 2 blastomeres from the non-contact perivitelline space of the 2-cell embryo **(Figure 13B)**. While the central junction of the vector angle was at the part where the 2 blastomeres were in contact, the measurement was made with the free ends extending towards the apical part of the 2 blastomeres separately. [90,215]. Angle between 2 blastomeres measurements was made with Zeiss ZEN Blue software.

3.6.3. Measurement the angle of compaction between blastomeres at the morula

Vector angle was used to evaluate the angle between the 2 blastomeres from the non-contact perivitelline space of the morula **(Figure 13C)**. Morula is the embryonal stage in which the cell boundaries between the blastomeres cannot be distinguished and the free surface angle between the blastomeres increases [90]. The contact surfaces at which the interblastomere angle was maximized were measured. Angle measurements were made for 3 different areas from each morula.

3.6.4. Measurement of the blastocoel cavity area

During the measurement of the blastocoele cavity, the measurement was made from the area towards the TE cells by the ICM cells. Maximum cross-sectional axes of blastocysts were measured and averaged [216]. Each line on the measurement scale was represented in μm **(Figure 13D).**

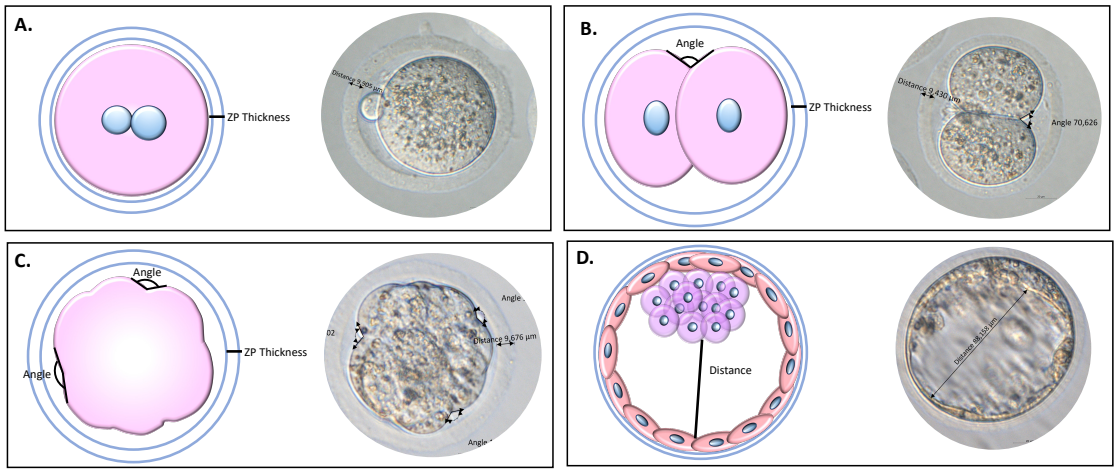

Figure 13: Schematic diagram of the parameters measured during embryo morphokinetic evaluation. A. ZP thickness measurement for zygote. B. ZP thickness measurement and angle between two blastomeres for 2-cell embryo. C. ZP thickness measurement and angle between two blastomeres for morula. D. blastocoel cavity distance for blastocyst.

3.7. Measuring Individual Blastomeres Areas of Blastocyst.

We used for ImageJ/FIJI program for measurment of cell area. First, we draw a line between two points of known distance and set scale. We choosed the first four buttons on the tool bar to surround an area on the image with a freehand shape. After selection, these areas analyzed. Images with E-cadherin immunofluorescence staining applied to blastocysts were used to calculate the blastomer area. (Figure 14).

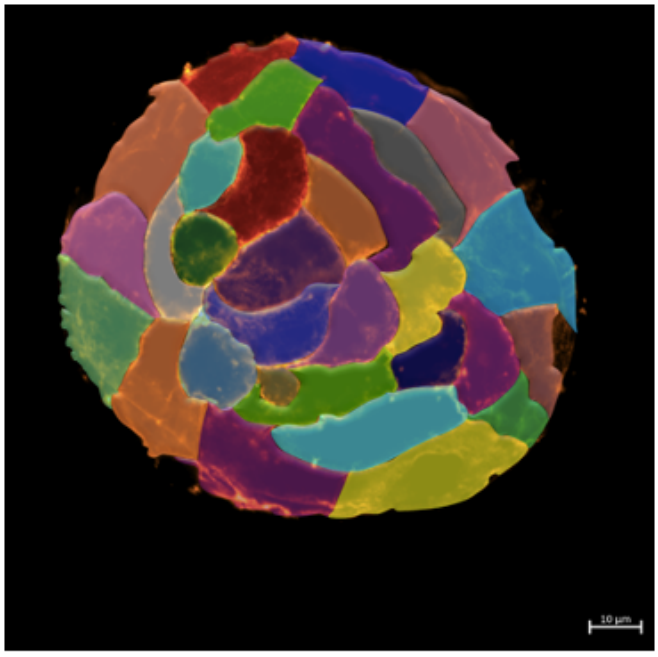

Figure 14: The graphic shows the measurement of the cell area in the blastomeres at the blastocyst.

3.8. Calculate the Number of Nucleus and Area of Nucleus in Blastocyst

We used for ImageJ/FIJI program for calculate the number of nucleus and area of nucleus in blastocyte. First, we converted the image to 8-bit grayscale and then 'threshold' the image. We choosen Analyze Particles, toggled 'show outlines' and checked ‘Display Results’. Selected OK and each counted nucleus outlined and numbered in a new window. Cell nucleus count and cell nucleus area measurement were calculated from 10 different embryos for each group.

3.9. Analysis of Apoptotic Bodies in the Preimplantation Embryo

We used for ImageJ/FIJI program for calculate the apoptotic bodies number in preimplantation embryo. First, we converted the image to 8-bit grayscale and then 'threshold' the image. We choosen Analyze Particles, toggled 'show outlines' and checked ‘Display Results’. Selected OK and each apoptotic bodies numbered in a new window. Apoptotic bodies numbers were calculated from 10 different embryos for each group. Apoptotic bodies were calculated from 10 different embryos for each group. Each apoptotic bodies idicated with oranged dots (Figure 15).

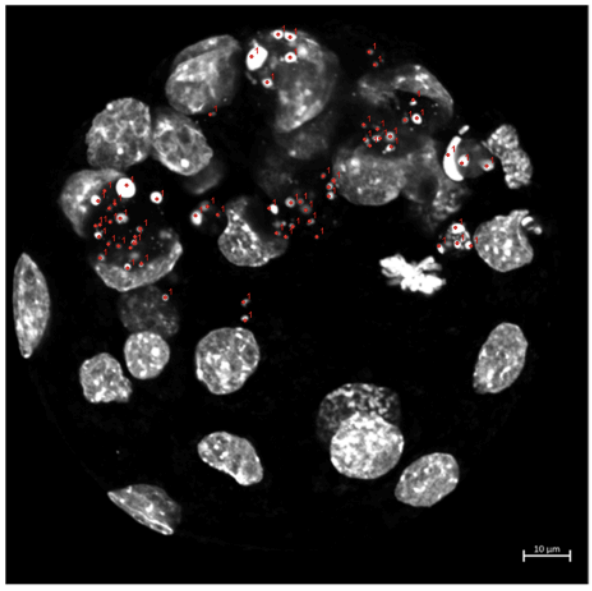

Figure 15: Detection of apoptotic bodies in mouse preimplantation embryos.

3.10. Immunofluorescence staining and analysis

The following antibodies were used to show how PDGF-AA and imatinib treatments used for c-Abl localization of proteins involved in the differentiation of inner cell mass and trophectoderm in blastocyst embryos in experimental groups. All antibodies used in this study are listed in Table 2.

Table 2: Primary and secondary antibodies used in the study

Primary Antibody List		
Name of antibody	Catalog number	Dilution
YAP	Cell Signalling, #1A12-12395	1:100
p-YAPY357	Invitrogen, #711259	1:100
c-Abl	Abcam, #ab15130	1:100
p-c-Abl (Tyr393)	Cell Signaling, #3671	1:100
NANOG	Abcam, #ab80892	1:100
p73	Cell Signaling, #14620S	1:100
TEAD4	Abcam, #ab97460	1:100
CDX2	Biogenex, #MU392-UC	1:100
PARD6	Invitrogen, #PA3-911	1:100
E-cadherin	Thermo Fisher Scientific, #13-1900	1:100
Goat Anti-Rat IgG H&L (Alexa Fluor® 647) preadsorbed	Abcam, #ab150167	1:750
Donkey Anti-Sheep IgG NorthernLights™ NL637-conjugated Antibody	R&D systems a biotechne brand, #NL011	1:750
Goat Anti-Mouse IgG H&L (Alexa Fluor® 568)	Abcam, #ab175473	1:750
Goat Anti-Rabbit IgG H&L (Alexa Fluor® 488)	Abcam, #ab150077	1:750
Donkey Anti-Goat IgG H&L (Alexa Fluor® 647)	Abcam, #ab150131	1:750

Immunofluorescence staining protocol:

- Isolated embryos were placed in KSOM medium
- Washed 3 times with 1% Bovine Serum Albumin (BSA) (Sigma, #A9418). (BSA diluted in distilled water)

- Incubated with 4% Paraformaldehyde (PFA) (Sigma, 158127) (for 20 min at room temperature for fixation. PFA is prepared in Phosphate buffered saline (PBS) (Sigma, #P4417-100TAB).
- After fixation, washing with 1% BSA was performed again.
- Permeabilization procedure is applied to the fixed embryos with 2% BSA+Triton-X (Merck, #112298). This process is carried out at room temperature for 1 hour and after 1 hour the embryos are washed again.
- Embryos were then incubated in primary antibody overnight at +4°C.
- Following primary antibody incubation, embryos were incubated with secondary antibody prepared in 1% BSA-PBS containing 0.01% Tween-20 (Merck, #822184.0500) for 1.5 hours at room temperature.
- Droplets was created with DAPI mounting medium (Sigma, F6057) for nucleus staining, and after embryos were placed in this droplet, imaging was performed under a confocal microscope. All images were acquired using a Zeiss confocal microscope (Zeiss, LSM700). We used 63X objextive with oil, 1024x1024 frame size, 8 avareged number ve best signal (Figure 16). All analyses were carried out using open-source image analysis software 'Fiji'.

Fluorescence intensity analysis was performed on images taken under a laser scanning confocal microscope. Images were taken as a Z-stack and the slice with the clearest visibility was selected. Fluorescence intensity was then measured by histogram analysis using ImageJ/FIJI software. After selecting each antibody image area, the average of the histogram mean values measured in the program was calculated.

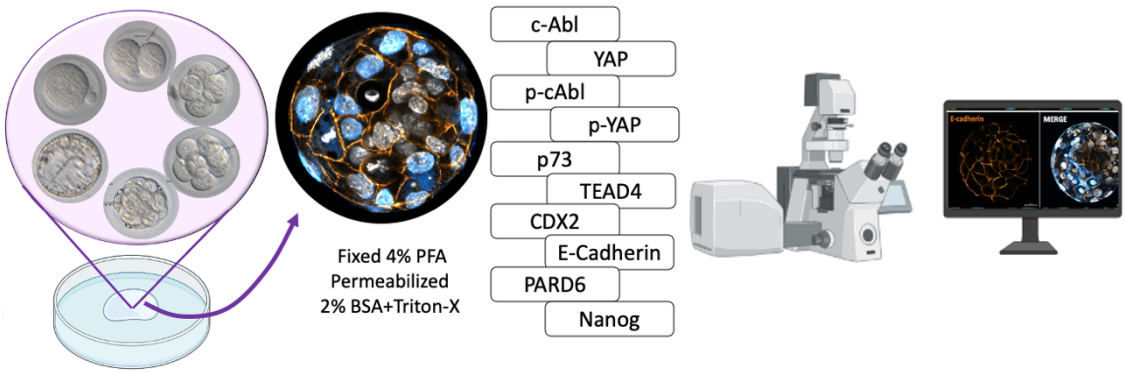

Figure 16: Immunofluorescence staining and imaging were schematized.

3.11. Quantitative Real-Time Polymerase Chain Reaction (qRT-PCR) and Analysis

The Real Time Polymerase Chain Reaction was used to reveal the relationship between *c-Abl* and *Yap* in the process of cell fate determination in early embryonic development. About 25 embryos were used for all experimental groups. Embryos were homogenized in 100 µl lysis buffer. After homogenization, the samples were transferred to filter tubes and RNA isolation and cDNA were obtained. After the cDNA synthesis process was completed, the samples were stored at -20°C. *c-Abl, Yap, Tead, Cdx2, Oct4, Nanog* genes will be determined at the mRNA level by using cDNAs obtained from the samples, SYBR Green Master mix and the primers specified in Table 2. *β-Actin* will be used as control. The data to be obtained were calculated as suggested by the kit and statistically evaluated **(Figure 17).**

Total RNA Purification Kit-Column Kit, (#PP210S), Jena Bioscience
Preparation of contents

1. Lysis Buffer: For 1 ml of lysis buffer before use, add 10 µl of 2-Mercaptoethanol.
2. First Washing Buffer: 8 ml of 100% ethanol is added to 32 ml of First Washing Buffer.
3. Second Washing Buffer: Add 32 ml of 100% ethanol to 8 ml of Second Washing Buffer.

RNA isolation.

1. Samples were placed in 50 µl Lysis Buffer
2. 2-propanol was added to the samples at 0.6 times the amount of Lysis Buffer it contained (60 µl was added).
3. The filtered column and 2 ml eppendorfs from the kit were prepared. 100 µl activation buffer was added to the filters.
4. It was centrifuged for 30 seconds at 10,000 g. Then the part under the eppenforf discard the flow-through.
5. After adding 2-propanol to the samples, they were transferred to the column. Centrifuged for 30 seconds at 10,000 g. Then the part under the eppenforf discard the flow-through.
6. Added 700 µl first washing buffer on the column. Centrifuged for 30 seconds at 10,000 g. Then the part under the eppenforf discard the flow-through.
7. Added 700 µl second washing buffer on the column.

8. Centrifuged for 30 seconds at 10,000 g. Then the part under the eppenforf discard the flow-through.
9. After the eppendorf was flow-through, the empty eppendorf and column were centrifuged again at 10,000 g for 2 min (to remove any remaining alcohol in the filter).
10. The column is transferred to DNase/RNase-free eppendorf.
11. Added 40 µl elution buffer on it.
12. Incubated for 1 min at room temperature.
13. Centrifuged at 10,000 g for 1 min and obtained RNA was stored at -20 °C.

Obtaining cDNA

SCRIPT cDNA Synthesis Kit, (#PCR511S), Jena Bioscience

Denaturation and primer annealing

Oligo dT	0.5 µl
Sample (RNA)	9.5 µl

As the first step of cDNA synthesis, the samples are incubated at 75 °C for 5 minutes by adding oligo dT.

Oligo dT	0.5 µl
Sample (RNA)	9.5 µl

Reaction mix. Preparation

SCRIPT RT Buffer	4 µl
dNTP Mix	1 µl
DTT Stock Solution	1 µl
RNase inhibitör	1 µl
SCRIPT Reverse Transcriptase	0.5 µl
RNase-free Water	2.5 µl
	10 µl mix

10 µl of the reaction mix was transferred to PCR tubes. Samples preperad with 10 µL of oligo dT were also added to the PCR tubes. It was first incubated at 42 °C for 10 min and then at 50 °C for 60 min. cDNA was obtained.

qRT-PCR reaction mix

Maxima SYBR Green qPCR Master Mix (2x)	7 µl
Forward Primer	1 µl (1 µM)
Reverse Primer	1 µl (1 µM)
Sample cDNA	1 µl

In our study, 6 different genes were determined at the mRNA level by qRT-PCR. cDNA and primer concentrations were normalized. Maxima SYBR Green qPCR Master Mix (2X) (Thermo Scientific) kit was used for real time PCR reactions. The programs for the genes evaluated in the study are provided separately below.

Table 3: *c-Abl* and *Yap* RT-PCR program.

94 °C 5 min	1 Cycle
94 °C 20 min	35 Cycle
52 °C 30 min	
72 °C 30 min	

Table 4: *Tead4* and *Nanog* RT-PCR program.

94 °C 5 min	1 Cycle
94 °C 20 min	35 Cycle
53 °C 30 min	
72 °C 30 min	

Table 5: *Cdx2* RT-PCR program.

94 °C 5 min	1 Cycle
94 °C 20 min	35 Cycle
54 °C 30 min	
72 °C 30 min	

Table 6: *Oct4* RT-PCR program.

94 °C 5 min	1 Cycle
94 °C 20 min	35 Cycle
52 °C 30 min	
72 °C 30 min	

Primer List

Table 7: The list of primers used for qRT-PCR.

Cdx2	**F** TCAACCTCGCCACAACCTTCCC **R** TGGCTCAGCCTGGGATTGCT	217
Nanog	**F** CTTACAAGGGTCTGCTACTGAGATGC **R** TGCTTCCTGGCAAGGACCTT	217
Yap1	**F** 5'-GACTCCGAA TGCAGTGTCTTC-3' **R** 5'-TGTTGAGGAAGTCGTCTGGG-3'	113
Tead4	**F** 5'-GGAGTATGCCCGCTATGAGA -3' **R** 5'-TCCTGTGTGTCTCGGTTGGT-3'	113
Oct4	**F** 5'- CCGGAAGAGAAAGCGAACTA -3' **R** 5'- CTCATACTCTTCTCGTTGGGAAT -3'	217
c-Abl	**F** CGG GAC CAT GTT GGA GAT **R** TTC ATA CCG CAG CGA GATG	218
β-Actin	**F** GAT GAC GAT ATC GCT GCG CTG **R** GTA CGA CCA GAG GCA TAC AGG	218

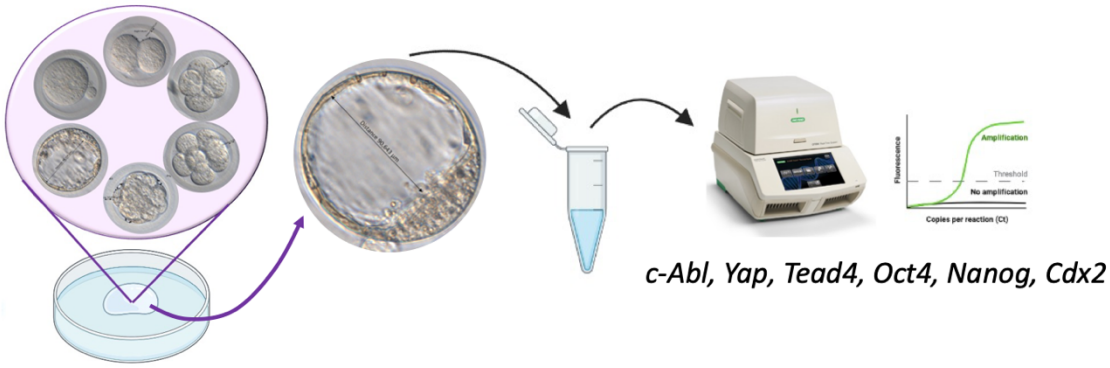

Figure 17: The Real Time Polymerase Chain Reaction schematized.

3.12. Statistical analysis

Morphological development data were analysed with 2-Way ANOVA (for ZP thickness) and One-way ANOVA (used Geisser-Greenhouse correction). Immunofluorescence intensity levels were determined using ImageJ. For the immunofluorescence intensity results and qRT-PCR results statistical analysis was performed with GraphPad Prism. Normally distributed data were analysed by a Two-Way ANOVA test to compare multiple groups. Differences were considered significant when $p<0.05$.

4. RESULTS

4.1. Development and morphological evaluation of embryos from zygote to the blastocyst

The cultured embryos imaging was performed with the Axio Observer-Invert microscope to evaluate the morphology. As a result of the evaluation, an evaluation was made in the light of the literature and considering the criteria. Imaging was performed to evaluate morphology using an Axio Observer-Invert microscope. As a result of the evaluation, an evaluation was made in the light of the literature, taking into account the relevant criteria [212,213].

Whether the embryo culture was successful or not was evaluated according to the morphological criteria we previously determined. As a result of the evaluation;

Evaluation of the 1st day zygote **(Figure 18A);**

- Both pronuclei appeared in the zygote.
- The second polar body was seen in the embryo.
- The zona pellucida was smooth.
- No vacuoles or granule-like structures were detected in the cytoplasm.
- Embryo mass occupied 60% of the perivitelline space as expected.

Evaluation of 2-cell embryo on day 2 of culture **(Figure 18B)**;

- It was observed that the embryos transitioned to the 2-cell 18-20 hours after they were cultured at the zygote. The 1st cleavge of embryos occurred at the expected time.
- Nuclei of both blastomeres were visible, there was no multinucleation.
- Polar body was visible.
- It was determined that the blastomeres were mononuclear and the nuclei were centrally located.
- The nuclei of the blastomeres looked healthy.
- The zona pellucida had a smooth structure.
- Cytoplasm was normal. No vacuoles or granule-like structures were detected.
- Perivitelline space was normal.
- The 2-cell embryo mass occupied 70% of the perivitelline space, as expected.

Evaluation of 4-cell embryo on day 3 of culture **(Figure 18C);**

- It was observed that the embryos transitioned to the 4-cell 36-38 hours after the start of culture at the zygote.
- The volumes of the blastomer were equal.

- The nuclei of the blastomeres were visible.
- The zona pellucida was smooth.
- The cytoplasmic image was normal. No vacuoles or granule-like structures were detected.
- Perivitelline space was normal.
- The 4-cell embryo mass occupied 70% of the perivitelline space, as expected.

Evaluation of 8-cell embryo on day 3 of culture **(Figure 18D);**

- After culturing the embryos at the zygote, it was observed that they transitioned to the 8-cell after approximately 46-48 hours.
- The volumes of the blastomer were equal.
- The nuclei of the blastomeres were visible.
- The zona pellucida was smooth.
- The cytoplasmic image was normal. No vacuoles or granule-like structures were detected.
- Perivitelline space was normal.
- The 8-cell embryo mass occupied 70% of the perivitelline space, as expected.

Evaluation of the morula embryo on the 4th day of culture **(Figure 18E);**

- After culturing the embryos at the zygote, it was observed that they transitioned to the morula approximately 65-67 hours later.
- Successful compaction (the blastomeres lose their cell boundaries and adhere to each other by junctional complexes) occurred as expected.
- Perivitelline space was normal.
- The embryo mass at the morula covered 80% of the perivitelline space, as expected.

Evaluation of the blastocyst embryo on day 4 of culture **(Figure 18F**);

- It was observed that the embryos transitioned to the blastocyst 70-72 hours after the start of culture at the zygote.
- It was observed that the blastocoele cavity of the embryo merged.
- The zona pellucida thickness decreased as expected due to the expansion of the blastocoele space and the pressure exerted by the embryo on the zona pellucida.
- Inner cell mass and outer cell mass were distinguishable.
- The inner cell mass was seen as compact.
- Embryo mass at the blastocyst covered 90% of the perivitelline space.

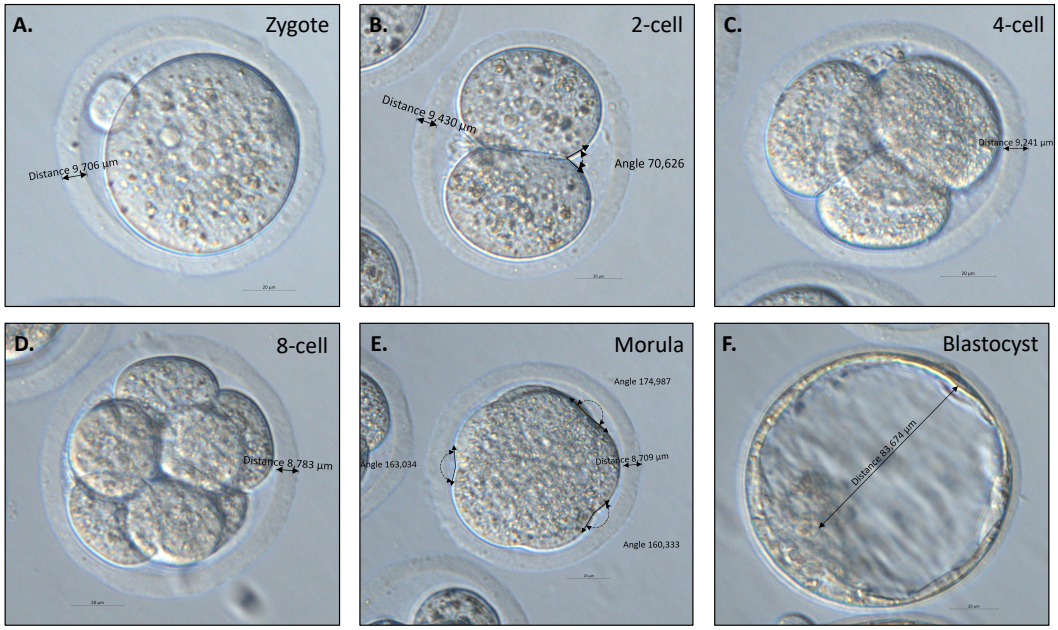

Figure 18: After superovulation, zygotes were cultured *in vitro* until they developed to the blastocyst. A.1. day zygote, B. Day 2 of culture 2-cell embryo, C. Day 3 of culture 4-cell embryo, D. Day 3 of culture 8-cell embryo, E. Day 4 of culture embryo at morula, 1F. Embryo at the blastocyst on day 4 of culture.

4.2. The development of mice preimplantation embryos after PDGF-AA treatment

Embryo development following PDGF-AA treatment was compared with control embryos. The morphological results obtained were shown comparatively. **(Figure 19A).** There was no difference between the control, 20 ng/mL and 50 ng/mL PDGF-AA groups in terms of morphological difference and developmental rate/duration. Control and 50 ng/mL PDGF-AA embryos showed an 81% success rate, while embryos cultured with 20 ng/mL PDGF-AA showed 78%, success rate **(Figure 19B and Figure 19C)**.

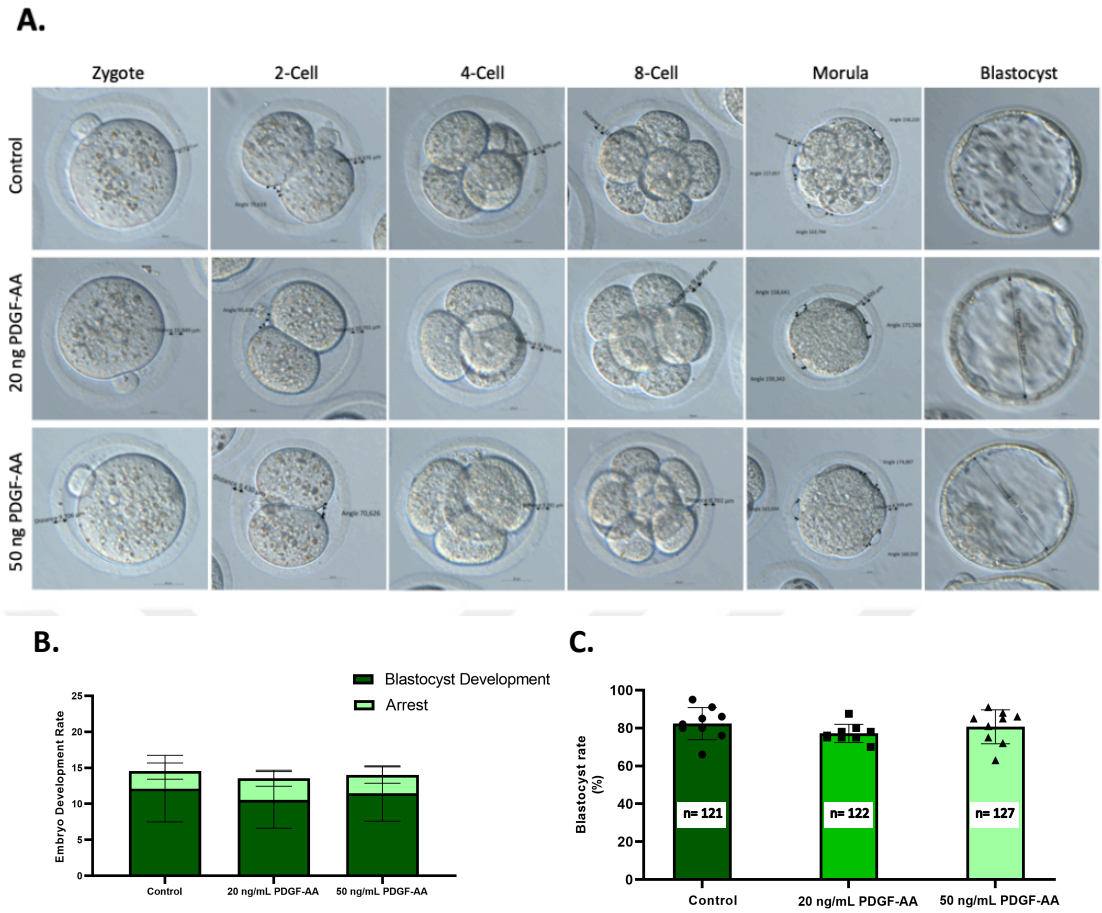

Figure 19: Morphological comparison of the developmental potentials of PDGF-AA groups. A. Morphological comparison of the control, 20 ng/mL and 50 ng/mL PDGF-AA groups of mouse embryos obtained by superovulation and cultured from zygote to blastocyst. B. and C. Comparison of groups by statistically evaluating the developmental potential of PDGF-AA treatment group on embryonic development. (8 different cultures were assessed for their average developmental potential).

As a result of the morphological examination, comparisons were made between the groups in which PDGF-AA treatment and the control group. In these comparisons, ZP thickness, the angle between blastomeres in the 2-cell, the angle between compacted blastomeres in the morula embryo and the blastocoele space in the blastocyst embryo were evaluated. At the end of this evaluation, there was no significant difference between the ZP thickness, the angle between blastomeres at the morula and the blastocoele space. However, when the angle between the blastomeres at the 2-cell was compared between the groups, it was seen that this angle increased in the 20 ng/mL PDGF-AA group **(Figure 20).**

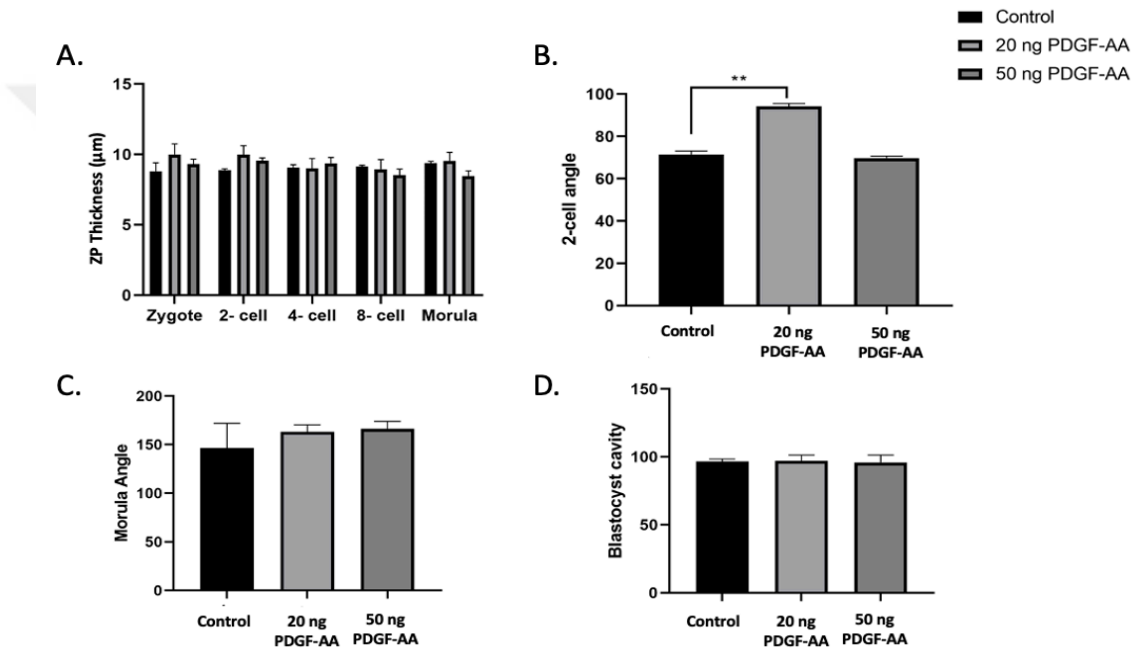

Figure 20: Statistical evaluation of the morphology of PDGF-AA groups. Control, 20 ng/mL PDGF-AA and 50 ng/mL PDGF-AA groups; the thickness of the ZP (A), the measurement of the angle between the 2 blastomeres in the 2-cell (B), the measurement of the angle between the 2 blastomeres in the morula (C), and the blastocoele cavity formed in the blastocyst (D) embryos were evaluated (n=10) (**p< 0.01).

4.3. Comparison of immunofluorescent staining and intensities in groups after PDGF-AA treatment

We demonstrated whether p73-mediated YAP/TEAD signaling affects polarization, TE epithelialization and TE/ICM cell fate determination as a result of PDGF-AA treatment in preimplantation embryo development cultured from zygote to blastocyst. After PDGF-AA treatment, we determined that the expression of YAP in the control groups was localized in the nuclei of TE cells, as expected. However, we determined that YAP expression in both the 20 ng/mL PDGF-AA and the 50 ng/mL PDGF-AA groups was localized in the cytoplasm in addition to the nuclear localization in TE cells. While c-Abl localization was nuclear in some of the TE cells in the control group, c-Abl expression was cytoplasmic in TE cells in 20 ng/mL PDGF-AA and 50 ng/mL PDGF-AA groups. While ICM showed a uniform distribution in the control and 20 ng/mL PDGF-AA groups, the ICM distribution was more widespread in the 50 ng/mL PDGF-AA group (dotted area). Expressions in nuclei of TE cells were marked with arrowheads. Interblastomere bridge-like structure seen in control and 20 ng/mL PDGF-AA of c-Abl are marked with arrows. c-Abl localization is interblastomere bridge-like structure between blastomeres in addition to cytoplasm and nucleus. These interblastomere bridge-like structures were negligible at 50 ng/mL PDGF-AA. The c-Abl localization seen in the nuclei of some cells in the control group, was not detected in the nucleus in the 20 ng/mL and 50 ng/mL PDGF-AA groups. It was observed that c-Abl exhibited a membranous staining especially in the 20 ng/mL PDGF-AA group **(Figure 21A).** We compared the IF intensity of c-Abl and YAP between the groups. As a result of PDGF-AA treatment, we detected an increase in the expression level of c-Abl in both the 20 ng/mL PDGF-AA and the 50 ng/mL PDGF-AA compared to the control group. When the change in localization was evaluated according to the IF intensity ratio, it was observed that there was more intense expression in the cytoplasm in the PDGF-AA administered groups. YAP expression was significantly increased only in the 20 ng/mL PDGF-AA group. It is possible to see the effect of YAP expression localized in the cytoplasm in addition to the nucleus **(Figure 21B).**

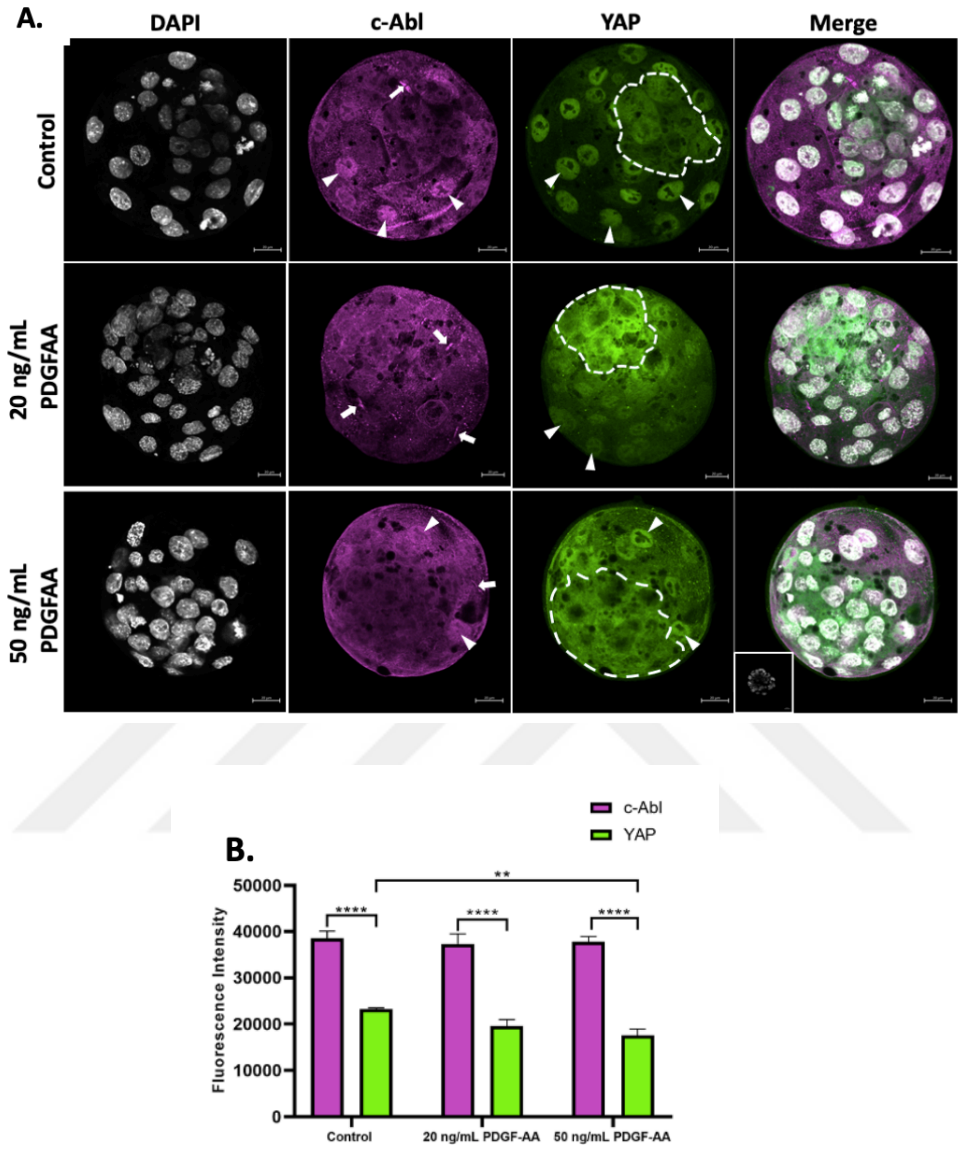

Figure 21: Evaluation of c-Abl and YAP localizations by immunofluorescence staining in control, 20 ng/mL and 50 ng/mL PDGF-AA groups. A. Evaluation of cellular localizations of c-Abl and YAP would change with PDGF-AA treatment. After PDGF-AA treatment, YAP localization was determined in the cytoplasm in addition to the nucleus in TE cells in PDGF-AA groups. B. Comparison of immunofluorescence intensities between groups (*p<0.05, **p <0.01, ****p <0.0001). Dotted area: ICM, Arrowhead: TE nucleus, White arrow: Interblastomere bridge-like structure. (C (control), n=8; 20 ng/mL, n=5; 50 ng/mL, n=6)

The expression of p-c-Abl in the control, 20 ng/mL PDGF-AA and 50 ng/mL PDGF-AA groups was imaged with a confocal microscope. Localization of p-c-Abl was observed around the nucleus and cytoplasm in all groups **(Figure 22A)**. In addition, there was no significant difference when the immunofluorescence intensities were statistically compared **(Figure 22B).**

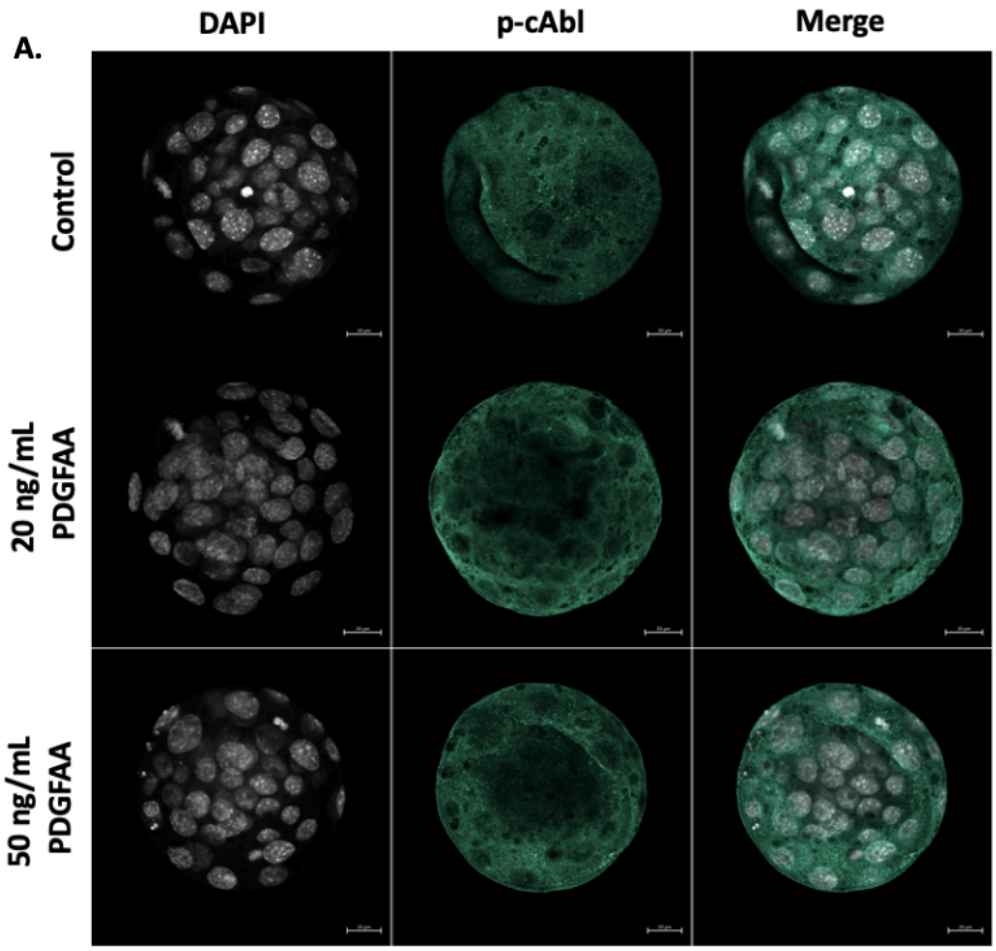

Figure 22: Evaluation of p-c-Abl localizations by immunofluorescence staining in control, 20 ng/mL and 50 ng/mL PDGF-AA groups. A. Localization of p-c-Abl in cells was determined after PDGF-AA treatment. p-c-Abl localization was determined around the nucleus and in the cytoplasm in all groups. B. There was no statistically significant difference between the groups when comparing the immunofluorescence intensity. (C (control), n=4; 20 ng/mL, n=4; 50 ng/mL, n=4)

p-YAP expression in the control, 20 ng/mL PDGF-AA and 50 ng/mL PDGF-AA groups was imaged with a confocal microscope. In all groups, p-YAP localization was determined around the peri-nuclear area and in the cytoplasm **(Figure 23A)**. In addition, when the immunofluorescence intensities were statistically compared, p-YAP expression was found to be significantly decreased in the 20 ng/mL PDGF-AA group compared to the 20 ng/mL PDGF-AA and control group **(Figure 23B).**

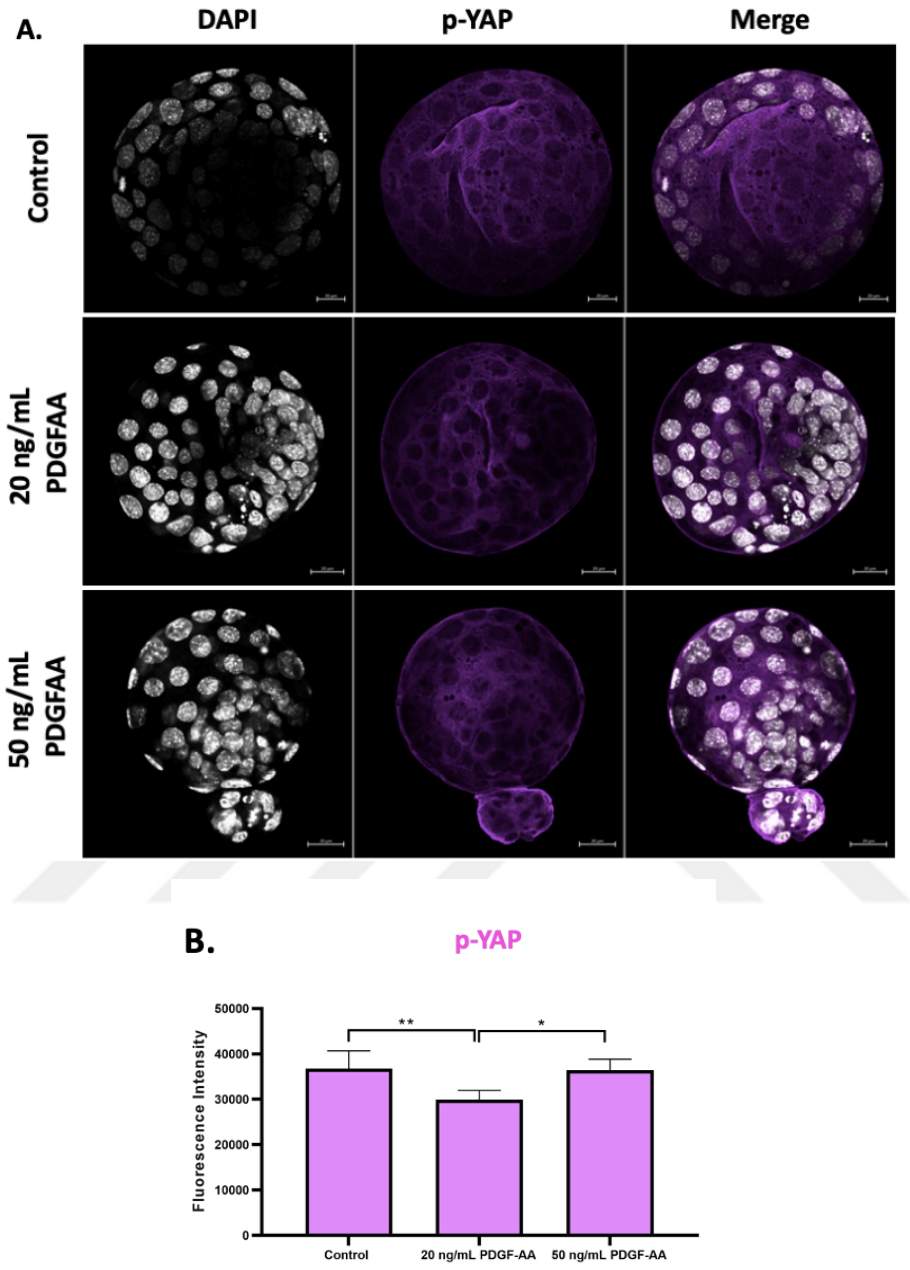

Figure 23: Evaluation of p-YAP localizations by immunofluorescence staining in control, 20 ng/mL and 50 ng/mL PDGF-AA groups. A. Cellular localization of p-YAP after PDGF-AA treatment. p-YAP localization was determined around the nucleus and cytoplasm in all groups B. When immunofluorescence intensity was compared between the groups, it was observed that the p-YAP level was significantly decreased in the 20 ng/mL and 50 ng/mL PDGF-AA groups (*$p<0.05$, **$p<0.01$). (C (control), n=5; 20 ng/mL, n=5; 50 ng/mL, n=5)

Expression of p73 was examined after PDGF-AA treatment. c-Abl is known to perform p73-mediated upregulation of YAP. In the control group, p73 expression was seen intensely in the cytoplasm. P73 expression was also seen in the cytoplasm in the 20 ng/mL PDGF-AA and 50 ng/mL PDGF-AA groups, similar to the control group. However, the p73 expression level was decreased compared to the control group. Cumulative expression of p73 in the cytoplasm of blastomeres was seen in the control group. However in PDGF-AA treatment groups, p73 expression was found to be decreased in blastomeres cytoplasm **(Figure 24A)**. Comparison of p73 IF intensity levels between groups showed that p73 expression intensity increased with PDGF-AA treatment compared to the control group **(Figure 24B)**.

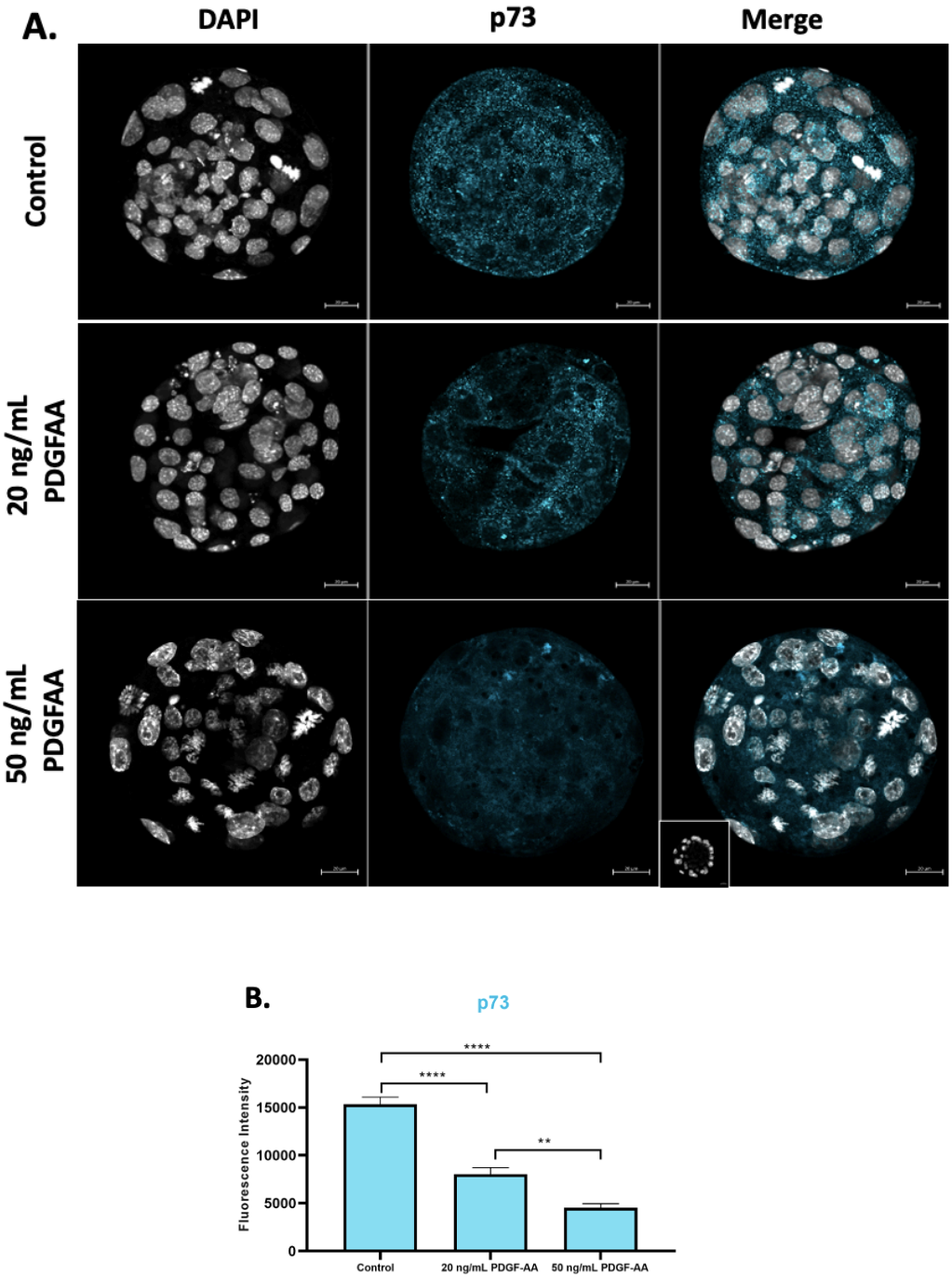

Figure 24: Evaluation of p73 localization by immunofluorescence staining in control, 20 ng/mL and 50 ng/mL PDGF-AA groups. A. Cellular localizations of p73 would change with the 20 ng/mL and 50 ng/mL PDGF-AA treatment compared to the control group. After PDGF-AA treatment. B. Comparison of p73 immunofluorescence intensities between groups (**p <0.01, ****p <0.0001). (C (control), n=4; 20 ng/mL, n=4; 50 ng/mL, n=4)

It is known that TEAD4 determines the fate of TE cells via CDX2. After PDGF-AA treatment, *Tead4* induces TE-specific factor *Cdx2*, enabling cells to acquire TE character [101]. We detected TEAD4 in the nuclei of TE cells as it should in the control blastocyst. However, after PDGF-AA treatment, TEAD4 was not detected in the nuclei of TE cells in both 20 ng/mL and 50 ng/mL PDGF-AA groups. In PDGF-AA treatment groups, cytoplasmic TEAD4 localization was determined. Nuclei of TE cells are marked with white arrowheads **(Figure 25A)**. The intensity of the TEAD4 expression pattern was significantly reduced in the PDGF-AA treatment groups compared to the control group **(Figure 25B)**.

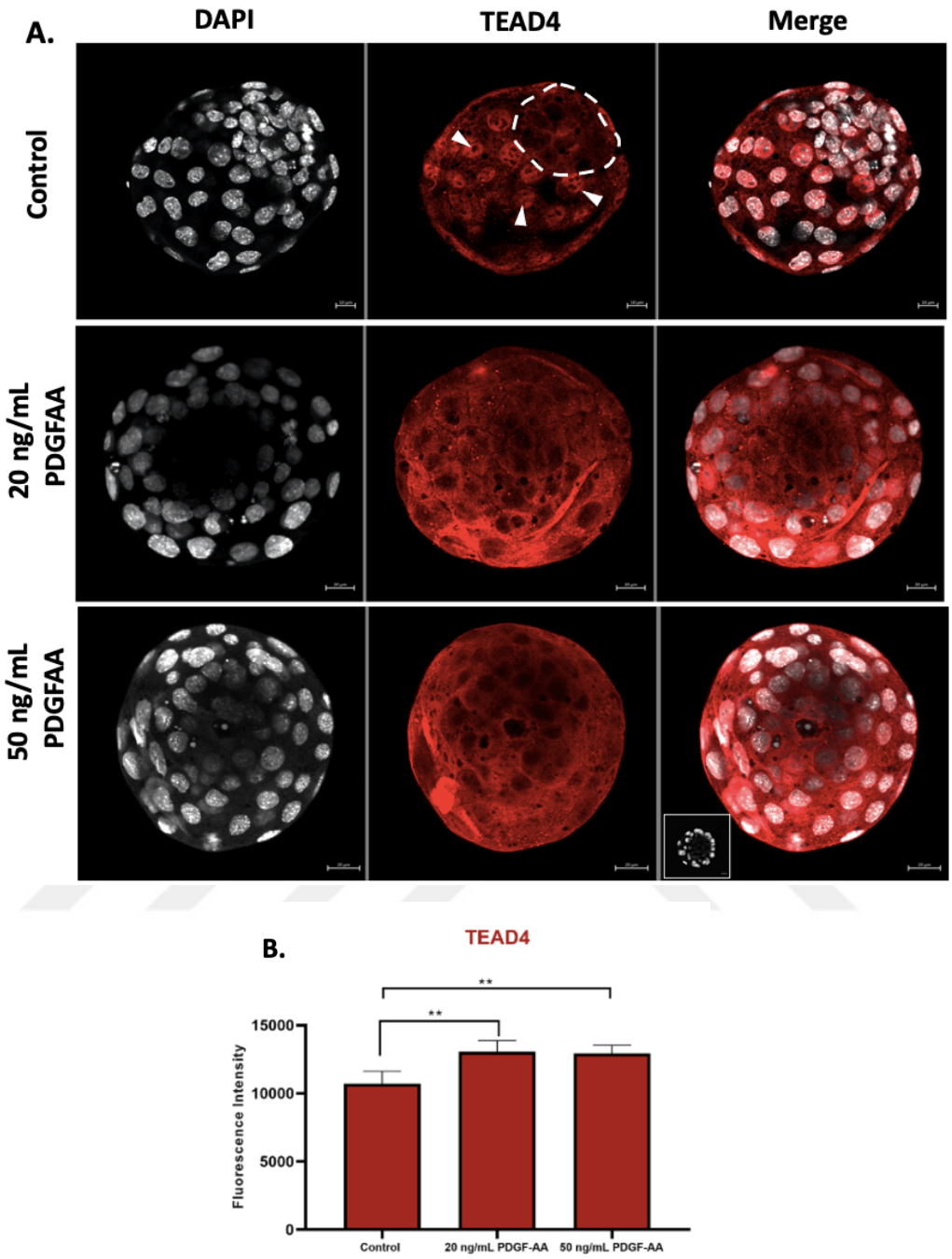

Figure 25: Evaluation of TEAD4 localization by immunofluorescence staining in control, 20 ng/mL and 50 ng/mL PDGF-AA groups. A. Cellular localizations of TEAD4 would change with the 20 ng/mL and 50 ng/mL PDGF-AA treatment compared to the control group. After PDGF-AA treatment, TEAD4 was gradually expressed in the cytoplasm in TE cells. Expression of TEAD4 in the nucleus of TE cells were seen in the control group. B. Comparison of TEAD4 immunofluorescence intensities between groups (**p <0.01, ****p <0.0001). Arrowhead: TE nucleus. (C (control), n=4; 20 ng/mL, n=5; 50 ng/mL, n=6)

It was observed that PARD6 localization, which is used as an apical polarization marker in TE cells, was distributed from the apical regions of the cell to the cytoplasm after PDGF-AA treatment. The increase of cytoplasmic PARD6 in the PDGF-AA treatment groups compared to the control group indicates the potential role that c-Abl may plays in polarization. Polarization regions determined by PARD6 in cells are marked with white arrows **(Figure 26A)**. Also, when comparing IF intensity, the increased intensity of PARD6 expression compared to the control group was due to its distribution into the cytoplasm **(Figure 26B)**.

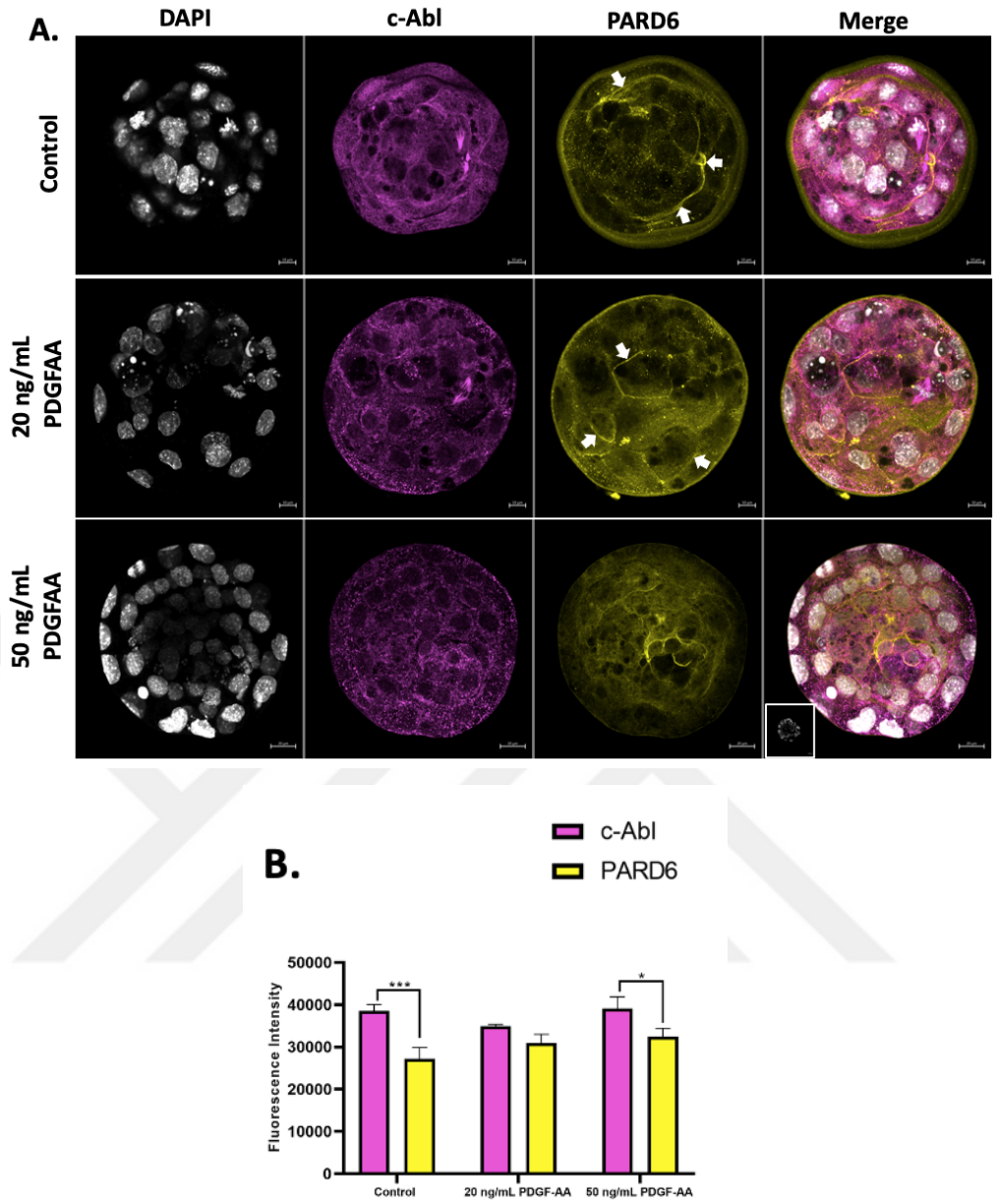

Figure 26: Evaluation of c-Abl and PARD6 localization by immunofluorescence staining in control, 20 ng/mL and 50 ng/mL PDGF-AA groups. A. Cellular localizations of c-Abl and PARD6 change with the PDGF-AA treatment compared to the control group. After PDGF-AA treatment, no significant changes were seen in the PARD6 pattern. B. Comparison of immunofluorescence intensities between groups (*p<0.05, ***p <0.001). White Arrow: Polarization regions. (C (control), n=4; 20 ng/mL, n=5; 50 ng/mL, n=5)

It is known that TEAD4 determines the fate of TE cells via CDX2 [101]. Therefore, we evaluated the CDX2 expression pattern. However, although PDGF-AA treatment induced the translocation of TEAD4 from the nucleus to the cytoplasm, it did not change the expression pattern of CDX2. This suggested that c-Abl-TEAD4 mediated signal should be evaluated on another signal, not CDX2 **(Figure 27A)**. At the same time, the E-cadherin pattern, which is an important marker of cell-cell connections in preimplantation embryo development, was evaluated. E-cadherin expression showed the same pattern in all groups **(Figure 27A)**. In a study conducted in 2013, the expression of E-cadherin in preimplantation embryo development was examined and it was shown that it forms the filopodia structure that allows the shape of the cells to be determined during compaction in blastomeres [219]. We examined in detail the cell-cell connections under a confocal microscope in PDGF-AA treatment groups. As a result of our imaging, we identified filopodia-like structures with E-cadherin in all groups. Especially in the 50 ng/mL PDGF-AA group, we found an increase in the number and length of filopodia compared to the control group **(Figure 27B)**. We did not detect any significant difference in E-cadherin and CDX2 expression intensity levels **(Figure 27C)**.

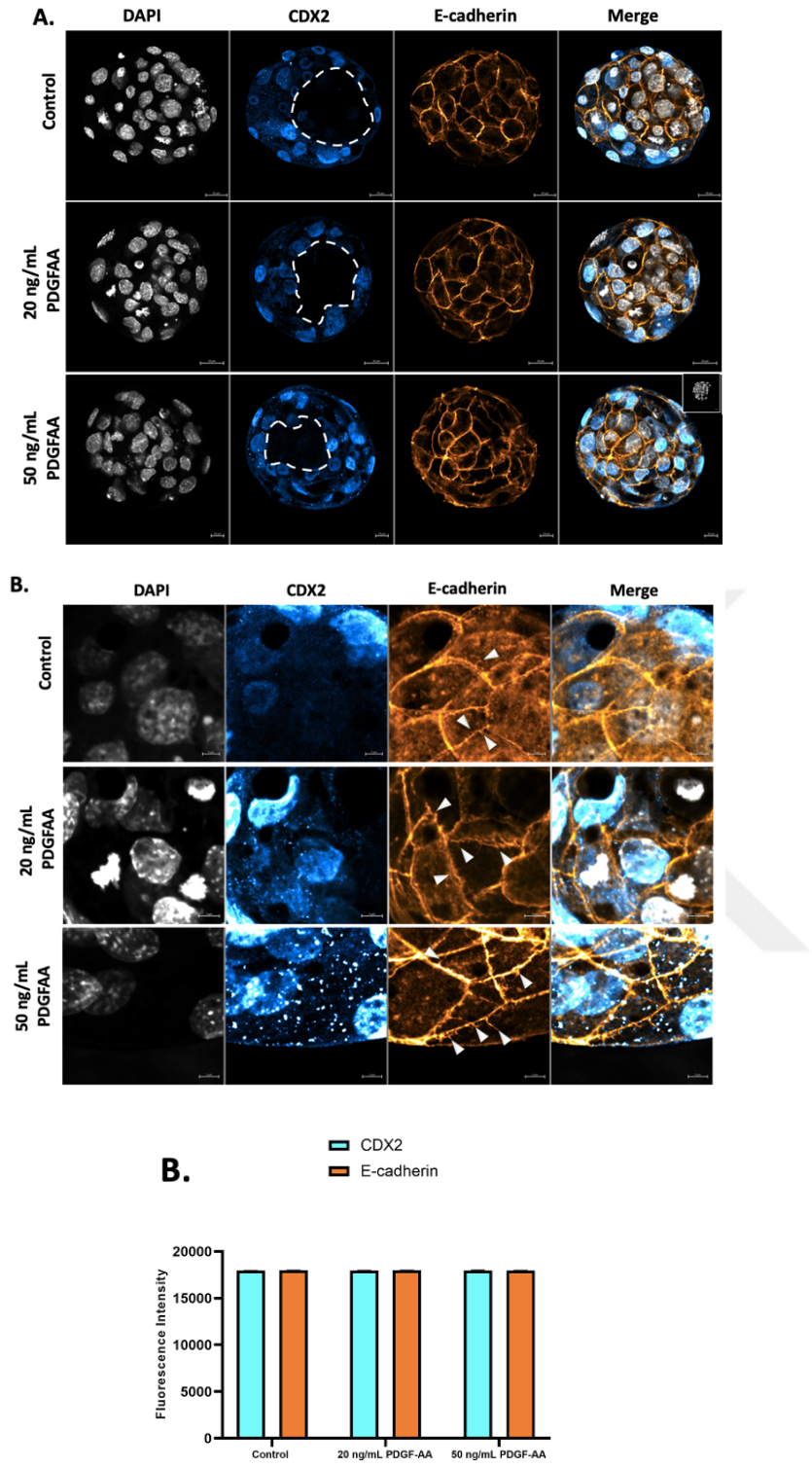

Figure 27: Evaluation of CDX2 and E-cadherin localization by immunofluorescence staining in control, 20 ng/mL and 50 ng/mL PDGF-AA groups. A. Cellular localizations of CDX2 and E-cadherin would change with the PDGF-AA treatment. There are no significant changes were seen in the CDX2 and E-cadherin patterns. B. E-cadherin and filopodia structures formed between blastomeres were determined. Especially in the 50 ng/mL PDGF-AA group, the filopodia were increased and exhibited a longer pattern compared to the control and 20 ng/mL PDGF-AA group. C. Comparison CDX2 and E-cadherin of

immunofluorescence intensities between groups (*p<0.05, **p<0.01, ***p <0.001, ****p <0.0001). Dotted area: ICM. (C (control), n=4; 20 ng/mL, n=4; 50 ng/mL, n=5)

We observed that CDX2, a TE cell marker, was not affected according to pattern by PDGF-AA treatment. However, we showed that it decreased in intensity. We evaluated ICM characterization with the ICM marker NANOG after PDGF-AA treatment. When we evaluated the Nanog pattern in the control and PDGF-AA treatment groups; We found that NANOG expression was expressed in ICM as expected in the control group. We found that NANOG was expressed in mostly ICM and some TE cells in 20 ng/mL PDGF-AA and 50 ng/mL PDGF-AA groups **(Figure 28A)**. There was no significant difference between the groups for immunofluorescence intensity **(Figure 28B).**

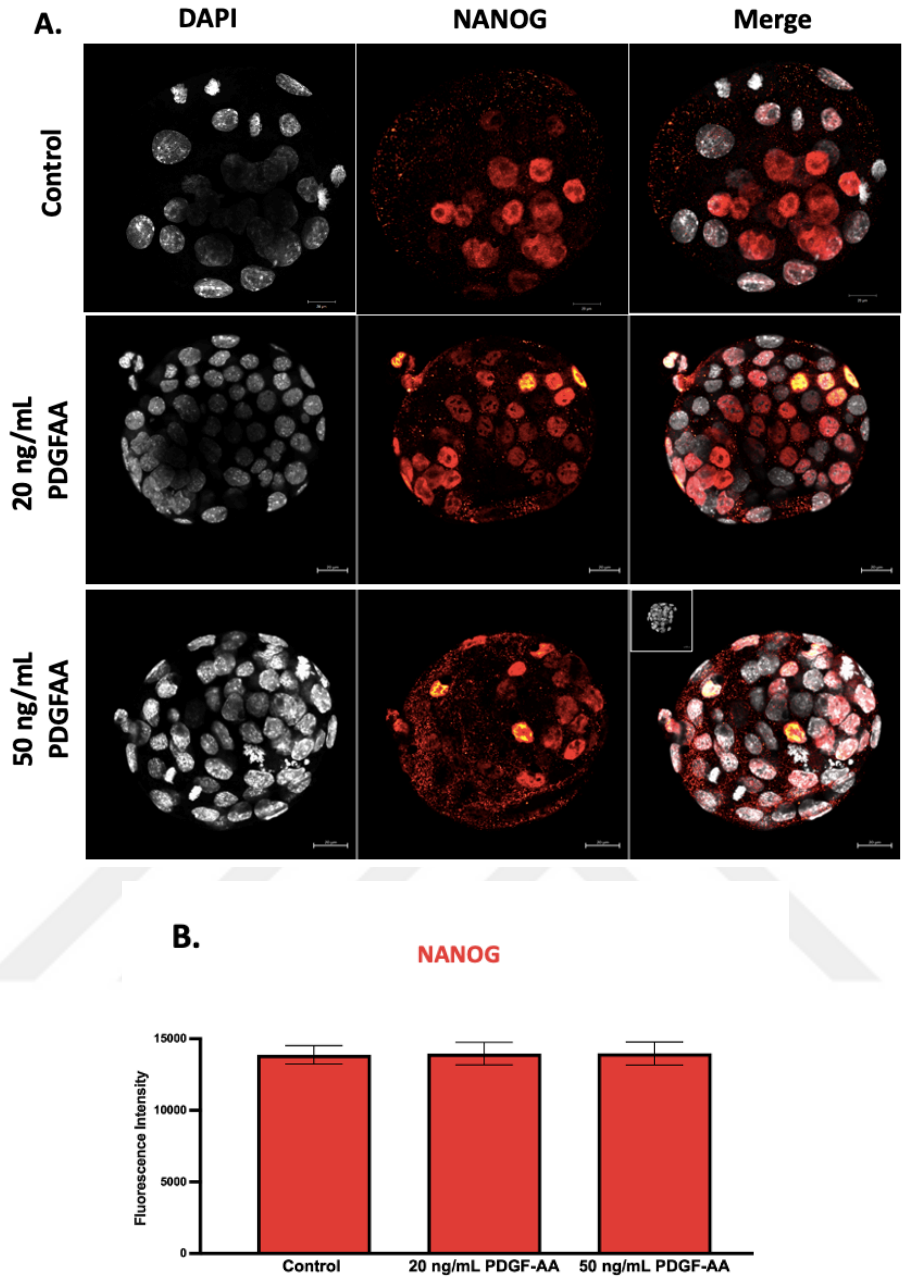

Figure 28: Evaluation of NANOG localization by immunofluorescence staining in contro 20 ng/mL and 50 ng/mL PDGF-AA groups. A. Cellular localizations of Nanog would change with the PDGF-AA treatment compared to the control group. In control group NANOG expression was determined in ICM. In 20 ng/mL and 50 ng/mL PDGF-AA groups Nanog expression determined in ICM, but we determined weak expression in TE cells. B. Comparison NANOG of immunofluorescence intensities between groups (*p<0.05, **p <0.01, ****p <0.0001). (C (control), n=4; 20 ng/mL, n=5; 50 ng/mL, n=5)

4.4. Comparison of *c-Abl, Yap, Tead4, Cdx2, Nanog* and *Oct4* mRNA levels in groups after PDGF-AA treatment

c-Abl, Yap, Tead4, Cdx2, Nanog and *Oct4* mRNA levels were compared in embryos that developed into blastocyst stage after PDGF-AA treatment. Considering the mRNA levels measured by qRT-PCR; As expected, PDGF-AA treatment and mRNA level of *c-Abl* significantly increased in the PDGF-AA treated groups compared to the control group. *Yap* mRNA level, on the other hand, showed a tendency to increase with c-Abl activation, but no significant difference was found. However, *Tead4* localized in the nuclei of TE cells was detected in groups with PDGF-AA treatment compared to the control group **(Figure 29A)**.

It was observed that *Cdx2*, which is a TE cell marker, decreased significantly at the mRNA level in PDGF-AA treatment groups. There was no significant difference between the groups in the levels of *Nanog* and *Oct4* mRNA, which is the ICM marker **(Figure 29B)**.

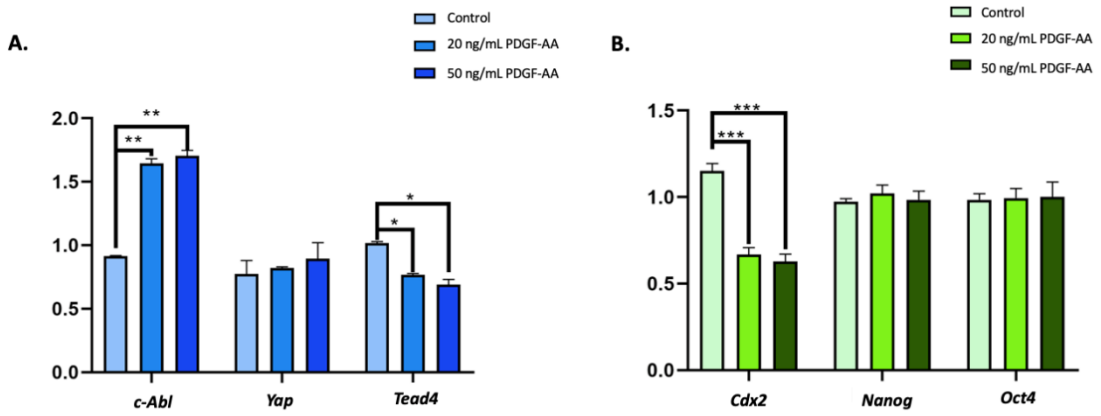

Figure 29: Determination of mRNA levels between groups following PDGF-AA treatment. A. After PDGF-AA treatment, *c-Abl, Yap, Tead4* mRNA levels were compared between control, 20ng/mL PDGF-AA and 50ng/mL PDGF-AA groups. While *c-Abl* mRNA level increased significantly in PDGF-AA groups, *Tead4* mRNA level decreased significantly in PDGF-AA groups. B. TE and ICM markers were compared between the control, 20ng/mL PDGF-AA and 50ng/mL PDGF-AA groups. While the TE marker *Cdx2* mRNA level decreased in the groups treated with PDGF-AA, the ICM markers *Nanog* and *Oct4* did not differ significantly.

4.5. The development of preimplantation embryos after imatinib treatment

We aimed to determine how it would affect preimplantation embryo development for inhibiting ATP binding site by treated with imatinib. Embryo development following imatinib treated was compared with that of control embryos. The morphological results obtained were shown comparatively **(Figure 30A).** The rates of reaching the blastocyst of zygote embryos cultured with imatinib compared to control embryos were compared. When the control group and the groups in which imatinib treatment was applied were compared in terms of developmental potentials, it was observed that the growth potentials in the blastocyst decreased significantly as the imatinib dose increased. Control embryos showed an 81% success rate, while embryos cultured with 1 μM imatinib showed 58.5%, embryos cultured with 5 μM imatinib showed a 54% success rate **(Figure 30B and Figure 30C)**. Zygotes cultured with 10 μM imatinib did not reach the blastocyst. Therefore, we continued our experiments with 1 μM and 5 μM imatinib.

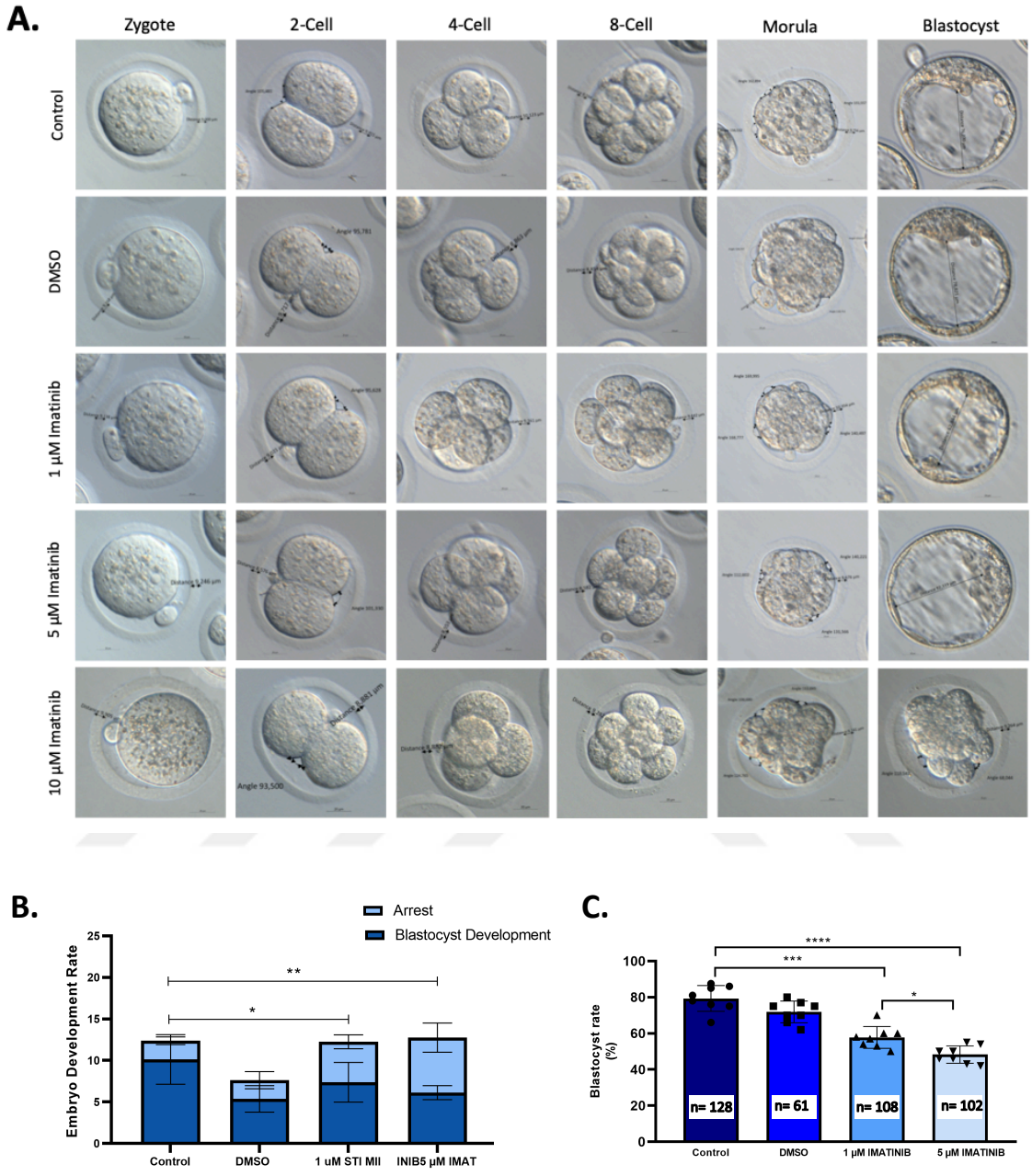

Figure 30: Morphological comparison of the developmental potentials of imatinib groups. A. Morphological comparison of the control, DMSO, 1 µM, 5 µM and 10 µM Imatinib groups of mouse embryos obtained by superovulation and cultured from zygote to blastocyst. B. and C. Statistical evaluation of the developmental potential of imatinib treatment on embryonic development (*p<0.05, **p<0.01, ***p<0.001). (8 different cultures were assessed for their average developmental potential).

As a result of the morphological examination, comparisons were made between the groups in which imatinib and the control groups. In these comparisons, ZP thickness, the angle between blastomeres in the 2-cell, the angle between compacted blastomeres in the morula embryo and the blastocoele space in the blastocyst embryo were evaluated. At the end of this evaluation, there was no significant difference between the ZP thickness and the angle between blastomeres at the 2-cell **(Figure 31A and 31B)**. However, when the angle between blastomeres was compared in embryos at the morula, it was seen that; In the groups where imatinib treatment were performed, the angle between blastomeres decreased. A decrease in the angle between the blastomeres indicates a weak connection between the 2 blastomeres [220]. In addition, as the dose of imatinib increased in culture medium, the angle between blastomeres decreased **(Figure 31C).** When the blastocyst cavity ratio is compared, the cavity ratio in the 1 µM imatinib group decreased compared to the control group. In the 5 µM imatinib group, the cavity ratio increased compared to the control group **(Figure 31D).**

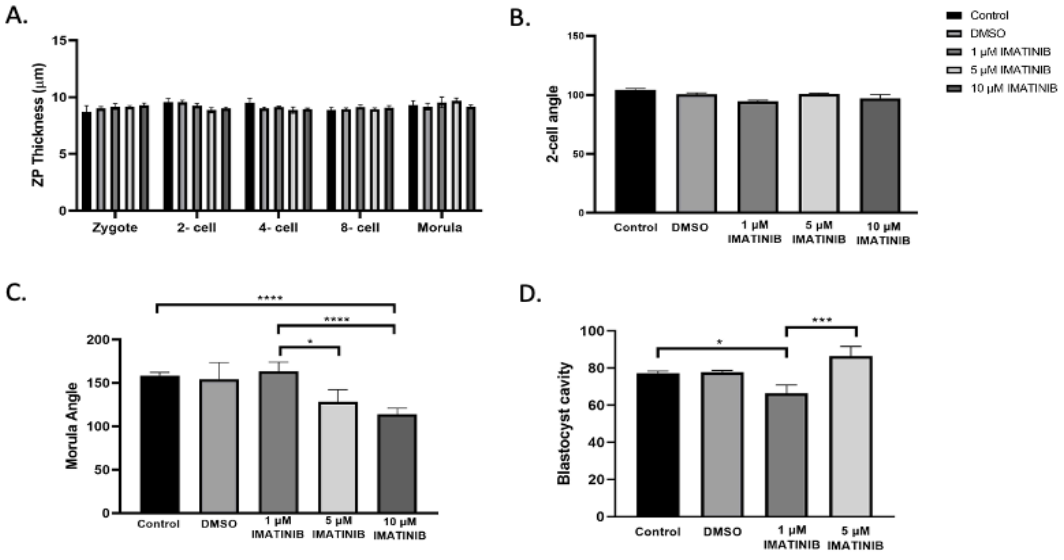

Figure 31: Statistical evaluation of the morphology of imatinib groups. Control, DMSO, 1 µM, 5 µM and 10 µM imatinib groups; The thickness of the ZP (A), the measurement of the angle between the 2 blastomeres in the 2-cell (B), the measurement of the angle between the 2 blastomeres in the Morula (C), and the blastocoele cavity formed in the blastocyst (D) embryos were evaluated (n=10) (*p <0.05, ****p<0.0001).

4.6. Comparison of immunofluorescent staining patterns and intensities in groups after imatinib treatment

We demonstrated whether p73-mediated YAP/TEAD signaling affects polarization, TE epithelialization and TE/ICM cell fate determination as a result of imatinib treatment in preimplantation embryo development cultured from zygote to blastocyst. First we determined that the expression of YAP in the control groups was localized in the nuclei of TE cells, as expected. After imatinib treatment we determined that YAP expression in both the 1 μM and 5 μM imatinib group was localized in the nucleus localization of TE cells as control group **(Figure 32A).** c-Abl was especially localized in the cell membrane and nuclei of mitotic cells **(Figure 32A).** The expression of YAP in ICM was detected in the cytoplasm of the cells. In addition, although the protein localizations of c-Abl and YAP did not change, as a result of the fluorescence intensity analysis of the staining, it was determined that the levels of c-Abl and YAP decreased **(Figure 32B).**

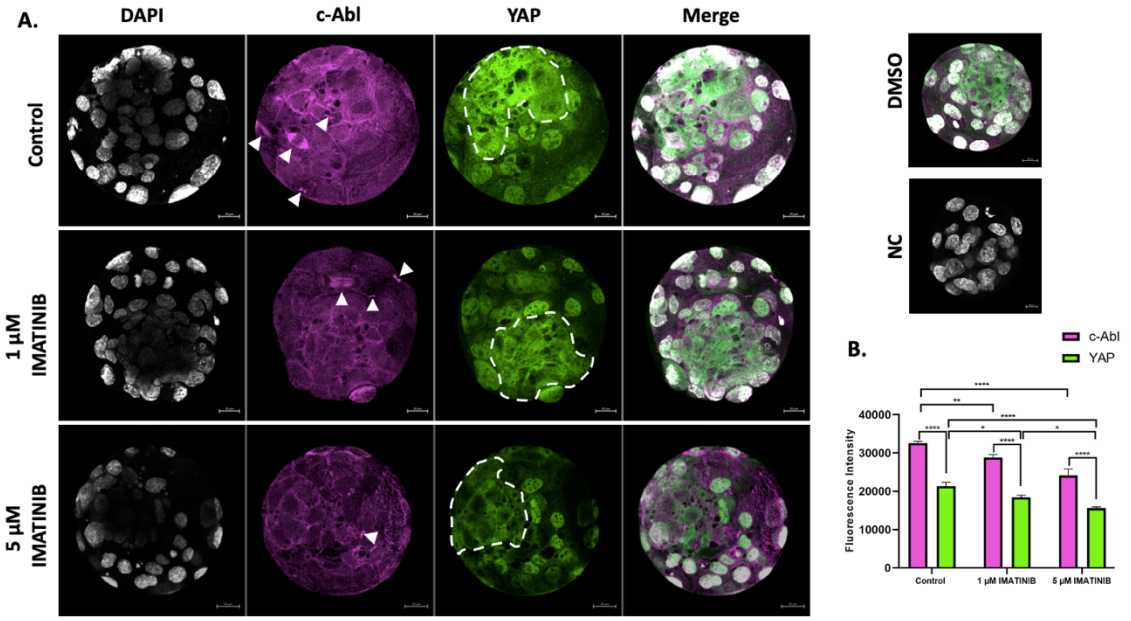

Figure 32: Evaluation of c-Abl and YAP localization by immunofluorescence staining in control, 1 µM and 5 µM imatinib groups. A. Cellular localizations of c-Abl and YAP would change with the imatinib treatment. In the control, 1 µM and 5 µM imatinib groups, c-Abl expression was seen in the cytoplasm. In addition to the cytoplasm, it was seen intensely in the nuclei of mitotic cells. YAP expression was determined in the nuclei of TE cells and in the cytoplasm of ICM cells. B. Although the c-Abl and YAP localization patterns did not change, when the immunofluorescence intensities were examined; It was determined that c-Abl and YAP intensity levels decreased in imatinib treatment (*p<0.05, **p <0.01, ***p <0.001, ****p <0.0001). (C (control), n=5; 1 µM, n=5; 5 µM, n=5)

Expression of p-c-Abl was examined after imatinib treatment. In the control group, p-c-Abl expression was seen intensely in the cytoplasm and cell boundries. In the 1 µM and 5 µM imatinib groups p-c-Abl expression was seen in the cytoplasm and cell boundries but weaker than control groups. A more intense cumulative pattern was seen in the 1 µM and 5 µM imatinib groups compared to the control group **(Figure 33A).** Comparison of p-c-Abl immunofluorescence intensity levels between groups showed that; p-c-Abl expression intensity decreased with imatinib treatment compared to the control group **(Figure 33B).**

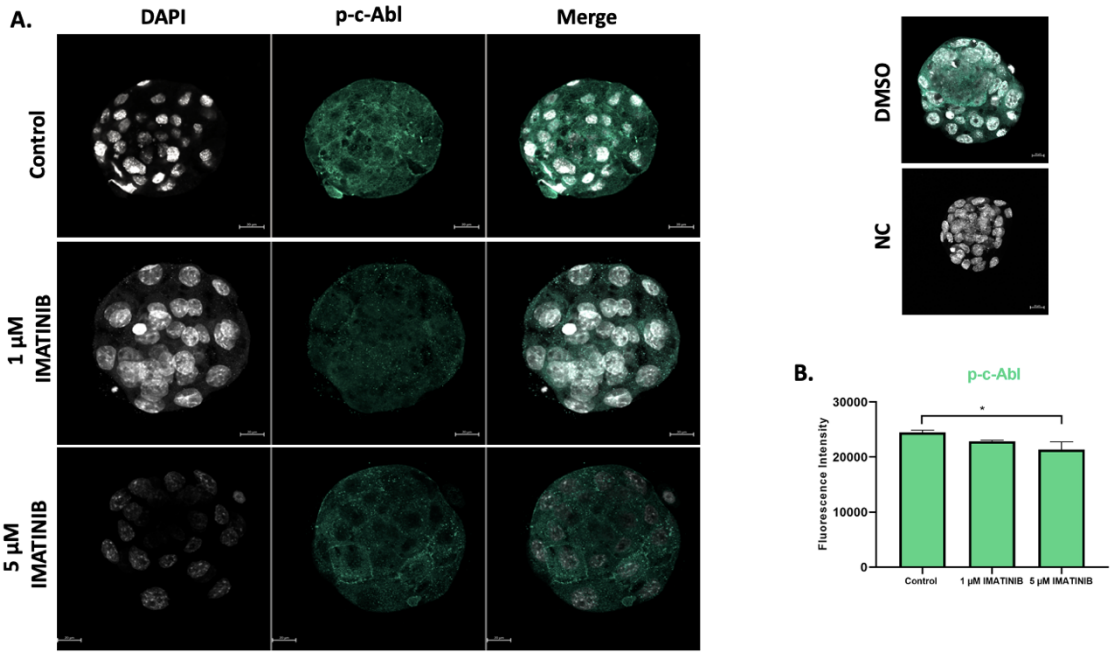

Figure 33: Evaluation of p-c-Abl localization by immunofluorescence staining in control, 1 µM and 5 µM imatinib groups. A. Cellular localizations of p-c-Abl would change with the imatinib treatment in the control, 1 µM and 5 µM imatinib groups with the immunofluorescence staining. In the control group p-c-Abl expression pattern was seen in the cytoplasm and cell boundries. In the 1 µM and 5 µM imatinib groups, p-c-Abl cumulative expression pattern was seen in the cytoplasm. B. When the immunofluorescence intensities were examined; It was determined that p-c-Abl intensity levels decreased in 5 µM imatinib treatment group (*p <0.05). (C (control), n=4; 1 µM, n=5; 5 µM, n=5)

Expression of p-YAP was examined after imatinib treatment. In the control group, p-YAP expression was seen intensely in the cytoplasm. In the 1 µM and 5 µM Imatinib groups p-YAP expression was seen in the cytoplasm and peri-nuclear area. However, in the 5 µM imatinib group, p-YAP was also found to be expressed in the nuclei of some cells **(Figure 34A).** Comparison of p-YAP IF intensity levels; In the 1 µM and 5 µM imatinib groups p-YAP expression levels higher than control group **(Figure 34B).**

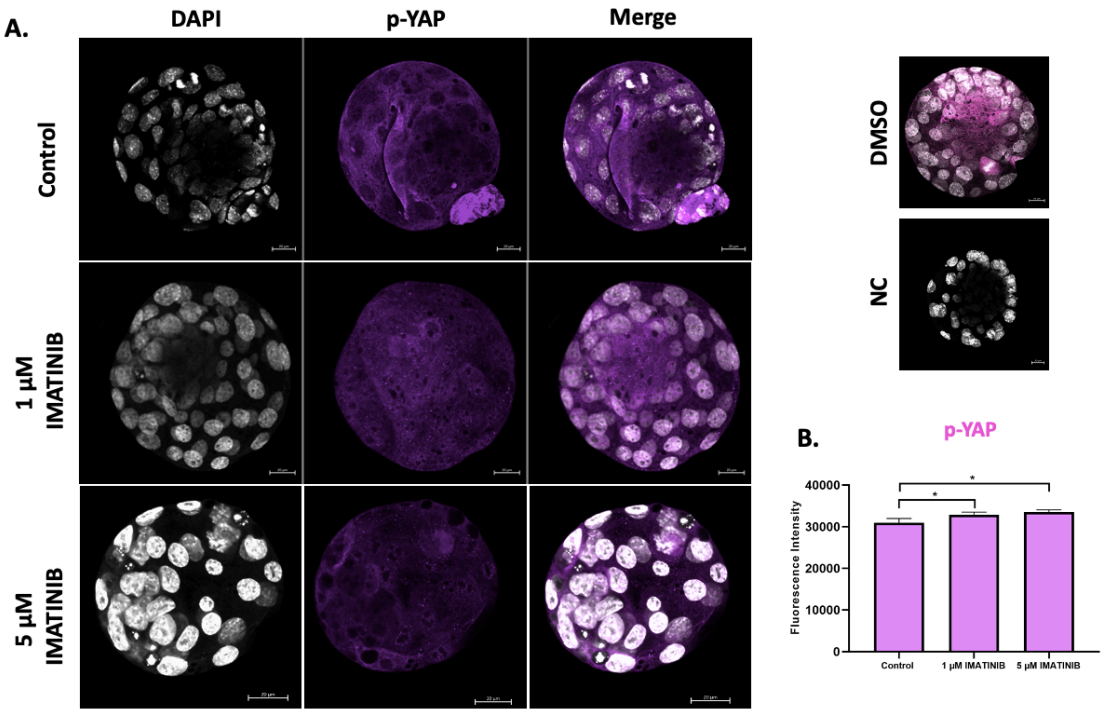

Figure 34: Evaluation of p-YAP localization by immunofluorescence staining in control 1 µM and 5 µM imatinib groups. A. Cellular localizations of p-YAP change with the imatinib treatment. In the control group p-YAP expression pattern was seen in the cytoplasm. In the 1 µM and 5 µM imatinib groups, p-YAP expression pattern was seen in the cytoplasm and peri-nuclear area. B. When the immunofluorescence intensities were examined; It was determined that p-YAP intensity levels increased in imatinib treatments (*p<0.05, ****p <0.0001). (C (control), n=4; 1 µM, n=4; 5 µM, n=4)

Expression of p73 was examined after imatinib treatment. c-Abl is known to perform p73-mediated upregulation of YAP. In the control group, p73 expression was seen intensely in the cumulative cytoplasm expression. p73 expression was also seen in the cytoplasm in the 1 µM and 5 µM imatinib groups. However, the p73 expression levels and cumulative patterns were decreased in the 1 µM and 5 µM imatinib groups compared to the control group **(Figure 35A).** Comparison of p73 immunofluorescence intensity levels between groups showed that p73 expression intensity decreased with imatinib treatment compared to the control group **(Figure 35B).**

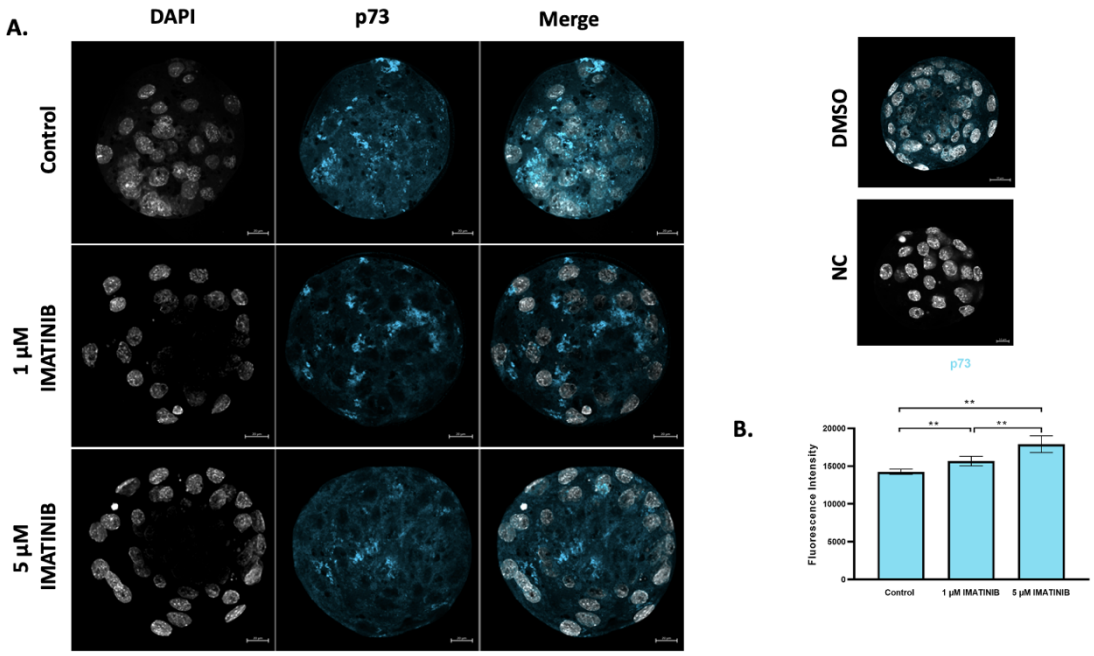

Figure 35: Evaluation of p73 localization by immunofluorescence staining in control, 1 µM and 5 µM imatinib groups. A. Cellular localizations of p73 would change with the imatinib treatment. In the control, 1 µM and 5 µM imatinib groups, p73 cumulative expression pattern was seen in the cytoplasm. B. When the immunofluorescence intensities were examined, it was determined that p73 intensity levels decreased in imatinib treatment groups (****p <0.0001). (C (control), n=5; 1 µM, n=6; 5 µM, n=8)

We detected TEAD4 in the nuclei of TE cells as it should in the control blastocyst. However, after imatinib treatment, it was not detected in the nuclei of TE cells in both 1 µM and 5 µM imatinib groups. In imatinib treatment groups, cytoplasmic TEAD4 localization was determined. Nuclei of TE cells are marked with white arrowheads **(Figure 36A)**. The intensity of the TEAD4 expression pattern was significantly reduced in the imatinib treatment groups compared to the control group **(Figure 36B)**.

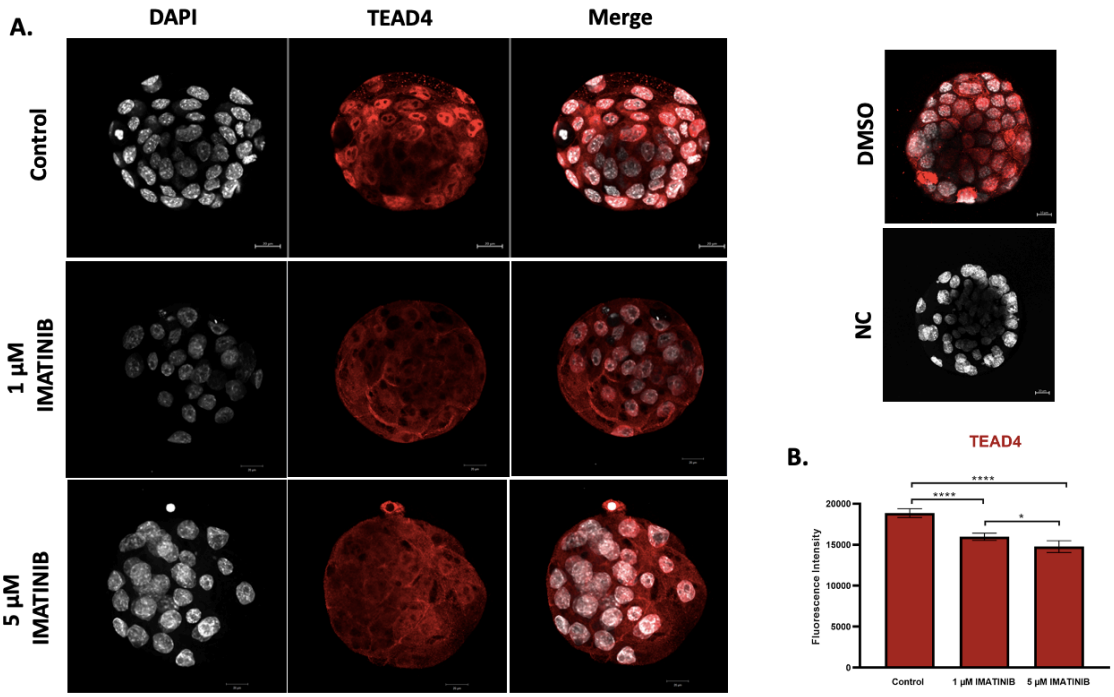

Figure 36: Evaluation of TEAD4 localization by immunofluorescence staining in control, 1 µM and 5 µM imatinib groups. A. Cellular localizations of TEAD4 would change with the imatinib treatment. In the control, 1 µM and 5 µM imatinib groups, TEAD4 expression pattern was seen in the cytoplasm. B. When the immunofluorescence intensities were examined, it was determined that TEAD4 intensity levels decreased in imatinib treatment groups (*p<0.05, ***p <0.001, ****p <0.0001). (C (control), n=4; 1 µM, n=6; 5 µM, n=6)

To demonstrate the effect of imatinib treatment for PARD6 expression, c-Abl and PARD6 expression in control, 1 µM and 5 µM imatinib groups were visualized with a confocal microscope. In the control group, PARD6 localization was intensely determined at the cell borders. It was detected weakly in the cytoplasm of the cells. In the 1 µM and 5 µM imatinib groups, it was determined that PARD6 was more intensely distributed in the cytoplasm **(Figure 37A).** In addition, when immunofluorescence levels were compared, PARD6 was significantly increased in the 1 µM and 5 µM imatinib groups compared to the control group, as it was distributed in the cytoplasm **(Figure 37B).**

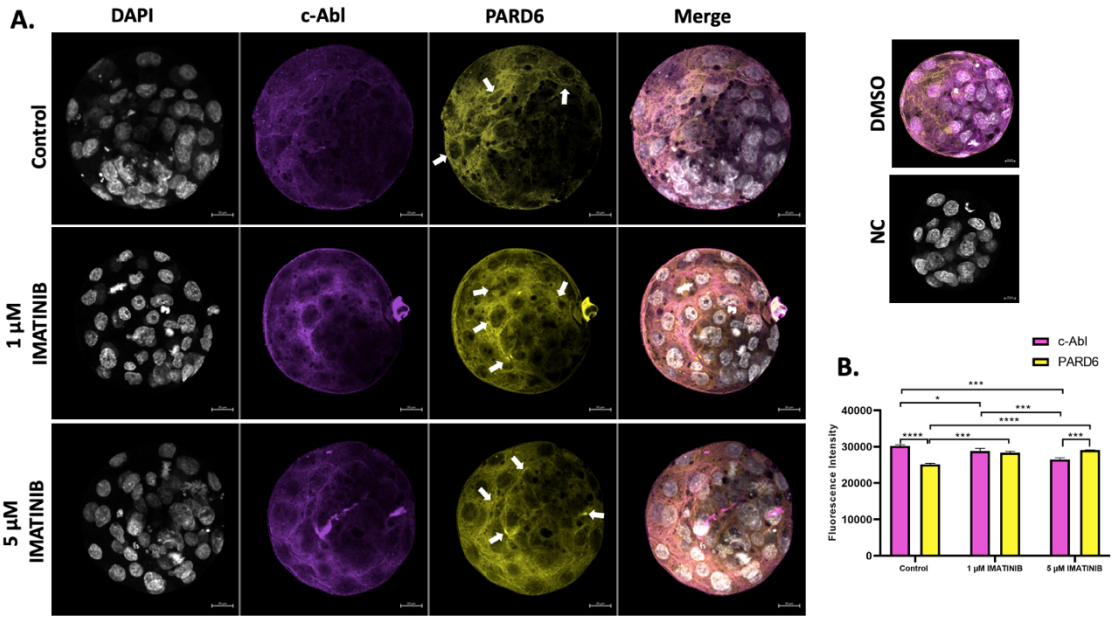

Figure 37: Evaluation of c-Abl and PARD6 localization by immunofluorescence staining in control 1 µM and 5 µM imatinib groups. A. Cell localizations of c-Abl and PARD6 were determined after imatinib treatment. In the control group, PARD6 localization showed intense localization at the borders of the cells, while it was determined that it spread towards the cytoplasm of the cells in the 1 µM and 5 µM imatinib groups. B. PARD6 expression level was significantly increased in the 1 µM and 5 µM imatinib groups (*p<0.*05*, ***p<0.001, ****p<0.0001). (C (control), n=5; 1 µM, n=5; 5 µM, n=5)

E-cadherin expression decreased with increasing imatinib dose **(Figure 38A).** In addition when we used higher zoom in scan area for 63X objective in the confocal microscope, we determined that the filipodial-like structures present in the control groups gradually decreased in the 1 µM and 5 µM imatinib groups. Especially in the 5 µM imatinib group, instead of filipodia structures, the E-cadherin pattern was seen forming chain-like hollow structures at the cell borders **(Figure 38B).** When immunofluorescence intensities were compared between groups; CDX2 and E-cadherin levels were significantly reduced in the 5 µM imatinib group **(Figure 38C).**

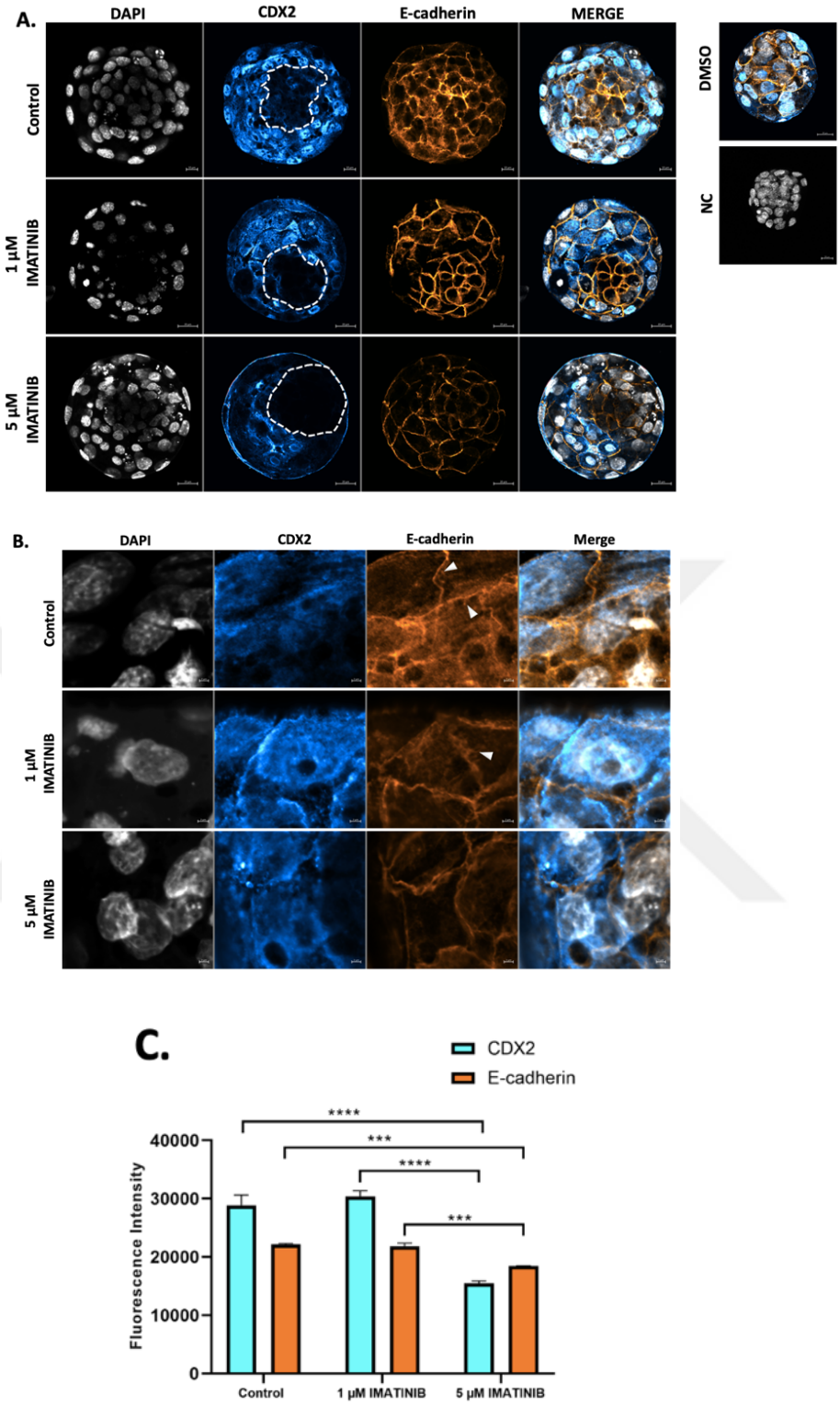

Figure 38: Evaluation of CDX2 and E-cadherin localization by immunofluorescence staining in control 1 µM and 5 µM imatinib groups. A. Cellular localizations of CDX2 and E-cadherin were determined in control, 1 µM and 5 µM imatinib groups. In the control group, CDX2 localization seen in nuclei, while it was determined that it cytoplasm of the cells in the 1 µM and 5 µM imatinib groups. E-cadherin expression was determined at cell borders in all groups. B. E-cadherin and filopodia structures formed between blastomeres were determined. While filopodia structures were visible in the control group, it was seen that

it decreased in the 1 µM group, and the structures took a chain-like shape in the 5 µM group. C. CDX2 expression level was significantly increased in the 5 µM imatinib groups and E-cadherin level was significantly increased in 1µM and 5 µM imatinib groups (***p<0.001, ****p<0.0001). (C (control), n=4; 1 µM, n=4; 5 µM, n=5)

Expression of the ICM marker Nanog was evaluated in the control, 1 µM and 5 µM imatinib groups. After imatinib treatment, Nanog expression was observed especially in the nuclei of TE cells **(Figure 39A).** In addition, when the expression levels were compared, it was determined that Naog expression levels higher in 1 µM and 5 µM imatinib groups than control group **(Figure 39B).**

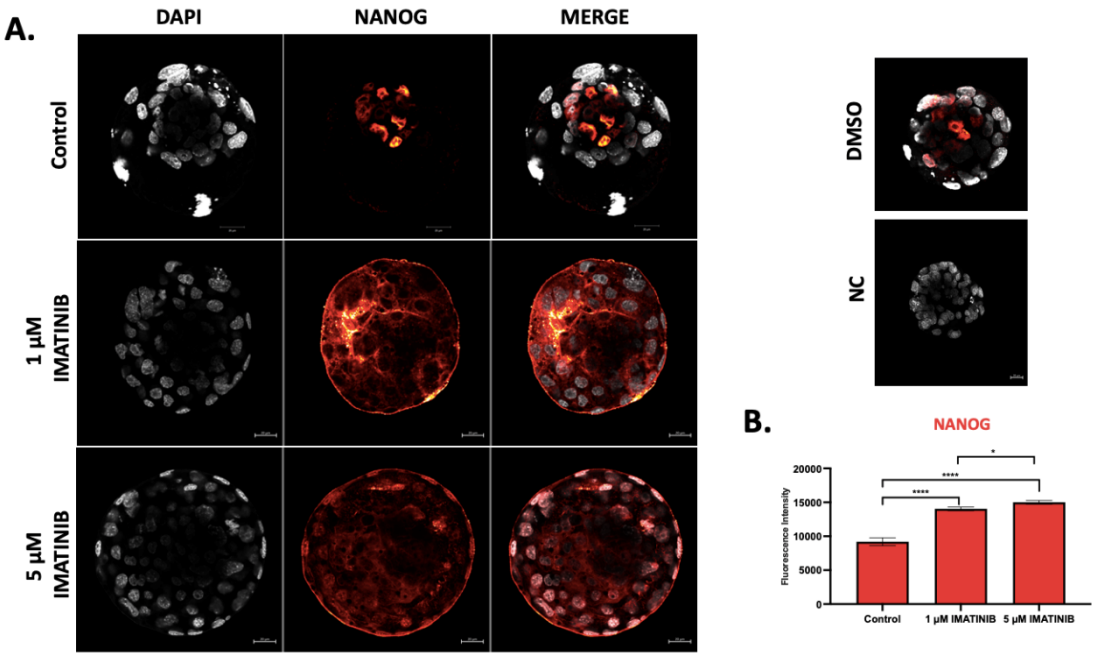

Figure 39: Evaluation of NANOG localization by immunofluorescence staining in control 1 µM and 5 µM imatinib groups. Cellular localizations of NANOG would change with the imatinib treatment. In control group Nanog expression was determined in ICM. In 1 µM and 5 µM imatinib groups NANOGg expression determined in TE, but we determined weak expression in TE cells. B. Comparison NANOG of immunofluorescence intensities between groups (*p<0.05, ****p <0.0001). (C (control), n=3; 1 µM, n=4; 5 µM, n=4)

4.7. Comparison of *c-Abl, Yap, Tead4, Cdx2, Nanog* and *Oct4* mRNA levels in groups after imatinib treatment

After imatinib treatment, *c-Abl, Yap, Tead4, Nanog, Oct4* and *Cdx2* mRNA levels were determined in preimplantation mouse embryos. The markers we evaluated with immunofluorescence staining were translational evaluations. Then, we evaluated the selected markers at the transcriptional level by qRT-PCR. As the dose of imatinib increased, *c-Abl* mRNA level decreased. The level of *Yap* mRNA was significantly reduced in the 5 µM imatinib group, while there was no significant transcriptional difference in the level of *Tead4* mRNA **(Figure 40A).** While no significant change was observed in *Oct4* mRNA level, which is an ICM cell marker, it was determined that *Nanog* mRNA level decreased significantly in the 1 µM and 5 µM imatinib groups. The TE cell marker *Cdx2* was significantly decreased with imatinib concentration **(Figure 40B)**. The results suggest that imatinib treatment may have an effect on TE cell fate determination.

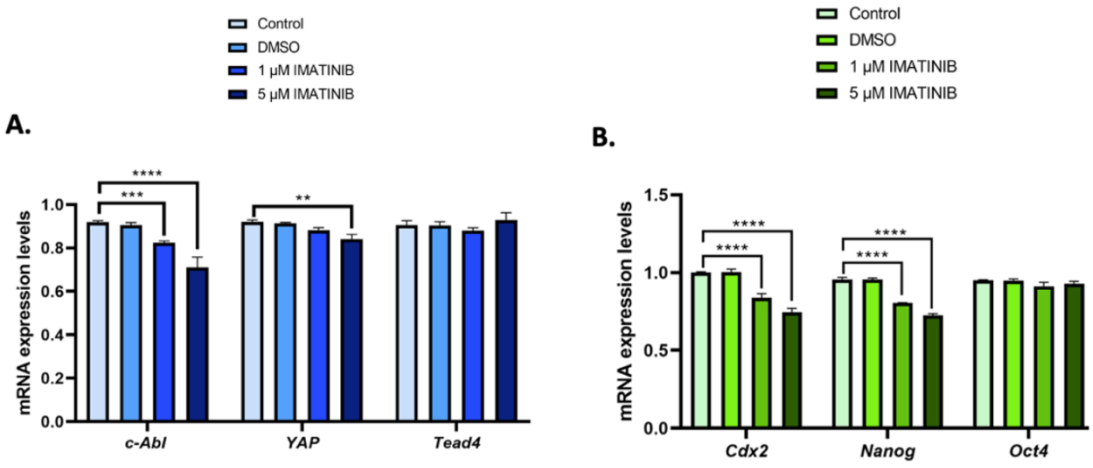

Figure 40: Comparison of *c-Abl, Yap, Tead4, Cdx2, Nanog* and *Oct4* mRNA levels after imatinib treatment (*p<0.05, **p<0.01, ***p<0.001, ****p<0.0001).

4.8. c-Abl siRNA microinjection results

siRNA is a double-stranded RNA (dsRNA) that recognizes and disrupts its homologous RNA, resulting in sequence-specific gene silencing. We suggested that c-Abl siRNA microinjection could be an excellent approach to selectively determine the molecular mechanism of c-Abl with high efficiency and low side effects, thereby establishing a model. In Figure 37, the morphological findings obtained from the control, scrambled and *c-Abl* siRNA microinjection groups are given comparatively. The morphologies of the embryos at each developmental stage were compared **(Figure 35).** No morphological differences were detected between the control, scrambled and c-Abl siRNA groups in the zygote to 2-cell and transition from 2-cell to 4-cell.

During the preimplantation period embryo development, within 12 hours after the transition from the 4-cell to 8-cell, the spaces between the blastomeres disappear and compaction takes place. This stage is also the stage where the blastomeres gain polarization [1,93]. When we looked at the c-Abl siRNA group, it was determined that the embryos stopped at the 4-cell and could not pass to the 8-cell. It was observed that the embryos in the control and scrambled groups could reach the blastocyst **(Figure 41).**

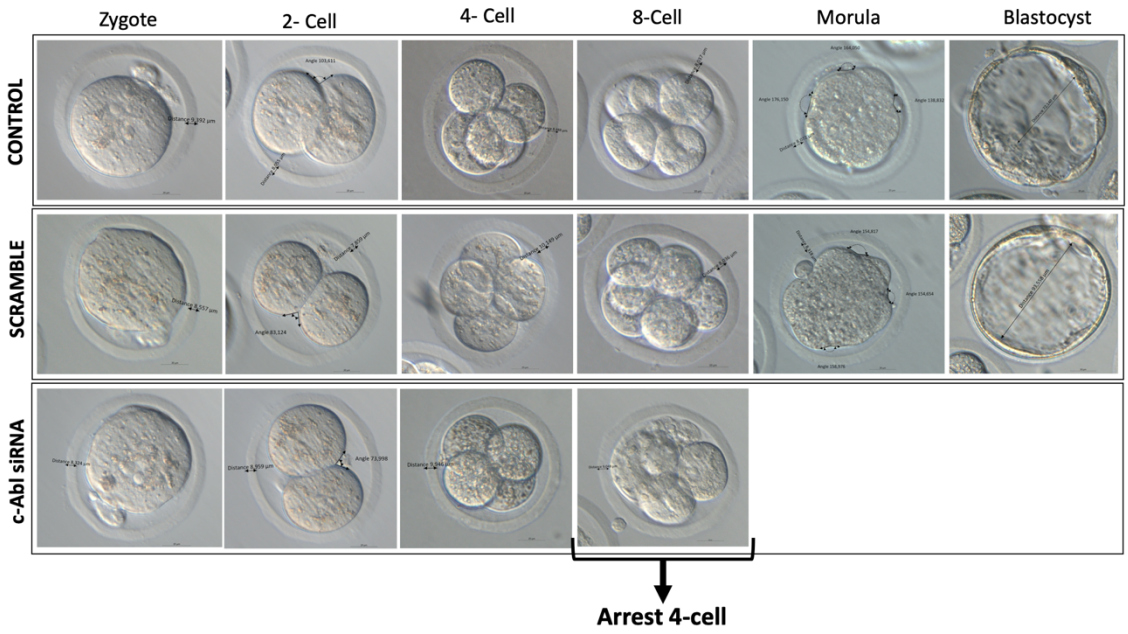

Figure 41: Morphological comparison of developmental potentials of embryos in control, scrambled, c-Abl siRNA groups. (3 different siRNA injection were assessed for evaliation of average developmental potential).

In the group in which c-Abl was silenced by siRNA injection, it was observed that the embryos could not develop beyond the 4-cell. In the control, scrambled and *c-Abl* siRNA groups, the zona pellucida thickness of the embryos and the angle between the blastomeres at the 2-cell were compared. As a result of morphokinetic analysis, no significant difference was determined between the groups **(Figure 42).**

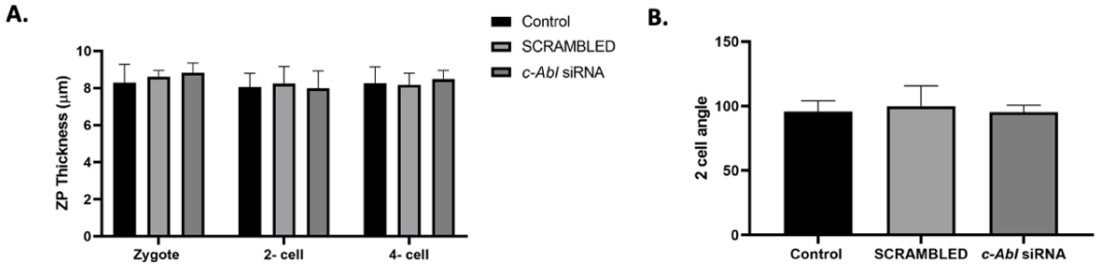

Figure 42: Morphokinetic evaluation of embryonal development following c-Abl siRNA microinjection. A. Comparison of ZP thickness of embryos between control, scrambled and c-Abl siRNA groups. B. Comparison of the interblastomere angle in 2-cell embryos between control, scrambled and c-Abl siRNA groups.

4.9. Evaluation of qRT-PCR results after *c-Abl* siRNA microinjection

c-Abl, Yap, Tead4, Nanog, Cdx2 and *Oct4* mRNA levels were determined in control, scrambled and *c-Abl* siRNA groups and the groups were compared. No significant difference was determined between the groups **(Figure 43).**

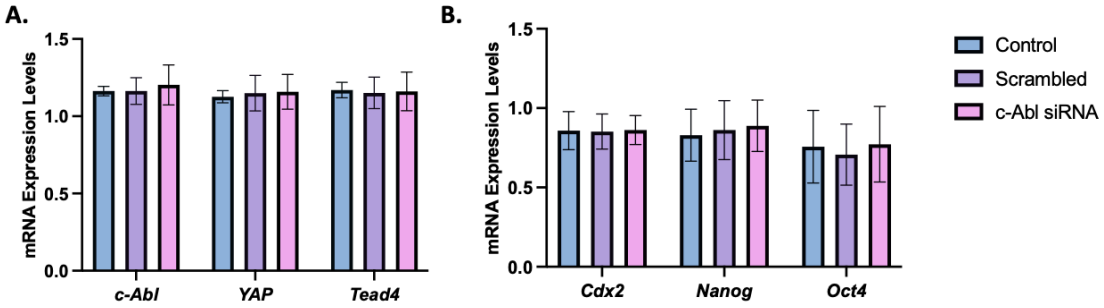

Figure 43: Comparison of *c-Abl, Yap, Tead4, Cdx2, Nanog* and *Oct4* mRNA levels in embryonal development following c-Abl siRNA microinjection. A. Comparison of *c-Abl, Yap* and *Tead4* mRNA levels in experimental groups. B. Comparison of *Nanog, Cdx2* and *Oct4* mRNA levels in experimental groups.

4.10. Analysis of area and apoptosis of PDGF-AA and imatinib treated groups

4.10.1. Analysis of cell area measurements of blastomers

After PDGF-AA and imatinib treatment, the blastomere areas of embryos that reached the blastocyst were measured **(Figure 44)**, and the groups were compared. After calculating the blastomere areas, it was observed that the blastomere areas were significantly reduced in both PDGF-AA treatment groups and imatinib treatment groups **(Figure 45)**.

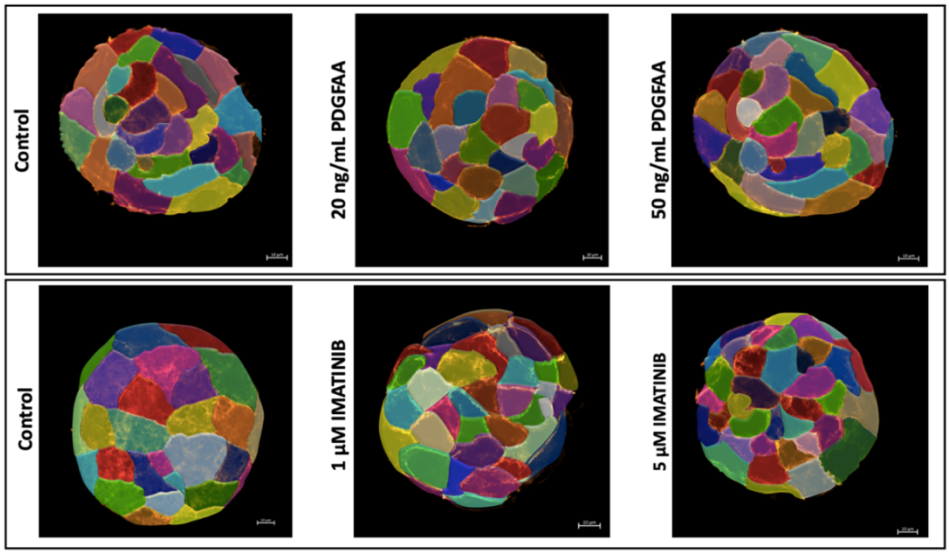

Figure 44: The figure shows the areas of blastomeres measured in embryos developing the blastocyst in the PDGF-AA and imatinib groups.

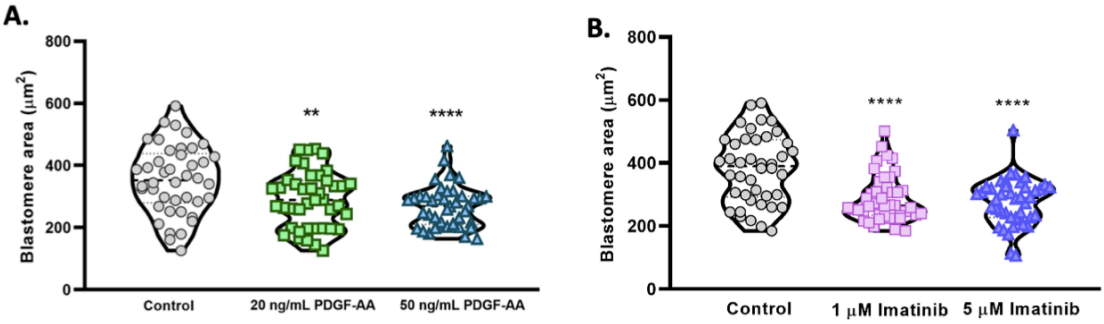

Figure 45: Comparison of area measurements of blastomeres in embryos developing blastocyst in PDGF-AA and imatinib groups. A. After PDGF-AA treatment, blastomere areas were significantly reduced in the 20 ng/mL and 50 ng/mL PDGF-AA groups. B. After imatinib treatment, blastomere areas were found to be significantly reduced in the 1 µM and 5 µM imatinib groups (n=44) (**p<0.01, ****p<0.0001).

4.10.2. Counting the Number of Cell Nucleus in the Blastocyst

After PDGF-AA treatment and imatinib treatment, nuclei of embryos reaching blastocyst were counted, their core areas were measured, and comparisons were made between groups. Considering the number of nuclei, there was no significant difference in the c PDGF-AA treatment compared to the control groups, while the number of nuclei in the 5 µM imatinib group from the imatinib treatment groups was significantly reduced **(Figures 46A and 46B)**. When the areas of nuclei were compared between the groups, no significant difference was determined **(Figure 46C).**

A. **Nucleus Number**

	Embriyo 1	Embriyo 2	Embriyo 3	Embriyo 4	Embriyo 5	Embriyo 6	Embriyo 7	Embriyo 8	Embriyo 9	Embriyo 10
Control	40	37	53	52	51	31	56	41	58	49
20 ng/ml PDGF-AA	41	30	42	28	51	39	36	34	49	53
50 ng/ml PDGF-AA	24	43	51	52	44	41	39	33	50	49
1 µM IMATINIB	50	39	45	31	33	38	36	38	35	39
5 µM IMATINIB	36	40	23	38	49	36	42	34	25	35

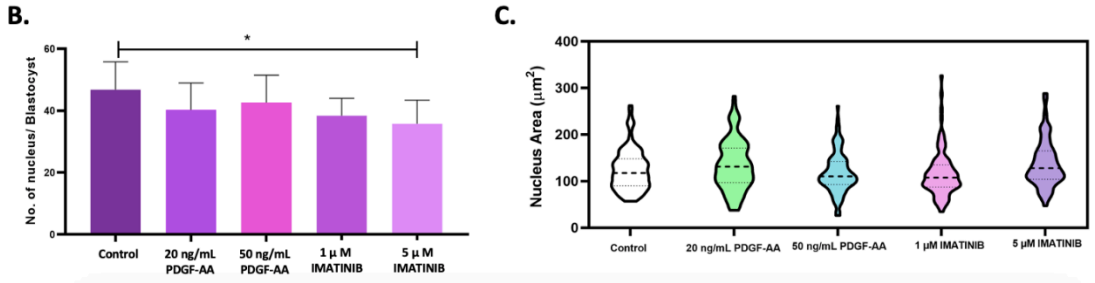

Figure 46: Comparison of the number of nuclei and area measurements of nuclei in embryos that can reach the blastocyst in the PDGF-AA and imatinib groups. The number of nucleus and the area of nucleus did not differ significantly in the 20 ng/mL and 50 ng/mL PDGF-AA groups. After imatinib treatment, the number of nuclei in the 1 µM and 5 µM imatinib groups was significantly reduced in the 5 µM imatinib group, while the core areas did not show a significant change (*$p<0.05$).

4.10.3. Analysis of Apoptotic Bodies in Embryos

After PDGF-AA treatment and imatinib treatment, we visualized the apoptotic bodies that we determined as a result of immunofluorescent staining **(Figure 47)**. We counted the apoptotic bodies in all experimental groups as schematized in Figure 32, then compared them numerically between groups **(Figures 48A and 48B).** We determined that apoptotic bodies increased significantly especially in the 20 ng/mL PDGF-AA group and in the 5 μM imatinib group **(Figure 48C).**

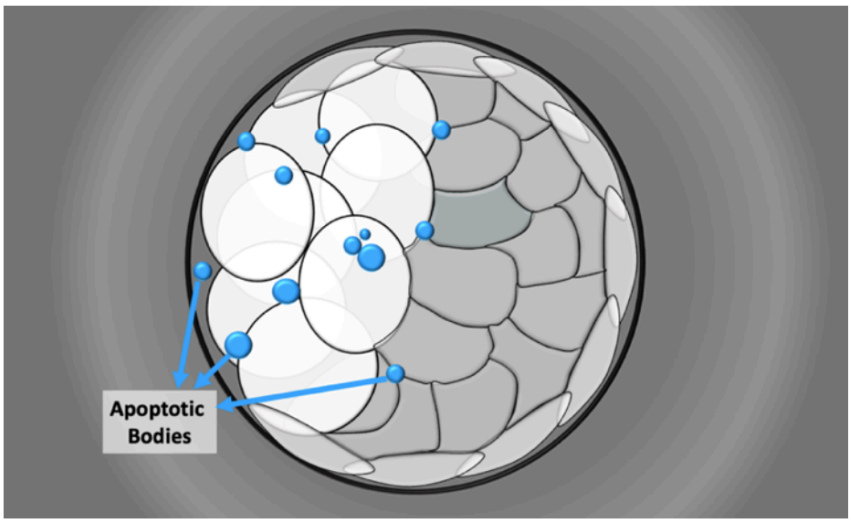

Figure 47: Apoptotic bodies identified in preimplantation embryos developing through the blastocyst.

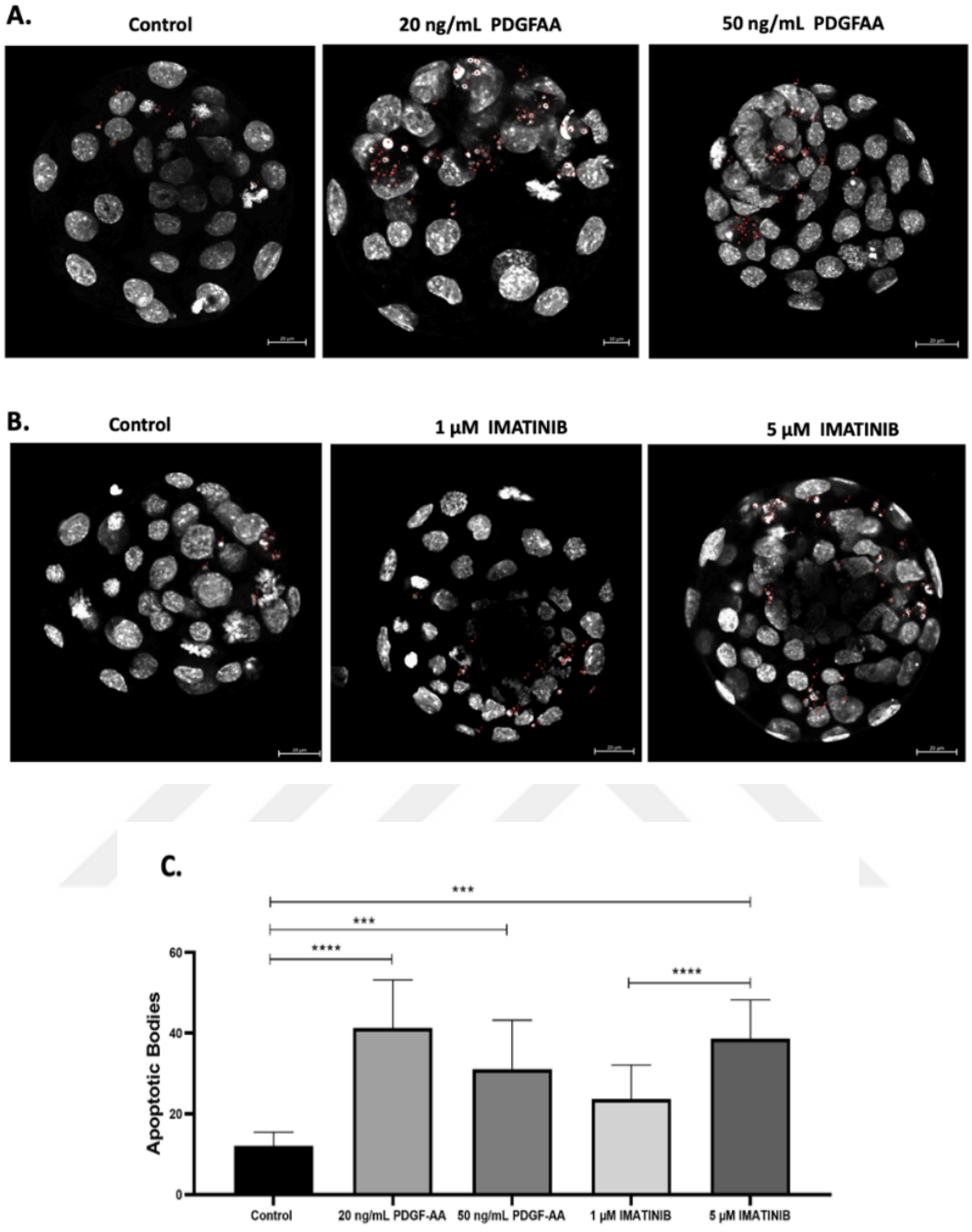

Figure 48: Image of apoptotic bodies formed in embryos reaching blastocyst in PDGF-AA and imatinib groups and comparison between groups. A. PDGF-AA treatment and B. imatinib treatment followed by apoptotic bodies in groups. C. Apoptotic bodies were significantly increased in the 20 ng/mL PDGF-AA group and the 5 µM imatinib group (**p<0.01, ****p<0.0001).

5. DISCUSSION

Early embryonic development is a complex process that involves the progression of a single-cell zygote, formed through fertilization, into multicellular stages through numerous mitotic divisions. Understanding the mechanisms involved in this process is a fundamental question in developmental biology. Key mechanisms in embryonic development include zygotic genome activation, polarization, compaction, determination of cell fate, and the formation of the blastocyst. Following fertilization, an 8-cell embryo is formed after three mitotic divisions. Mechanisms for polarization and compaction are established in the late 8-cell. Subsequently, the fate of TE cells, which contribute to placental development, and ICM cells, which contribute to embryonic development, is determined [91]. Although embryonic development occurs synchronously in terms of morphokinetics, the developmental potential exhibited by individual embryos can vary molecularly. This raises the question of how equal and homogeneous the blastomeres are in terms of the mechanisms involved in embryonic development. The embryo at the zygote lacks polarity. Acquisition of polarization by the embryo occurs as the embryonic process progresses. Therefore, the process of polarization is a crucial mechanism in embryonic development [13].

Both PDGF-AA and imatinib treatment were applied to determine the effect of c-Abl tyrosine kinase on morphology during preimplantation embryo development. In addition, the N-terminus from the SH3 domain was targeted with *cAbl* siRNA. The c-Abl tyrosine kinase is involved in various cellular processes including but not limited to the halt of cell division in response to DNA damage, facilitation of DNA repair mechanisms, control of programmed cell death, cell proliferation, and safeguarding genomic integrity [221]. In our study, we hypothesized that c-Abl could be involved in determining cell fate through a p73/YAP-mediated pathway. Therefore, we aimed to demonstrate the functional role of c-Abl in preimplantation embryonic development. After culturing zygotes with PDGF-AA and imatinib until the blastocyst stage, we compared the differences observed in c-Abl/p73/YAP-mediated embryos. In addition to targeting the activation domain and ATP-binding site, we manipulated the N-terminal region of the c-Abl SH3 domain through c-Abl siRNA microinjection. As a result of our study, we completed evaluations regarding the markers of crucial events in determining cell fate when developing to the blastocyst from zygote.

PDGF-AA has been shown in studies to activate c-Abl, and this activation is dependent on the activity of Src tyrosine kinase. In response to PDGF, it affects the

reorganization of the cellular cytoskeleton and entry into the S phase. Activation of Abl leads to the mediation of signaling pathways associated with cell morphology and cell motility, which are also influenced by receptor molecules attached to the cell membrane [154]. The specific function of PDGF-AA treatment in preimplantation embryonic development has not been entirely elucidated. Tyrosine kinases act as catalysts, mediating the transfer of a phosphate group from ATP to the amino acid tyrosine. Imatinib, in particular, selectively attaches itself to the region situated between the N- and C-lobes within the kinase domain of Bcr-Abl. Imatinib, the initial treatment identified as an ATP binding inhibitor for abl, finds extensive application in the management of Chronic Myeloid Leukemia (CML). The efficacy of imatinib in CML therapy emphasizes the potential of targeting c-Abl in particular disease contexts [129-131]. The differences between Bcr-Abl and c-Abl occur above the SH3 domain, and therefore, imatinib inhibits c-Abl by targeting its kinase domain. By binding to the kinase domain, imatinib prevents the activation of downstream signaling pathways associated with aberrant tyrosine kinase activity [222]. Imatinib also binds to the ATP-binding site, leading to the enzyme remaining in an inactive conformation. In the process, Abl inhibition can occur through two mechanisms: 1) Phosphorylation of the activation loop is a dynamic process and can be transiently suppressed. Imatinib binds to the enzyme, resulting in decreased kinase activity. 2) Imatinib can bind to newly synthesized Bcr-Abl kinase and prevent its activation if it does not allow phosphorylation and modification. [138]. This highlights the importance of Abl in regulating actin dynamics and cellular processes involved in tissue development and organization.

In the PDGF-AA treatment experimental groups, we did not find any significant differences in the morphological findings, except for an increase in the angle between blastomeres in the 2-cell embryo. The increase in blastomere angle at the 2-cell stage suggested a tendency for slower transition to the 4-cell stage. After imatinib treatment, morphological evaluations were performed. In our experiments to determine the imatinib dose, we incubated with 10 μM, 20 μM, and 50 μM imatinib treatment. However, embryos were not developed in the 10, 20, and 50 μM imatinib groups. Therefore, we determined our imatinib doses for embryo development evaluation as 1 μM and 5 μM. Compared to the control group, the proportion of arrested embryos was significantly higher in the 1 μM and 5 μM imatinib groups. The number of developing embryos into the blastocyst stage decreased according to the imatinib dose increased. Morphokinetic evaluations revealed a reduction in the angle between blastomeres at the morula stage

with higher imatinib doses, indicating that the blastomeres in the morula stage embryo were not compacted. It was suggested that the reason for compaction failure could be due to the inability to form connections between blastomeres, a decrease in the number and density of filopodia, and the deficiency of blastomeres to merge their boundaries.The sharper boundary and lower angle between blastomeres suggest that intercellular connections were not established. In the 10 μM imatinib group, embryos could not complete the transition from the morula to the blastocyst. Embryos in the 10 μM imatinib treatment group did not exhibit similar morphology as control embryos. The inability to progress from the morula to the blastocyst indicated that c-Abl may play an important role in compaction.

After PDGF-AA treatment and imatinib treatment, *c-Abl* was targeted from the N-terminal end of the SH3 domain mediated by siRNA. As a result of the morphological evaluation, it was observed that there was 4-cell arrest in the embryos. Development to the 8-cell could not be achieved. The use of siRNA microinjection as a sensitive and specific gene silencing method explains the cessation of development in earlier stages seen in the imatinib treatment. Furthermore, it was determined that imatinib dose of 10 μM or higher, similar to the specific region-based c-Abl siRNA microinjection, halted development. The SH3 domain contains protein-binding peptide motifs in the cell. In addition, the SH3 region of c-Abl plays an actin regulatory role in the cell by working with actin, microtubules and the Ena/VASP family member [223,224]. The results indicated the potential significance of silencing *c-Abl* by targeting the SH3 region N-terminus site, especially concerning processes like polarization and compaction.

PDGF-AA treatment and imatinib treatment may play a role in determining cell fate by influencing the localization of markers involved in important stages of preimplantation embryo development. Based on this suggestion, we evaluated specific stages in preimplantation embryo development such as polarization, compaction, and ICM/TE cell markers by immunofluorescence staining. Especially we evaluated members of the Hippo signaling pathway, YAP-TEAD, was performed in the groups where PDGF-AA treatment and imatinib treatment were carried out.

The PDGF-AA treatment represents an important mechanism in intracellular signal transduction and regulation of biological responses. The lack of nuclear localization of c-Abl observed in some cells of the control group, particularly in the 20 ng/mL PDGF-AA group, and its presence in the cytoplasm and membrane, indicates the involvement of PDGF-AA-mediated c-Abl in membrane ruffling events during preimplantation embryo

development. Firstly, c-Abl localization was evaluated following PDGF-AA treatment. It has been shown that PDGF-AA treatment may caused c-Abl tyrosine kinase membrane ruffling. Membrane ruffling refers to the dynamic protrusion and retraction of the cell membrane, which is important for cell migration and changes in cell shape. c-Abl's involvement in membrane ruffling suggests its role in regulating cytoskeletal dynamics and cell movement [154]. In the imatinib treatment groups, examination of c-Abl localization revealed that in the control group, c-Abl appeared membranous and additionally localized in the nuclei of dividing cells. It was also observed as an intercellular extension structure between blastomeres. Furthermore, in the 1 and 5 μM imatinib groups, a decrease in c-Abl expression intensity was observed. Considering that imatinib treatment leads to a weakened expression pattern, which is observed in blastocysts.

It is known that c-Abl directly phosphorylates and stabilizes the transcriptional co-activator *Yap1*, thereby contributing to the selective transcriptional co-activation of proapoptotic target genes of p73 [9]. In the control group, as expected, YAP localization was observed in the nuclei of TE cells. However, after PDGF-AA treatment, YAP translocated to the cytoplasm. Following imatinib treatment, the translocation of YAP to the cytoplasm decreased compared to the PDGF-AA group. In the imatinib treatment groups, YAP expression was preserved in the nucleus, but the expression intensity level decreased compared to the control group. These results suggest that c-Abl can determine the localization of YAP during preimplantation embryo development. The significance of YAP localization as an important marker in preimplantation embryo development which supports the idea that c-Abl tyrosine kinase can regulate cell fate through YAP signaling.

The C-lobe of c-Abl is the lobe that participates in the active site in terms of the activation cycle, which is a dynamic structural feature for many kinases. In the Abl activation cycle, phosphorylation of a single tyrosine residue is sufficient to induce the open conformation of the active site through electrostatic interactions with a neighboring arginine [225]. After PDGF-AA treatment and imatinib treatment, we evaluated the phosphorylated form of c-Abl at the Tyr393 site. In the PDGF-AA treatment groups, no changes were observed in the phosphorylated form of c-Abl (Tyr393) that could be regulated by PDGF-AA. This suggests that PDGF-AA does not affect the phosphorylation of the c-Abl Tyr393 region. The Tyrosine 393 (Tyr393) site of c-Abl is located in the activation loop of the Bcr-Abl kinase domain, and its phosphorylation signifies the opening of the activation loop region. When phosphorylated, imatinib cannot access the Tyr393 region of the Bcr-Abl kinase domain. This condition leads to a decrease in the inhibitory function of imatinib [226]. The lack of change in p-cAbl expression at a dose of 1 uM in the Imatinib treatment groups indicates that Imatinib cannot reach and affect this phosphorylated region. However, the decrease in p-cAbl at 5 uM Imatinib suggests that a higher dose of imatinib partially affects the activation of the Tyr393 region.

In our study, we evaluated the impact of PDGF-AA treatment and imatinib treatment on YAP phosphorylation during preimplantation mouse embryo development. In the PDGF-AA treatment groups, the dose-dependent changes in YAP phosphorylation levels suggest that PDGF-AA induces different molecular conformations of c-Abl in preimplantation embryos, which, although not affecting the localization of phospho-YAP, alters its intensity levels. In the imatinib treatment groups, the nuclear localization of phospho-YAP, in addition to its cytoplasmic localization, indicates that imatinib treatment through imatinib binding to the ATP-binding site triggers nuclear entry independently of the Hippo signaling pathway. Since the external conditions in the culture environment are constant, these changes in phospho-YAP levels and localization suggest that they occur at the biochemical level. YAP phosphorylation is regulated by the Hippo signaling pathway at the biochemical level [227]. At the mechanical level, the regulation of YAP activity is influenced by various mechanical cues, including extracellular matrix (ECM) stiffness, shear stress, and cell adhesion area. Cells can respond according to the physical characteristics of their environment. These mechanical cues can influence YAP localization and activity [228-230]. The mechanical regulation at the cellular level encompasses various components, including cell cytoskeletal integrity, adhesive structure

of the cytoskeleton, myosin contractility, and other force-generating mechanisms [228,230,231]. Another factor involved in the regulation of YAP localization is other kinase families, including NLK and the Src kinase family [232,233]. Phosphorylation of YAP on Serine residues serves as a negative regulator for maintaining YAP in a stable state. Additionally, phosphorylation of tyrosine 357 by Src is associated with nuclear localization and increased YAP activity [233,234]. The interaction between the transcription factors YAP and TEAD of pY357-YAP at high levels was observed in human muscle cells with the $LMNA^{\Delta K32}$ gene mutation, resulting in nuclear retention. [235]. In a study conducted with human muscle stem cells, it was shown that treatment with Dasatinib (a Src family kinase inhibitor) led to the translocation of pY357-YAP into the nucleus [235]. Based on our findings, the regulation of YAP phosphorylation and its nuclear-cytoplasmic localization remains uncertain in terms of the molecular signals involved.

Studies conducted to date have mostly evaluated the localization of p73 over the apoptotic pathway. During the preimplantation embryo development, there is a lack of literature information regarding the pattern of p73. However, changes observed in the cytoplasmic localization of p73 in both PDGF-AA treatment and imatinib treatment groups. p73 is exported to the cytoplasm during preimplantation embryo development, and this cytoplasmic export is likely to be crucial for the interaction and modulation of proteins such as c-Abl, YAP, and p73. Studies have reported that p73 acts as a transcription factor that binds to DNA and facilitates the transcription of genes such as p21 and Bax. It maintains this role while being localized in the nucleus [236]. It has also been reported that p73 promotes apoptosis through nuclear and non-nuclear pathways. In the non-nuclear pathway of p73, it has been reported that there is a direct translocation in the mitochondria, thus localizing in the cytoplasm [237]. Considering that c-Abl and YAP can localize both in the cytoplasm and the nucleus based on their functions, the following question arises: In which cellular compartment do c-Abl and YAP interact with p73? To determine this, we examined the localization of p73 using immunofluorescence staining under a confocal microscope in preimplantation embryos subjected to both PDGF-AA treatment and imatinib treatment. Upon analyzing the results, we found that in both cases, p73 was localized in the cytoplasm. In the PDGF-AA treatment group, we observed a decrease in p73 expression as the dosage of PDGF-AA increased. Conversely, in the groups where imatinib treatment, an increase in p73 levels compared to the control group was detected. This finding suggests that c-Abl may affect the retention of p73. Furthermore, we proposed that c-Abl has a greater impact on the cytoplasmic

transcriptional activity of p73 rather than its nuclear apoptotic activity. It has also been suggested that p73 may present its functional role through endoplasmic reticulum ot mithochondria in the preimplantation embryos.

The findings obtained suggest that the subcellular localization of TEAD4 changes between the nucleus and cytoplasm during preimplantation embryo development. When considering the studies, it can be seen that the differential expression of TEAD4 between ICM and TE cells is determined by the cooperative action of components in the Hippo signaling pathway. In our study, the regulation of TEAD coactivation by c-Abl-mediated YAP was investigated. The localization of TEAD4 was examined during preimplantation embryo development following PDGF-AA treatment and imatinib treatment. In the groups where PDGF-AA-treatment was performed, TEAD4 localization was determined in the cytoplasm of TE cells in response to PDGF-AA treatment. This cytoplasmic distribution of localization resulted in an increase in expression intensity. In the imatinib treatment groups, similar to the PDGF-AA treatment group, TEAD4 localization was observed to be distributed in the cytoplasm of TE cells. This indicates that changes occurring in c-Abl significantly affect the subcellular localization of TEAD4.During preimplantation embryo development, the molecular mechanisms of transcription profiles differ between inner and outer cells. Positive TEAD4 localization is observed in the nuclei of blastomeres at various stages of development, including the 4-cell, 8-cell, morula, and blastocyst in mice. This finding suggests that TEAD4 expression is initiated during EGA and structurally maintained in the nucleus [238]. There are studies indicating that transcription of TEAD4, which is a specific marker for the TE, is directly regulated by TEAD4 itself [239]. In another study conducted using Human embryonic kidney 293 cells (HEK293A) cells, after treatment with NaCl, TEAD4 was found to localize not only to the nucleus but also to the cytoplasm [240]. As observed in different studies, it is not possible to evaluate the subcellular localization of TEAD4 through a single signaling pathway.

Considering the roles of c-Abl tyrosine kinase and PARD6 in polarity, there are notable commonalities. PARD6 has been shown to participate in the establishment of cellular non-muscle myosin-mediated polarity, while Abl tyrosine kinase's roles in determining polarity and AJ localization may involve similar mechanisms. Moreover, manipulation of c-Abl tyrosine kinase during preimplantation embryo development could potentially impact the formation of junctions between blastomeres and the apical accumulation of PARD6. Although the localization of PARD6 was preserved in the apical

region upon PDGF-AA treatment, it was observed to be distributed in the cytoplasm as well. The disruption of PARD6 in conjunction with imatinib treatment, similar to PDGF-AA treatment groups, may play an important role in determining cell fate. The cessation of development after the 4-cell in preimplantation embryos where c-Abl tyrosine kinase was silenced by siRNA implies that blastomere polarization may not be achieved. Polarity formation is achieved through actomyosin-mediated cortical dynamics that physically transport anterior PAR protein complexes to the front of the cell [241,242]. It has been proposed that although PARD6 localizes in both the nucleus and cytoplasm, it is not actually a shuttle protein. In order to examine the dynamic localization of PARD6 and determine whether it undergoes shuttling between the cytoplasm and nucleus or remains stably localized in both compartments, researchers treated MDCK and HeLa cells with leptomycin B (LMB), a specific inhibitor of CRM1-mediated nuclear export [243]. According to the results, they demonstrated that the nuclear and cytoplasmic localization of PARD6 (and membrane-associated PARD6 localization in MDCK cells) remained unchanged after treatment with LMB in both cell types. However, in cells expressing GFP-tagged PARD6 stably, they showed that LMB caused the accumulation of the overexpressed protein in the nucleus [243]. Studies on Abl in the context of polarity have shown that loss of Abl disrupts actin organization-mediated cell coordination in various epithelial tissues, including ovarian follicle cells, neural development during embryogenesis, and embryonic epidermis [244,245]. Considering the crosstalk between c-Abl and cellular cytoskeletal dynamics, it can be anticipated that manipulations such as PDGF-AA treatment and imatinib treatment may alter the localization of PARD6 during embryonic development **(Figure 49).**

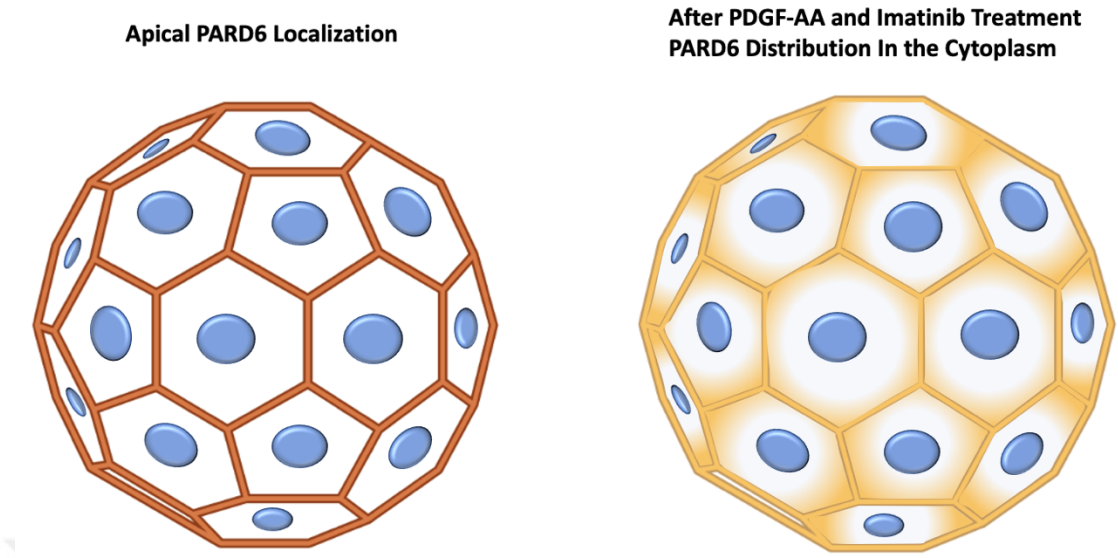

Figure 49: Cellular distribution of PARD6 following PDGF-AA treatment and imatinib treatment in mouse blastocyst. Following PDGF-AA treatment and imatinib treatment, the localization of PARD6 in the blastomeres shifts from the apical region to the cytoplasm.

Cdx2 is activated through the YAP/TEAD4 pathway and serves as a key regulator of TE fate. The activation of *Cdx2* by YAP/TEAD4 plays a crucial role in determining the TE lineage during early embryonic development [98]. When we look at the mechanism, it is known that *Cdx2* is regulated by OCT4 and NANOG [99]. An analysis of the groups in which PDGF-AA treatment was performed revealed that CDX2 expression was appropriately localized in the nuclei of TE cells. This suggests that PDGF-AA treatment does not induce any transcriptional changes in TE cells. However, in the imatinib treatmen groups was performed using 1 µM and 5 µM imatinib, CDX2 expression did not exhibit nuclear localization in TE cells. These results indicate that imatinib treatment induced changes at the transcriptional level in TE cells. The observation of CDX2 in the cytoplasm following imatinib treatment suggests that c-Abl normally plays a role in facilitating the nuclear localization of CDX2 in preimplantation embryos. On the other hand, imatinib treatment could hinder the nuclear functions of CDX2. Considering all these possibilities, it is possible that c-Abl interacts with other factors or serves as a marker that regulates the nuclear localization of CDX2. The imatinib treatment may disrupt this interaction, leading to the translocation of CDX2 from the nucleus to the

cytoplasm. The imatinib treatment could trigger the transition of CDX2 from the nucleus to the cytoplasm by blocking an active process in the nucleus. However, further research is needed to elucidate this mechanism observed during preimplantation embryonic development.

E-cadherin expression is observed in the early stages of embryonic development. Initially, it is maternally provided within the oocyte, and the synthesis of new E-cadherin in the zygote commences during the 2-cell embryo [30]. Zygotes that lack E-cadherin expression cannot maintain their viability during the early stages of embryonic development. Although they undergo compaction facilitated by maternal E-cadherin, they are unable to successfully develop to the blastocyst [246]. In the 2-cell, when E-cadherin is silenced by siRNA in one blastomere, the blastomeres lacking E-cadherin are unable to integrate into the developing embryo during the compaction [219]. It has been noted that in embryos lacking E-cadherin both maternally and zygotically, the formation of the blastocyst structure is impaired, and the blastomeres appear as loose cell clusters instead of compacting [34]. Previous studies have demonstrated the essential role of Abl tyrosine kinases in the maintenance of adherens junctions. To investigate the impact of Abl kinases on adherens junction stability, researchers employed imatinib to inhibit Abl activity in Nara Bladder Tumor II (NBT-II) epithelial cells. Following a 6-hour treatment of STI571, a reduction in the levels of β-catenin and E-cadherin, along with disrupted localization of adherens junctions, was observed [128]. The downregulation of Abl/Arg expression using RNAi in MCF-10A cell lines has shown a decrease in E-cadherin levels in cell-cell adhesion. These results indicate the role of the Abl family and kinase activity in the formation of adherens junctions [128]. In the PDGF-AA treatment groups blastocyst embryo has been shown to result in a dense localization pattern of E-cadherin at cell boundaries. However, upon imatinib treatment, a weakening of E-cadherin expression and the formation of a chain-like pattern were observed. It is expected that E-cadherin, as an intercellular junction complex, should be localized on the cell membrane with a regular and homogeneous distribution. The increase in E-cadherin localization on the cell membrane upon c-Abl activation suggests that c-Abl may have an enhancing effect on the translocation of E-cadherin to the membrane and its synthesis. On the other hand, imatinib treatment resulting in reduced membrane localization of E-cadherin and the formation of a chain-like structure indicates that imatinib treatment may disrupt the integrity of E-cadherin. The imatinib treatment could prevent E-cadherin from remaining on the membrane or hinder its targeting to the membrane. These findings suggest that c-

Abl may have a mechanism supporting the membrane retention or stabilization of E-cadherin in preimplantation embryos.

In our study, we found that PDGF-AA treatment resulted in an increase in filopodia formation during the blastocyst of preimplantation embryos. However, in the groups imatinib treatmen, a decrease in filopodia structures was observed. Recent research has revealed that in addition to its presence at adherens junctions, E-cadherin is also found in elongated cellular extensions known as 'filopodia,' especially during the compaction process [219]. Lamellipodia and filopodia are membrane protrusions that form at the leading edges of cells to facilitate cell migration [247]. These filopodia extend from the contact points of the blastomeres towards the membranes of neighboring blastomeres, and E-cadherin attaches to these regions through trans-interactions. Filopodia maintain tension on the blastomere membranes, bringing them closer together and facilitating compaction [219]. Previous studies have shown that PDGF-AA induces the formation of lamellipodia in MDA-MB-231 cells [248,249]. These findings suggest that c-Abl plays a role in filopodia formation and dynamics. Considering that c-Abl is an important protein kinase involved in cell migration and cytoskeleton regulation, it is plausible to speculate that it is also involved in the mechanisms of filopodia formation in preimplantation embryos. PDGF-AA treatment may stimulate and promote filopodia through affected signaling pathways within the cells. Similarly, imatinib treatment may impact the intercellular filopodia mechanisms, leading to their decrease. Since a decrease in filopodia impairs successful compaction, we propose that E-cadherin may participate in compaction through c-Abl-mediated processes **(Figure 50).**

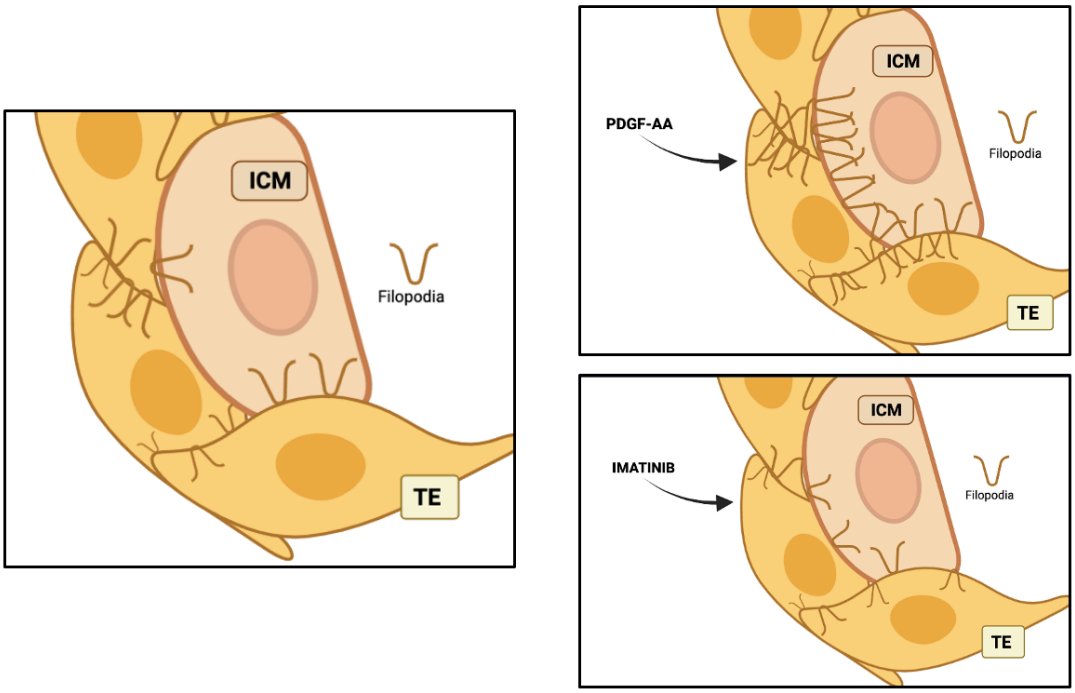

Figure 50: PDGF-AA treatment and imatinib treatment affect the localization of E-cadherin, which is crucial for compaction, as well as the length and number of filopodia during preimplantation embryo development.

Cdx2 transcription is necessary for the segregation of ICM and TE cell lineages in the blastocyst embryo by suppressing OCT4 and NANOG. However, the factors underlying this suppression mechanism are still largely unknown [250]. In a study conducted using Med20 gene KO and KD blastocyst models, ectopic NANOG expression was observed in CDX2-positive TE cells, and it was determined that NANOG was expressed in the nuclei of TE cells [250]. Based on our findings, in the PDGF-AA treatment groups was performed, NANOG expression was observed in the nuclei of ICM cells, whereas in the imatinib treatment groups were performed, NANOG expression gradually shifted to the nuclei of TE cells. These data suggest that c-Abl may be necessary for the suppression of NANOG in TE cells. Additionally, the coordination of the suppression mechanism of NANOG in TE cells through c-Abl and the factors involved in this process are still unknown.

c-Abl can affect the genes crucial for determining cell fate during preimplantation embryo development at the transcriptional level. In our study, we observed that in the PDGF-AA treatment groups, the TE marker TEAD4 was localized in the cytoplasm instead of the nucleus. We did not observe any significant difference in translational stage for CDX2 after PDGF-AA treatment. However, when evaluated at the transcriptional

level, both *Cdx2* mRNA and *Tead4* mRNA levels were significantly decreased in the PDGF-AA treatment groups. Our findings indicate that PDGF-AA treatment may lead to a mechanism that reduces the transcriptional effects of *Tead4* and *Cdx2*. This suggests that PDGF-AA treatment may interact with *Tead4* and *Cdx2*, playing an inhibitory role in the transcriptional system.

In preimplantation embryo imatinib treatment resulted in a decrease in the transcriptional levels of *Yap, Cdx2,* and *Nanog*. These findings suggest that affecting imatinib treatment and the ATP binding site may interfere with the interaction of c-Abl with transcription factors or prevent transcription factors from binding to DNA. Consequently, this localization of E-cadherin in filopodia can result in reduced transcriptional activity and expression levels of critical factors such as *Yap, Cdx2*, and *Nanog*. Our thesis findings provide an evidence for the involvement of c-Abl in the regulation of these crucial transcription factors and reveal that c-Abl exerts may control over their activity through its ATP-binding site.

In contrast to the results obtained from PDGF-AA treatment and imatinib treatment, c-Abl siRNA microinjection in preimplantation embryos did not show any significant difference in the mRNA levels of *c-Abl, Yap, Tead4, Cdx2, Nanog*, and *Oct4*. The embryos where c-Abl was silenced by siRNA exhibited a developmental arrest at the 4-cell, so the mRNA levels were measured at the pre-compaction (8-cell). Silencing c-Abl specifically from a certain region prevented the embryos from progressing beyond the 4-cell. Considering that critical events determining cell fate (polarization, compaction, symmetric/asymmetric division) occur after the 8-cell, it can be concluded that *c-Abl, Yap, Tead4, Cdx2, Nanog,* and *Oct4* levels are not transcriptionally affected when c-Abl is silenced in pre-compaction embryos.

PDGF-AA treatment and imatinib treatment may be effective in determining cell size in preimplantation mouse embryos. It has been demonstrated through various studies that cell size plays a role in controlling cell fate during embryonic development. In oocytes and early embryos, the distribution of RNAs and proteins exhibits polarity. This polarized distribution of molecules can have an impact on cell size due to the uneven allocation of factors that dictate cell fate within each individual cell [251,252]. In another study conducted in 2019, it was proposed that cell size regulates polarity and division asymmetry in *C. elegans* embryos [253]. The impact of PARD6 protein on polarity can vary depending on cell size. This finding has been supported by studies in *C. elegans* embryos, where genetic and physical manipulations of embryo size were conducted [254]. Although

various studies have investigated the influence of cell size on cell fate, it has not yet been established whether this relationship holds true for vertebrates or mammals.

The utilization of changes in cell size and shape during early development has been discussed as regulatory mechanisms that trigger subsequent responses, including vital events in early embryogenesis. These changes play a crucial role in orchestrating the progression of early embryonic development. It has also been shown that reduction in blastomere cell size leads to alterations in a range of physicochemical parameters [255].

Studies have demonstrated how cytokinesis regulates cell-cell adhesion, the contractile ring, and mechanical stiffness in somatic cells. During cytokinesis, cell-cell adhesion is actively regulated to ensure proper separation of daughter cells. During cell division, the contractile ring, which consists of actin and myosin filaments, undergoes contraction to generate the force required for the process of cytokinesis [256,257]. In a study conducted in 2022 using mouse embryos, it was reported that blastomere size affects the rate of cell division [258]. It has been reported that ICM cells exhibit a slower rate of cell division compared to TE cells. As known, TE cells display a flatter morphology compared to ICM cells due to E-cadherin-mediated compaction. To determine whether the division rate is dependent on morphology, in the late 16-cell e, the medium was depleted of calcium to induce rounder morphology in the outer cells, similar to ICM cells. However, it was observed that the division rate was still faster in TE cells. This suggests that the division rate may be determined by intrinsic characteristics of the cells rather than morphology [258]. These findings indicate that the division rates of outer and inner cells are determined by their intrinsic characteristics rather than their morphologies. In a study conducted in 2023, it was reported that during the late 16-cell in preimplantation embryos, cell fate determination is also influenced by RNA localization during cell division [259]. Based on all these studies, it is evident that the cell's division pattern and volume serve as guiding factors for cell fate determination. In our study, we compared the blastomere sizes in embryos that reached the blastocyst after PDGF-AA treatment and imatinib treatment. Our results showed that both PDGF-AA treatment and imatinib treatment led to a decrease in blastomere areas compared to the control group. Considering that cell shape and volume are determinant mechanisms in cell fate, the disruption of c-Abl stability through PDGF-AA treatment or imatinib treatment during preimplantation embryo development can be seen as a factor that affects the cell's volume. Moreover, considering the involvement of c-Abl in cellular mechanisms such as cell proliferation and apoptosis, the disruption of c-Abl stability can explain the impaired proliferation and

cytokinesis of the cell. Considering that this phenomenon may vary depending on specific conditions and cell types, further investigation is needed, including the involvement of cytoskeletal elements, to explore whether c-Abl can influence cell fate through cell volume during preimplantation embryo development.

Recent studies have proposed several similar models regarding the control of nucleus size in cells. One of these models suggests that the ratio of nucleus to cytoplasm remains constant. This implies that cytoplasmic volume determines the size of the nucleus [260-262]. However, subsequent studies investigating the influence of nucleus size on cell size have been limited and inadequate. Detailed examination of the cytoplasm-nucleus relationship in determining cell size was aimed in a study conducted in 2016 using ex vivo mouse preimplantation embryos [263]. They described this ex vivo system as a manipulable system where blastomeres undergo equal division in each cell cycle. Micro-manipulation techniques were also used to alter cell size. As a result, they proposed a mechanism in which cytoplasm and nucleus size can be regulated by each other but through independent mechanisms [263]. Additionally, studies have demonstrated that the size of the nucleus in blastomeres is influenced by cytoplasmic factors, and it undergoes a reduction in size following consecutive mitotic divisions. Researchers have proposed that a cell size-sensing mechanism regulates the mechanism ensuring that larger cells tend to possess larger nuclei. This mechanism plays a role in maintaining proper nuclear-to-cytoplasmic ratios during embryonic development [263]. According to our study, although there were differences in blastomere sizes, the nuclear sizes did not show significant differences between groups. Only in the 5uM imatinib group, the number of nuclei decreased compared to the control group. Considering the results in line with previous studies, it is suggested that PDGF-AA treatment and imatinib treatment may not be a affected for nuclear size.

Possible causes of apoptosis of PDGF-AA treatment and imatinib treatment for preimplantation mouse embryos; Each cell has its own pathway that regulates apoptosis, and the molecular mechanisms and genes involved in cell death are continuously regulated. When a cell is stimulated by an inductive signal, it can activate or inhibit the suppression of genes responsible for the apoptotic mechanism [264]. During the pre-implantation embryo development, some blastomeres undergo rapid mitotic proliferation, while others are eliminated through apoptosis. Studies conducted with human blastocysts have identified the presence of degenerating blastomeres in the ICM and their ultrastructural features associated with micro-pinositotic activity, as described in a study

published in 1982. These studies conducted with human embryos have shown consistency with studies conducted in primate models [265,266]. The results of these studies showed that the apoptotic process serves a physiological role in the development of the ICM. Furthermore, during studies on assisted reproductive techniques, it has been proposed that both viable and developmentally arrested embryos contain a certain amount of apoptotic fragments, suggesting that cellular apoptosis may play a role during the developmental pause of embryos. A notable morphological characteristic of apoptosis observed during pre-implantation embryo development is the formation of apoptotic bodies through a process known as "blebbing." This process involves the budding and detachment of membrane-bound vesicles, which can encapsulate cytoplasmic remnants, organelles, and nuclear fragments. These apoptotic bodies are subsequently released into the extracellular space [267]. After being released, apoptotic bodies are typically phagocytosed and engulfed by phagocytes, where they undergo degradation and breakdown [267]. During early embryonic development, phagocytic competence has been evaluated. Following the culture of human blastocysts, phagocytic competence was assessed in TE cells using Transmission Electron Microscopy (TEM) and fluorescence microscopy, while no phagocytic activity was detected in ICM cells [268]. In our study, we determined that apoptotic bodies were predominantly more abundant in the ICM region. The reason for the higher density of apoptotic bodies in the ICM region could be attributed to the lack of phagocytic activity in ICM cells. Molecular mechanisms underlying this phenomenon have not been elucidated in previous studies.

Apoptotic bodies have been associated with important steps in preimplantation embryo development, such as embryonic genome activation and the development of cellular connections like gap junctions, as well as mitochondrial maturation. In particular, the lack of well-developed gap junctions in cleavage embryos, where apoptotic bodies are less frequently observed, has been considered as a molecular factor for the transmission of apoptotic signals due to the absence of cell-to-cell communication [269,270]. The mechanisms underlying the occurrence of apoptotic bodies in preimplantation embryo development still remain to be fully elucidated. Cellular mechanisms involved in the formation of fragmentation-like structures or the release into the blastocoel cavity/perivitelline space may be implicated in the control of various signaling pathways. However, understanding the impact of the source of the stimulus on the cell is crucial, as apoptotic cell death is associated with cellular structural disturbances. Based on the results, we believe that alterations in c-Abl levels during preimplantation embryo

development could potentially affect the proper development of blastomeres. The significant differences observed in apoptotic bodies, particularly in the 20 ng/mL PDGF-AA group and the 5uM Imatinib group compared to the control group, suggest that PDGF-AA treatment and imatinib treatment may influence this process, possibly in a dose-dependent manner. However, it is unlikely that these fragmented bodies observed in the perivitelline space are responsible for their own phagocytosis.

Preimplantation embryonic development includes many important mechanisms, starting from the zygote and developing into the blastocyst. Polarization markers begin to be expressed in the late 8-cell embryo in the developmental period. After this stage, following the determination of polarization, symmetric/asymmetric cell division begins.

Cells undergo symmetric/asymmetric cell division before becoming compacted. The fate of ICM and TE cells is profoundly affected by all of these stages of development. In our study, we aimed to show the relationship of the Hippo signaling pathway, which is known to be important in cell fate determination, with c-Abl. While we suggested that c-Abl might play an important role in the development of preimplantation embryos, we hypothesized that its mechanism might be mediated by c-Abl/p73/YAP. To reveal this mechanism in *in vitro* preimplantation embryo culture, we targeted c-Abl from 3 different sites. PDGF-AA treatment, imatinib treatment, and c-Abl siRNA microinjection provided with quantitative results to functionally evaluate the role of c-Abl tyrosine kinase.

Preimplantation embryo development is significantly dependent on the stability of c-Abl tyrosine kinase. We suggested that polarization, compaction, and TE-ICM cell fate determination in preimplantation embryos are dependent on the stability of c-Abl tyrosine kinase. The activation of c-Abl tyrosine kinase from the activation site by PDGF-AA treatment and inhibition from the ATP binding site by imatinib treatment can change PARD6 distribution, E-cadherin pattern, density and number of filopodia, as well as the localization of CDX2 and NANOG compared to the control group in blastomeres. The expression of TEAD4, in both PDGF-AA and imatinib treatment groups was determined in the cytoplasm instead of nucleus. However, changes in both translational and transcriptional expression levels of YAP also indicate that c-Abl is involved in this YAP-mediated process. The cytoplasmic expression seen in the p73 expression pattern in the preimplantation embryo differentiates our study from other studies that evaluated p73 in somatic cells via the apoptotic pathway. When examined at the p73, we propose that it operates in a manner distinct from the apoptotic path in the development of preimplantation embryos, and that this manner involves binding to cellular organelles.

The significance of c-Abl in embryo development gains even stronger ground with the observation that the PARD6 disperses in the cytoplasm when the stability of c-Abl is disrupted. Filopodia differences evaluated with E-cadherin expression in compaction, which is also a strategic stage, show how important the stability of c-Abl tyrosine kinase is for embryo compaction. The noticeable augmentation and elongation of the filopodia pattern following PDGF-AA treatment showed a contrasting decrease and weakening of expression in the imatinib-treated groups. This observation highlights the significance of c-Abl expression on filopodia, particularly during the compaction process. Moreover, any disruption in the fundamentally crucial c-Abl/YAP pathway leads to developmental abnormalities in the embryo, and delving deeper into this signaling mechanism will yield valuable insights into preimplantation embryo development. **(Figure 51).**

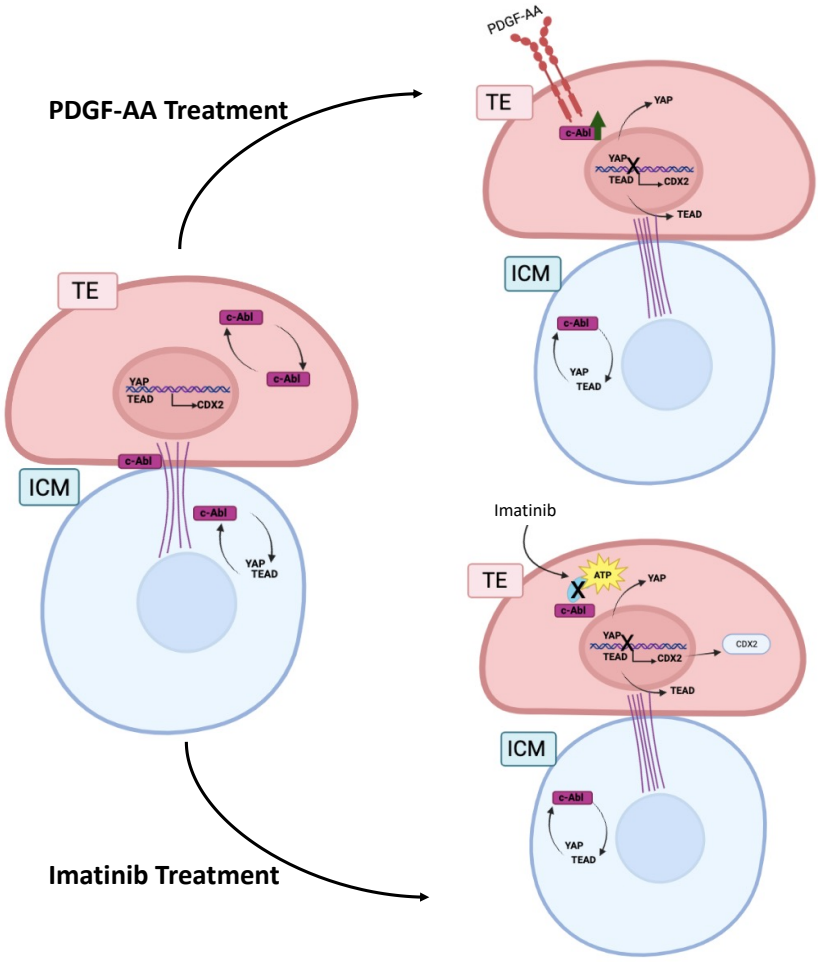

Figure 51: c-Abl participates in the determination of YAP location during the preimplantation stage of mouse embryonic development, which in effect determines cell fate.

6. REFERENCES

1. Johnson MH, Ziomek CA. The foundation of two distinct cell lineages within the mouse morula. *Cell*. 1981. 24(1):p. 71-80.

2. Harvey K, Tapon N. The Salvador-Warts-Hippo pathway - an emerging tumour-suppressor network. *Nature reviews Cancer*. 2007. 7(3):p. 182-91.

3. Camargo FD, Gokhale S, Johnnidis JB, et al. YAP1 increases organ size and expands undifferentiated progenitor cells. *Curr Biol*. 2007. 17(23):p. 2054-60.

4. Dong J, Feldmann G, Huang J, et al. Elucidation of a universal size-control mechanism in Drosophila and mammals. *Cell*. 2007. 130(6):p. 1120-33.

5. Posfai E, Petropoulos S, de Barros FRO, et al. Position- and Hippo signaling-dependent plasticity during lineage segregation in the early mouse embryo. *Elife*. 2017. 6:p.

6. Baskaran R, Wood LD, Whitaker LL, et al. Ataxia telangiectasia mutant protein activates c-Abl tyrosine kinase in response to ionizing radiation. *Nature*. 1997. 387(6632):p. 516-9.

7. Yaba A, Kayisli UA, Johnson J, Demir R, Demir N. The Abelson tyrosine kinase (c-Abl) expression on the mouse uterus and placenta during gestational period. *J Mol Histol*. 2011. 42(2):p. 91-6.

8. Agami R, Blandino G, Oren M, Shaul Y. Interaction of c-Abl and p73alpha and their collaboration to induce apoptosis. *Nature*. 1999. 399(6738):p. 809-13.

9. Levy D, Adamovich Y, Reuven N, Shaul Y. Yap1 phosphorylation by c-Abl is a critical step in selective activation of proapoptotic genes in response to DNA damage. *Mol Cell*. 2008. 29(3):p. 350-61.

10. Suwińska A. Preimplantation mouse embryo: developmental fate and potency of blastomeres. *Results Probl Cell Differ*. 2012. 55:p. 141-63.

11. Aiken CE, Swoboda PP, Skepper JN, Johnson MH. The direct measurement of embryogenic volume and nucleo-cytoplasmic ratio during mouse pre-implantation development. *Reproduction*. 2004. 128(5):p. 527-35.

12. Fleming TP, Johnson MH. From egg to epithelium. *Annu Rev Cell Biol*. 1988. 4:p. 459-85.

13. Chazaud C, Yamanaka Y. Lineage specification in the mouse preimplantation embryo. *Development*. 2016. 143(7):p. 1063-74.

14. Li L, Lu X, Dean J. The maternal to zygotic transition in mammals. *Molecular aspects of medicine*. 2013. 34(5):p. 919-38.

15. Chang MC. Fertilizing capacity of spermatozoa deposited into the fallopian tubes. *Nature*. 1951. 168(4277):p. 697-8.

16. Austin CR. Observations on the penetration of the sperm in the mammalian egg. *Australian journal of scientific research Ser B: Biological sciences*. 1951. 4(4):p. 581-96.

17. Bhakta HH, Refai FH, Avella MA. The molecular mechanisms mediating mammalian fertilization. *Development*. 2019. 146(15):p.

18. Ducibella T, Anderson E, Albertini DF, Aalberg J, Rangarajan S. Quantitative studies of changes in cortical granule number and distribution in the mouse oocyte during meiotic maturation. *Dev Biol*. 1988. 130(1):p. 184-97.

19. Piliszek A, Madeja ZE. Pre-implantation Development of Domestic Animals. *Curr Top Dev Biol*. 2018. 128:p. 267-294.

20. Latham KE, Solter D, Schultz RM. Acquisition of a transcriptionally permissive state during the 1-cell stage of mouse embryogenesis. *Dev Biol*. 1992. 149(2):p. 457-62.

21. Aoki F, Worrad DM, Schultz RM. Regulation of transcriptional activity during the first and second cell cycles in the preimplantation mouse embryo. *Dev Biol*. 1997. 181(2):p. 296-307.

22. Crosby IM, Gandolfi F, Moor RM. Control of protein synthesis during early cleavage of sheep embryos. *Journal of reproduction and fertility*. 1988. 82(2):p. 769-75.

23. Meirelles FV, Caetano AR, Watanabe YF, et al. Genome activation and developmental block in bovine embryos. *Animal reproduction science*. 2004. 82-83:p. 13-20.

24. Maddox-Hyttel P, Alexopoulos NI, Vajta G, et al. Immunohistochemical and ultrastructural characterization of the initial post-hatching development of bovine embryos. *Reproduction*. 2003. 125(4):p. 607-23.

25. Hamatani T, Ko M, Yamada M, et al. Global gene expression profiling of preimplantation embryos. *Human cell*. 2006. 19(3):p. 98-117.

26. Latham KE, Garrels JI, Chang C, Solter D. Analysis of embryonic mouse development: construction of a high-resolution, two-dimensional gel protein database. *Applied and theoretical electrophoresis : the official journal of the International Electrophoresis Society*. 1992. 2(6):p. 163-70.

27. Ruebel ML, Vincent KA, Schall PZ, Wang K, Latham KE. SMCHD1 terminates the first embryonic genome activation event in mouse two-cell embryos and contributes to a transcriptionally repressive state. *American journal of physiology Cell physiology*. 2019. 317(4):p. C655-c664.

28. White MD, Zenker J, Bissiere S, Plachta N. How cells change shape and position in the early mammalian embryo. *Curr Opin Cell Biol*. 2017. 44:p. 7-13.

29. Samarage CR, White MD, Álvarez YD, et al. Cortical Tension Allocates the First Inner Cells of the Mammalian Embryo. *Dev Cell*. 2015. 34(4):p. 435-47.

30. Vestweber D, Gossler A, Boller K, Kemler R. Expression and distribution of cell adhesion molecule uvomorulin in mouse preimplantation embryos. *Dev Biol*. 1987. 124(2):p. 451-6.

31. De Vries WN, Evsikov AV, Haac BE, et al. Maternal beta-catenin and E-cadherin in mouse development. *Development*. 2004. 131(18):p. 4435-45.

32. Torres M, Stoykova A, Huber O, et al. An alpha-E-catenin gene trap mutation defines its function in preimplantation development. *Proc Natl Acad Sci U S A*. 1997. 94(3):p. 901-6.

33. Haegel H, Larue L, Ohsugi M, Fedorov L, Herrenknecht K, Kemler R. Lack of beta-catenin affects mouse development at gastrulation. *Development*. 1995. 121(11):p. 3529-37.

34. Stephenson RO, Yamanaka Y, Rossant J. Disorganized epithelial polarity and excess trophectoderm cell fate in preimplantation embryos lacking E-cadherin. *Development*. 2010. 137(20):p. 3383-91.

35. Pey R, Vial C, Schatten G, Hafner M. Increase of intracellular Ca2+ and relocation of E-cadherin during experimental decompaction of mouse embryos. *Proc Natl Acad Sci U S A*. 1998. 95(22):p. 12977-82.

36. Diz-Muñoz A, Krieg M, Bergert M, et al. Control of directed cell migration in vivo by membrane-to-cortex attachment. *PLoS Biol*. 2010. 8(11):p. e1000544.

37. Kunda P, Pelling AE, Liu T, Baum B. Moesin controls cortical rigidity, cell rounding, and spindle morphogenesis during mitosis. *Curr Biol*. 2008. 18(2):p. 91-101.

38. Turlier H, Maître JL. Mechanics of tissue compaction. *Semin Cell Dev Biol*. 2015. 47-48:p. 110-7.

39. Fierro-González JC, White MD, Silva JC, Plachta N. Cadherin-dependent filopodia control preimplantation embryo compaction. *Nature Cell Biology*. 2013. 15(12):p. 1424-1433.

40. Eckert JJ, Fleming TP. Tight junction biogenesis during early development. *Biochim Biophys Acta*. 2008. 1778(3):p. 717-28.

41. Zenker J, White MD, Gasnier M, et al. Expanding Actin Rings Zipper the Mouse Embryo for Blastocyst Formation. *Cell*. 2018. 173(3):p. 776-791.e17.

42. Schwayer C, Sikora M, Slovakova J, Kardos R, Heisenberg CP. Actin Rings of Power. *Dev Cell*. 2016. 37(6):p. 493-506.

43. Conduit PT, Wainman A, Raff JW. Centrosome function and assembly in animal cells. *Nat Rev Mol Cell Biol*. 2015. 16(10):p. 611-24.

44. Canse C, Yildirim E, Yaba A. Overview of junctional complexes during mammalian early embryonic development. *Front Endocrinol (Lausanne)*. 2023. 14:p. 1150017.

45. Fededa JP, Gerlich DW. Molecular control of animal cell cytokinesis. *Nat Cell Biol*. 2012. 14(5):p. 440-7.

46. Clift D, Schuh M. A three-step MTOC fragmentation mechanism facilitates bipolar spindle assembly in mouse oocytes. *Nat Commun*. 2015. 6:p. 7217.

47. Houliston E, Pickering SJ, Maro B. Alternative routes for the establishment of surface polarity during compaction of the mouse embryo. *Dev Biol*. 1989. 134(2):p. 342-50.

48. Houliston E, Pickering SJ, Maro B. Redistribution of microtubules and pericentriolar material during the development of polarity in mouse blastomeres. *J Cell Biol*. 1987. 104(5):p. 1299-308.

49. Zenker J, White MD, Templin RM, et al. A microtubule-organizing center directing intracellular transport in the early mouse embryo. *Science*. 2017. 357(6354):p. 925-928.

50. Hawdon A, Aberkane A, Zenker J. Microtubule-dependent subcellular organisation of pluripotent cells. *Development*. 2021. 148(20):p.

51. Deguchi R, Shirakawa H, Oda S, Mohri T, Miyazaki S. Spatiotemporal analysis of Ca(2+) waves in relation to the sperm entry site and animal-vegetal axis during Ca(2+) oscillations in fertilized mouse eggs. *Dev Biol*. 2000. 218(2):p. 299-313.

52. Ajduk A, Ilozue T, Windsor S, et al. Rhythmic actomyosin-driven contractions induced by sperm entry predict mammalian embryo viability. *Nat Commun*. 2011. 2:p. 417.

53. Johnson MH, Maro B. A dissection of the mechanisms generating and stabilizing polarity in mouse 8- and 16-cell blastomeres: the role of cytoskeletal elements. *J Embryol Exp Morphol*. 1985. 90:p. 311-34.

54. Ziomek CA, Johnson MH. Cell surface interaction induces polarization of mouse 8-cell blastomeres at compaction. *Cell*. 1980. 21(3):p. 935-42.

55. Ducibella T, Ukena T, Karnovsky M, Anderson E. Changes in cell surface and cortical cytoplasmic organization during early embryogenesis in the preimplantation mouse embryo. *J Cell Biol*. 1977. 74(1):p. 153-67.

56. Ajduk A, Biswas Shivhare S, Zernicka-Goetz M. The basal position of nuclei is one pre-requisite for asymmetric cell divisions in the early mouse embryo. *Dev Biol*. 2014. 392(2):p. 133-40.

57. Louvet S, Aghion J, Santa-Maria A, Mangeat P, Maro B. Ezrin becomes restricted to outer cells following asymmetrical division in the preimplantation mouse embryo. *Dev Biol*. 1996. 177(2):p. 568-79.

58. Vinot S, Le T, Ohno S, Pawson T, Maro B, Louvet-Vallée S. Asymmetric distribution of PAR proteins in the mouse embryo begins at the 8-cell stage during compaction. *Dev Biol*. 2005. 282(2):p. 307-19.

59. Gao L, Macara IG. Isoforms of the polarity protein par6 have distinct functions. *J Biol Chem*. 2004. 279(40):p. 41557-62.

60. Lin D, Edwards AS, Fawcett JP, Mbamalu G, Scott JD, Pawson T. A mammalian PAR-3-PAR-6 complex implicated in Cdc42/Rac1 and aPKC signalling and cell polarity. *Nat Cell Biol*. 2000. 2(8):p. 540-7.

61. Bose R, Wrana JL. Regulation of Par6 by extracellular signals. *Curr Opin Cell Biol*. 2006. 18(2):p. 206-12.

62. Watts JL, Etemad-Moghadam B, Guo S, et al. par-6, a gene involved in the establishment of asymmetry in early C. elegans embryos, mediates the asymmetric localization of PAR-3. *Development*. 1996. 122(10):p. 3133-40.

63. Roh MH, Margolis B. Composition and function of PDZ protein complexes during cell polarization. *Am J Physiol Renal Physiol*. 2003. 285(3):p. F377-87.

64. Etienne-Manneville S, Hall A. Cell polarity: Par6, aPKC and cytoskeletal crosstalk. *Curr Opin Cell Biol*. 2003. 15(1):p. 67-72.

65. Liu Z, Yang Y, Gu A, et al. Par complex cluster formation mediated by phase separation. *Nat Commun*. 2020. 11(1):p. 2266.

66. Henrique D, Schweisguth F. Cell polarity: the ups and downs of the Par6/aPKC complex. *Curr Opin Genet Dev*. 2003. 13(4):p. 341-50.

67. Suzuki A, Ohno S. The PAR-aPKC system: lessons in polarity. *J Cell Sci*. 2006. 119(Pt 6):p. 979-87.

68. Etienne-Manneville S, Hall A. Cdc42 regulates GSK-3beta and adenomatous polyposis coli to control cell polarity. *Nature*. 2003. 421(6924):p. 753-6.

69. Etienne-Manneville S, Hall A. Integrin-mediated activation of Cdc42 controls cell polarity in migrating astrocytes through PKCzeta. *Cell*. 2001. 106(4):p. 489-98.

70. Johansson A, Driessens M, Aspenström P. The mammalian homologue of the Caenorhabditis elegans polarity protein PAR-6 is a binding partner for the Rho GTPases Cdc42 and Rac1. *J Cell Sci*. 2000. 113 (Pt 18):p. 3267-75.

71. Noda Y, Takeya R, Ohno S, Naito S, Ito T, Sumimoto H. Human homologues of the Caenorhabditis elegans cell polarity protein PAR6 as an adaptor that links the small GTPases Rac and Cdc42 to atypical protein kinase C. *Genes Cells*. 2001. 6(2):p. 107-19.

72. Balda MS, Matter K. Epithelial cell adhesion and the regulation of gene expression. *Trends Cell Biol*. 2003. 13(6):p. 310-8.

73. Benmerah A, Scott M, Poupon V, Marullo S. Nuclear functions for plasma membrane-associated proteins? *Traffic*. 2003. 4(8):p. 503-11.

74. Johnson MH. From mouse egg to mouse embryo: polarities, axes, and tissues. *Annual review of cell and developmental biology*. 2009. 25:p. 483-512.

75. Levy JB, Johnson MH, Goodall H, Maro B. The timing of compaction: control of a major developmental transition in mouse early embryogenesis. *J Embryol Exp Morphol*. 1986. 95:p. 213-37.

76. Smith HL, Stevens A, Minogue B, et al. Systems based analysis of human embryos and gene networks involved in cell lineage allocation. *BMC Genomics*. 2019. 20(1):p. 171.

77. Shi J, Chen Q, Li X, et al. Dynamic transcriptional symmetry-breaking in pre-implantation mammalian embryo development revealed by single-cell RNA-seq. *Development*. 2015. 142(20):p. 3468-77.

78. Zdravkovic T, Nazor KL, Larocque N, et al. Human stem cells from single blastomeres reveal pathways of embryonic or trophoblast fate specification. *Development*. 2015. 142(23):p. 4010-25.

79. White MD, Zenker J, Bissiere S, Plachta N. Instructions for Assembling the Early Mammalian Embryo. *Dev Cell*. 2018. 45(6):p. 667-679.

80. Zhu M, Leung CY, Shahbazi MN, Zernicka-Goetz M. Actomyosin polarisation through PLC-PKC triggers symmetry breaking of the mouse embryo. *Nat Commun*. 2017. 8(1):p. 921.

81. Maître J-L, Turlier H, Illukkumbura R, et al. Asymmetric division of contractile domains couples cell positioning and fate specification. *Nature*. 2016. 536(7616):p. 344-348.

82. Johnson MH, Maro B, Takeichi M. The role of cell adhesion in the synchronization and orientation of polarization in 8-cell mouse blastomeres. *J Embryol Exp Morphol*. 1986. 93:p. 239-55.

83. Korotkevich E, Niwayama R, Courtois A, et al. The Apical Domain Is Required and Sufficient for the First Lineage Segregation in the Mouse Embryo. *Dev Cell*. 2017. 40(3):p. 235-247.e7.

84. Johnson MH, Ziomek CA. Induction of polarity in mouse 8-cell blastomeres: specificity, geometry, and stability. *J Cell Biol*. 1981. 91(1):p. 303-8.

85. Cockburn K, Rossant J. Making the blastocyst: lessons from the mouse. *The Journal of clinical investigation*. 2010. 120(4):p. 995-1003.

86. Tarkowski AK, Wróblewska J. Development of blastomeres of mouse eggs isolated at the 4- and 8-cell stage. *J Embryol Exp Morphol*. 1967. 18(1):p. 155-80.

87. Yamanaka Y, Ralston A, Stephenson RO, Rossant J. Cell and molecular regulation of the mouse blastocyst. *Dev Dyn*. 2006. 235(9):p. 2301-14.

88. Sasaki H. Roles and regulations of Hippo signaling during preimplantation mouse development. *Dev Growth Differ*. 2017. 59(1):p. 12-20.

89. Posfai E, Rovic I, Jurisicova A. The mammalian embryo's first agenda: making trophectoderm. *The International journal of developmental biology*. 2019. 63(3-4-5):p. 157-170.

90. Martín Á, de los Santos MJ. The first choice of the preimplantation embryo: How compaction and polarity build cell identity. *Medicina Reproductiva y Embriología Clínica*. 2020. 7(1):p. 23-32.

91. Yildirim E, Bora G, Onel T, Talas N, Yaba A. Cell fate determination and Hippo signaling pathway in preimplantation mouse embryo. *Cell Tissue Res*. 2021. 386(3):p. 423-444.

92. Chisholm JC, Houliston E. Cytokeratin filament assembly in the preimplantation mouse embryo. *Development*. 1987. 101(3):p. 565-82.

93. Leung CY, Zhu M, Zernicka-Goetz M. Polarity in Cell-Fate Acquisition in the Early Mouse Embryo. *Curr Top Dev Biol*. 2016. 120:p. 203-34.

94. Etemad-Moghadam B, Guo S, Kemphues KJ. Asymmetrically distributed PAR-3 protein contributes to cell polarity and spindle alignment in early C. elegans embryos. *Cell*. 1995. 83(5):p. 743-52.

95. Anani S, Bhat S, Honma-Yamanaka N, Krawchuk D, Yamanaka Y. Initiation of Hippo signaling is linked to polarity rather than to cell position in the pre-implantation mouse embryo. *Development*. 2014. 141(14):p. 2813-24.

96. Plusa B, Frankenberg S, Chalmers A, et al. Downregulation of Par3 and aPKC function directs cells towards the ICM in the preimplantation mouse embryo. *J Cell Sci*. 2005. 118(Pt 3):p. 505-15.

97. Nishioka N, Inoue K, Adachi K, et al. The Hippo signaling pathway components Lats and Yap pattern Tead4 activity to distinguish mouse trophectoderm from inner cell mass. *Dev Cell*. 2009. 16(3):p. 398-410.

98. Kaneko KJ, DePamphilis ML. TEAD4 establishes the energy homeostasis essential for blastocoel formation. *Development*. 2013. 140(17):p. 3680-90.

99. Strumpf D, Mao CA, Yamanaka Y, et al. Cdx2 is required for correct cell fate specification and differentiation of trophectoderm in the mouse blastocyst. *Development*. 2005. 132(9):p. 2093-102.

100. Menchero S, Sainz de Aja J, Manzanares M. Our First Choice: Cellular and Genetic Underpinnings of Trophectoderm Identity and Differentiation in the Mammalian Embryo. *Curr Top Dev Biol*. 2018. 128:p. 59-80.

101. Niwa H, Toyooka Y, Shimosato D, et al. Interaction between Oct3/4 and Cdx2 determines trophectoderm differentiation. *Cell*. 2005. 123(5):p. 917-29.

102. Ralston A, Rossant J. Cdx2 acts downstream of cell polarization to cell-autonomously promote trophectoderm fate in the early mouse embryo. *Dev Biol*. 2008. 313(2):p. 614-29.

103. Chen YA, Lu CY, Cheng TY, Pan SH, Chen HF, Chang NS. WW Domain-Containing Proteins YAP and TAZ in the Hippo Pathway as Key Regulators in Stemness Maintenance, Tissue Homeostasis, and Tumorigenesis. *Front Oncol*. 2019. 9:p. 60.

104. Frum T, Watts JL, Ralston A. TEAD4, YAP1 and WWTR1 prevent the premature onset of pluripotency prior to the 16-cell stage. *Development*. 2019. 146(17):p.

105. Wicklow E, Blij S, Frum T, et al. HIPPO pathway members restrict SOX2 to the inner cell mass where it promotes ICM fates in the mouse blastocyst. *PLoS Genet*. 2014. 10(10):p. e1004618.

106. Frum T, Murphy TM, Ralston A. HIPPO signaling resolves embryonic cell fate conflicts during establishment of pluripotency in vivo. *Elife*. 2018. 7:p.

107. Hirate Y, Sasaki H. The role of angiomotin phosphorylation in the Hippo pathway during preimplantation mouse development. *Tissue Barriers*. 2014. 2(1):p. e28127.

108. Wu Z, Guan KL. Hippo Signaling in Embryogenesis and Development. *Trends in biochemical sciences*. 2021. 46(1):p. 51-63.

109. Hirate Y, Hirahara S, Inoue K, et al. Polarity-dependent distribution of angiomotin localizes Hippo signaling in preimplantation embryos. *Curr Biol*. 2013. 23(13):p. 1181-94.

110. Zhao B, Li L, Lu Q, et al. Angiomotin is a novel Hippo pathway component that inhibits YAP oncoprotein. *Genes & development*. 2011. 25(1):p. 51-63.

111. Li Y, Zhou H, Li F, et al. Angiomotin binding-induced activation of Merlin/NF2 in the Hippo pathway. *Cell Res*. 2015. 25(7):p. 801-17.

112. Schier AF. The maternal-zygotic transition: death and birth of RNAs. *Science*. 2007. 316(5823):p. 406-7.

113. Yu C, Ji SY, Dang YJ, et al. Oocyte-expressed yes-associated protein is a key activator of the early zygotic genome in mouse. *Cell Res*. 2016. 26(3):p. 275-87.

114. Ralston A, Cox BJ, Nishioka N, et al. Gata3 regulates trophoblast development downstream of Tead4 and in parallel to Cdx2. *Development*. 2010. 137(3):p. 395-403.

115. Hashimoto M, Sasaki H. Epiblast Formation by TEAD-YAP-Dependent Expression of Pluripotency Factors and Competitive Elimination of Unspecified Cells. *Dev Cell*. 2019. 50(2):p. 139-154.e5.

116. Shaul Y. c-Abl: activation and nuclear targets. *Cell Death Differ*. 2000. 7(1):p. 10-6.

117. Van Etten RA, Jackson P, Baltimore D. The mouse type IV c-abl gene product is a nuclear protein, and activation of transforming ability is associated with cytoplasmic localization. *Cell*. 1989. 58(4):p. 669-78.

118. Nagar B, Hantschel O, Seeliger M, et al. Organization of the SH3-SH2 unit in active and inactive forms of the c-Abl tyrosine kinase. *Mol Cell*. 2006. 21(6):p. 787-98.

119. Miller AL, Wang Y, Mooseker MS, Koleske AJ. The Abl-related gene (Arg) requires its F-actin-microtubule cross-linking activity to regulate lamellipodial dynamics during fibroblast adhesion. *J Cell Biol*. 2004. 165(3):p. 407-19.

120. Colicelli J. ABL tyrosine kinases: evolution of function, regulation, and specificity. *Sci Signal*. 2010. 3(139):p. re6.

121. Bianchi C, Torsello B, Angeloni V, et al. Eight full-length abelson related gene (Arg) isoforms are constitutively expressed in caki-1 cell line and cell distribution of two isoforms has been analyzed after transfection. *Journal of cellular biochemistry*. 2008. 105(5):p. 1219-27.

122. Zhang J, Adrián FJ, Jahnke W, et al. Targeting Bcr-Abl by combining allosteric with ATP-binding-site inhibitors. *Nature*. 2010. 463(7280):p. 501-6.

123. Reuven N, Shaul Y. The c-Abl/YAP/p73 Apoptotic Module and the HIPPO Pathway. In: Oren M, Aylon Y, eds. *The Hippo Signaling Pathway and Cancer*. Springer New York; 2013:173-195.

124. Bradley WD, Koleske AJ. Regulation of cell migration and morphogenesis by Abl-family kinases: emerging mechanisms and physiological contexts. *J Cell Sci*. 2009. 122(Pt 19):p. 3441-54.

125. Boyle SN, Michaud GA, Schweitzer B, Predki PF, Koleske AJ. A critical role for cortactin phosphorylation by Abl-family kinases in PDGF-induced dorsal-wave formation. *Curr Biol*. 2007. 17(5):p. 445-51.

126. Sossey-Alaoui K, Li X, Cowell JK. c-Abl-mediated phosphorylation of WAVE3 is required for lamellipodia formation and cell migration. *J Biol Chem*. 2007. 282(36):p. 26257-65.

127. Bays JL, Peng X, Tolbert CE, et al. Vinculin phosphorylation differentially regulates mechanotransduction at cell-cell and cell-matrix adhesions. *J Cell Biol*. 2014. 205(2):p. 251-63.

128. Zandy NL, Playford M, Pendergast AM. Abl tyrosine kinases regulate cell-cell adhesion through Rho GTPases. *Proc Natl Acad Sci U S A*. 2007. 104(45):p. 17686-91.

129. Capdeville R, Buchdunger E, Zimmermann J, Matter A. Glivec (STI571, imatinib), a rationally developed, targeted anticancer drug. *Nature reviews Drug discovery*. 2002. 1(7):p. 493-502.

130. Heffron TP. Small Molecule Kinase Inhibitors for the Treatment of Brain Cancer. *Journal of medicinal chemistry*. 2016. 59(22):p. 10030-10066.

131. Kerkelä R, Grazette L, Yacobi R, et al. Cardiotoxicity of the cancer therapeutic agent imatinib mesylate. *Nature medicine*. 2006. 12(8):p. 908-16.

132. Druker BJ, Lydon NB. Lessons learned from the development of an abl tyrosine kinase inhibitor for chronic myelogenous leukemia. *The Journal of clinical investigation*. 2000. 105(1):p. 3-7.

133. Manley PW, Cowan-Jacob SW, Buchdunger E, et al. Imatinib: a selective tyrosine kinase inhibitor. *European journal of cancer (Oxford, England : 1990)*. 2002. 38 Suppl 5:p. S19-27.

134. Peng B, Lloyd P, Schran H. Clinical Pharmacokinetics of Imatinib. *Clinical Pharmacokinetics*. 2005. 44(9):p. 879-894.

135. Luttman JH, Colemon A, Mayro B, Pendergast AM. Role of the ABL tyrosine kinases in the epithelial–mesenchymal transition and the metastatic cascade. *Cell Communication and Signaling*. 2021. 19(1):p. 59.

136. Quintás-Cardama A, Kantarjian HM, Cortes JE. Mechanisms of primary and secondary resistance to imatinib in chronic myeloid leukemia. *Cancer control : journal of the Moffitt Cancer Center*. 2009. 16(2):p. 122-31.

137. Azam M, Latek RR, Daley GQ. Mechanisms of autoinhibition and STI-571/imatinib resistance revealed by mutagenesis of BCR-ABL. *Cell*. 2003. 112(6):p. 831-43.

138. Savage DG, Antman KH. Imatinib mesylate--a new oral targeted therapy. *The New England journal of medicine*. 2002. 346(9):p. 683-93.

139. Smith JM, Mayer BJ. Abl: mechanisms of regulation and activation. *Front Biosci*. 2002. 7:p. d31-42.

140. Alexandropoulos K, Baltimore D. Coordinate activation of c-Src by SH3- and SH2-binding sites on a novel p130Cas-related protein, Sin. *Genes Dev*. 1996. 10(11):p. 1341-55.

141. Smith JM, Katz S, Mayer BJ. Activation of the Abl tyrosine kinase in vivo by Src homology 3 domains from the Src homology 2/Src homology 3 adaptor Nck. *J Biol Chem*. 1999. 274(39):p. 27956-62.

142. Nagar B, Hantschel O, Young MA, et al. Structural basis for the autoinhibition of c-Abl tyrosine kinase. *Cell*. 2003. 112(6):p. 859-71.

143. Woodring PJ, Hunter T, Wang JY. Inhibition of c-Abl tyrosine kinase activity by filamentous actin. *J Biol Chem*. 2001. 276(29):p. 27104-10.

144. McWhirter JR, Wang JY. An actin-binding function contributes to transformation by the Bcr-Abl oncoprotein of Philadelphia chromosome-positive human leukemias. *Embo j*. 1993. 12(4):p. 1533-46.

145. Woodring PJ, Litwack ED, O'Leary DD, Lucero GR, Wang JY, Hunter T. Modulation of the F-actin cytoskeleton by c-Abl tyrosine kinase in cell spreading and neurite extension. *J Cell Biol*. 2002. 156(5):p. 879-92.

146. Salem W, Ho JR, Woo I, et al. Long-term imatinib diminishes ovarian reserve and impacts embryo quality. *J Assist Reprod Genet*. 2020. 37(6):p. 1459-1466.

147. Kong X, Yang S, Gong F, et al. The Relationship between Cell Number, Division Behavior and Developmental Potential of Cleavage Stage Human Embryos: A Time-Lapse Study. *PLoS One*. 2016. 11(4):p. e0153697.

148. Keshet R, Adler J, Ricardo Lax I, et al. c-Abl antagonizes the YAP oncogenic function. *Cell Death Differ*. 2015. 22(6):p. 935-45.

149. Chen J, Harris RC. Interaction of the EGF Receptor and the Hippo Pathway in the Diabetic Kidney. *J Am Soc Nephrol*. 2016. 27(6):p. 1689-700.

150. Li H, Huang Z, Gao M, et al. Inhibition of YAP suppresses CML cell proliferation and enhances efficacy of imatinib in vitro and in vivo. *J Exp Clin Cancer Res*. 2016. 35(1):p. 134.

151. Menchero S, Rayon T, Andreu MJ, Manzanares M. Signaling pathways in mammalian preimplantation development: Linking cellular phenotypes to lineage decisions. *Dev Dyn*. 2017. 246(4):p. 245-261.

152. McKay MM, Morrison DK. Integrating signals from RTKs to ERK/MAPK. *Oncogene*. 2007. 26(22):p. 3113-21.

153. Fincham VJ, Unlu M, Brunton VG, Pitts JD, Wyke JA, Frame MC. Translocation of Src kinase to the cell periphery is mediated by the actin cytoskeleton under the control of the Rho family of small G proteins. *J Cell Biol*. 1996. 135(6 Pt 1):p. 1551-64.

154. Plattner R, Kadlec L, DeMali KA, Kazlauskas A, Pendergast AM. c-Abl is activated by growth factors and Src family kinases and has a role in the cellular response to PDGF. *Genes & development*. 1999. 13(18):p. 2400-11.

155. Plusa B, Piliszek A, Frankenberg S, Artus J, Hadjantonakis AK. Distinct sequential cell behaviours direct primitive endoderm formation in the mouse blastocyst. *Development*. 2008. 135(18):p. 3081-91.

156. Soriano P. The PDGF alpha receptor is required for neural crest cell development and for normal patterning of the somites. *Development*. 1997. 124(14):p. 2691-700.

157. Artus J, Panthier JJ, Hadjantonakis AK. A role for PDGF signaling in expansion of the extra-embryonic endoderm lineage of the mouse blastocyst. *Development*. 2010. 137(20):p. 3361-72.

158. Barilá D, Superti-Furga G. An intramolecular SH3-domain interaction regulates c-Abl activity. *Nat Genet*. 1998. 18(3):p. 280-2.

159. Jackson P, Baltimore D. N-terminal mutations activate the leukemogenic potential of the myristoylated form of c-abl. *Embo j*. 1989. 8(2):p. 449-56.

160. Van Etten RA, Debnath J, Zhou H, Casasnovas JM. Introduction of a loss-of-function point mutation from the SH3 region of the Caenorhabditis elegans sem-5 gene activates the transforming ability of c-abl in vivo and abolishes binding of proline-rich ligands in vitro. *Oncogene*. 1995. 10(10):p. 1977-88.

161. Brasher BB, Van Etten RA. c-Abl has high intrinsic tyrosine kinase activity that is stimulated by mutation of the Src homology 3 domain and by autophosphorylation at two distinct regulatory tyrosines. *J Biol Chem*. 2000. 275(45):p. 35631-7.

162. Echarri A, Pendergast AM. Activated c-Abl is degraded by the ubiquitin-dependent proteasome pathway. *Curr Biol*. 2001. 11(22):p. 1759-65.

163. Hubbard SR. Src autoinhibition: let us count the ways. *Nat Struct Biol*. 1999. 6(8):p. 711-4.

164. Ting AY, Kain KH, Klemke RL, Tsien RY. Genetically encoded fluorescent reporters of protein tyrosine kinase activities in living cells. *Proc Natl Acad Sci U S A*. 2001. 98(26):p. 15003-8.

165. Greaves S. Ready and abl. *Nat Cell Biol*. 2002. 4(4):p. E74.

166. Frasca F, Vigneri P, Vella V, Vigneri R, Wang JY. Tyrosine kinase inhibitor STI571 enhances thyroid cancer cell motile response to Hepatocyte Growth Factor. *Oncogene*. 2001. 20(29):p. 3845-56.

167. Nihira K, Taira N, Miki Y, Yoshida K. TTK/Mps1 controls nuclear targeting of c-Abl by 14-3-3-coupled phosphorylation in response to oxidative stress. *Oncogene*. 2008. 27(58):p. 7285-95.

168. Yoshida K, Yamaguchi T, Natsume T, Kufe D, Miki Y. JNK phosphorylation of 14-3-3 proteins regulates nuclear targeting of c-Abl in the apoptotic response to DNA damage. *Nat Cell Biol*. 2005. 7(3):p. 278-85.

169. Zhao B, Wei X, Li W, et al. Inactivation of YAP oncoprotein by the Hippo pathway is involved in cell contact inhibition and tissue growth control. *Genes & development*. 2007. 21(21):p. 2747-61.

170. Cottini F, Hideshima T, Xu C, et al. Rescue of Hippo coactivator YAP1 triggers DNA damage-induced apoptosis in hematological cancers. *Nature medicine*. 2014. 20(6):p. 599-606.

171. Rosenbluh J, Nijhawan D, Cox AG, et al. β-Catenin-driven cancers require a YAP1 transcriptional complex for survival and tumorigenesis. *Cell*. 2012. 151(7):p. 1457-73.

172. Kim MK, Jang JW, Bae SC. DNA binding partners of YAP/TAZ. *BMB reports*. 2018. 51(3):p. 126-133.

173. Morgan SE, Kastan MB. p53 and ATM: cell cycle, cell death, and cancer. *Adv Cancer Res*. 1997. 71:p. 1-25.

174. Yuan ZM, Huang Y, Fan MM, Sawyers C, Kharbanda S, Kufe D. Genotoxic drugs induce interaction of the c-Abl tyrosine kinase and the tumor suppressor protein p53. *J Biol Chem*. 1996. 271(43):p. 26457-60.

175. Yuan ZM, Huang Y, Whang Y, et al. Role for c-Abl tyrosine kinase in growth arrest response to DNA damage. *Nature*. 1996. 382(6588):p. 272-4.

176. Sawyers CL, McLaughlin J, Goga A, Havlik M, Witte O. The nuclear tyrosine kinase c-Abl negatively regulates cell growth. *Cell*. 1994. 77(1):p. 121-31.

177. Daniel R, Cai Y, Wong PM, Chung SW. Deregulation of c-abl mediated cell growth after retroviral transfer and expression of antisense sequences. *Oncogene*. 1995. 10(8):p. 1607-14.

178. Yuan ZM, Shioya H, Ishiko T, et al. p73 is regulated by tyrosine kinase c-Abl in the apoptotic response to DNA damage. *Nature*. 1999. 399(6738):p. 814-7.

179. Barton CE, Pietenpol JA. p53 Family. In: Lennarz WJ, Lane MD, eds. *Encyclopedia of Biological Chemistry (Second Edition)*. Academic Press; 2013:379-383.

180. Downward J, Basu S. YAP and p73: A Complex Affair. *Molecular Cell*. 2008. 32(6):p. 749-750.

181. Marshall CB, Mays DJ, Beeler JS, et al. p73 Is Required for Multiciliogenesis and Regulates the Foxj1-Associated Gene Network. *Cell Rep*. 2016. 14(10):p. 2289-300.

182. Basu S, Totty NF, Irwin MS, Sudol M, Downward J. Akt phosphorylates the Yes-associated protein, YAP, to induce interaction with 14-3-3 and attenuation of p73-mediated apoptosis. *Mol Cell*. 2003. 11(1):p. 11-23.

183. Levy D, Adamovich Y, Reuven N, Shaul Y. The Yes-associated protein 1 stabilizes p73 by preventing Itch-mediated ubiquitination of p73. *Cell Death Differ*. 2007. 14(4):p. 743-51.

184. Qiu Z, Cang Y, Goff SP. Abl family tyrosine kinases are essential for basement membrane integrity and cortical lamination in the cerebellum. *J Neurosci*. 2010. 30(43):p. 14430-9.

185. Koleske AJ, Gifford AM, Scott ML, et al. Essential roles for the Abl and Arg tyrosine kinases in neurulation. *Neuron*. 1998. 21(6):p. 1259-72.

186. Gutierrez DA, Vargas LM, Chandia-Cristi A, de la Fuente C, Leal N, Alvarez AR. c-Abl Deficiency Provides Synaptic Resiliency Against Aβ-Oligomers. *Front Cell Neurosci*. 2019. 13:p. 526.

187. Richardson C, Horikoshi N, Pandita TK. The role of the DNA double-strand break response network in meiosis. *DNA Repair (Amst)*. 2004. 3(8-9):p. 1149-64.

188. Goff SP, Gilboa E, Witte ON, Baltimore D. Structure of the Abelson murine leukemia virus genome and the homologous cellular gene: studies with cloned viral DNA. *Cell*. 1980. 22(3):p. 777-85.

189. Shilo BZ, Weinberg RA. DNA sequences homologous to vertebrate oncogenes are conserved in Drosophila melanogaster. *Proc Natl Acad Sci U S A*. 1981. 78(11):p. 6789-92.

190. Goddard JM, Weiland JJ, Capecchi MR. Isolation and characterization of Caenorhabditis elegans DNA sequences homologous to the v-abl oncogene. *Proc Natl Acad Sci U S A*. 1986. 83(7):p. 2172-6.

191. Lev Z, Leibovitz N, Segev O, Shilo BZ. Expression of the src and abl cellular oncogenes during development of Drosophila melanogaster. *Mol Cell Biol*. 1984. 4(5):p. 982-4.

192. Walker G, Burgess D, Kinsey WH. Fertilization promotes selective association of the Abl [correction of AbI] kinase with the egg cytoskeleton. *Eur J Cell Biol*. 1996. 70(2):p. 165-71.

193. Dorey K, Barilá D, Gavin AC, Nebreda AR, Superti-Furga G. Regulation of human c-Abl tyrosine kinase activity in Xenopus oocytes and acceleration of progesterone-induced G2/M transition by oncogenic forms. *Biol Chem*. 1999. 380(2):p. 223-30.

194. Rawe VY, Payne C, Navara C, Schatten G. WAVE1 intranuclear trafficking is essential for genomic and cytoskeletal dynamics during fertilization: cell-cycle-dependent shuttling between M-phase and interphase nuclei. *Dev Biol*. 2004. 276(2):p. 253-67.

195. Hantschel O, Superti-Furga G. Regulation of the c-Abl and Bcr-Abl tyrosine kinases. *Nat Rev Mol Cell Biol*. 2004. 5(1):p. 33-44.

196. Hernández SE, Krishnaswami M, Miller AL, Koleske AJ. How do Abl family kinases regulate cell shape and movement? *Trends in cell biology*. 2004. 14(1):p. 36-44.

197. Schmandt RE, Broaddus R, Lu KH, et al. Expression of c-ABL, c-KIT, and platelet-derived growth factor receptor-beta in ovarian serous carcinoma and normal ovarian surface epithelium. *Cancer*. 2003. 98(4):p. 758-64.

198. O'Neill AJ, Cotter TG, Russell JM, Gaffney EF. Abl expression in human fetal and adult tissues, tumours, and tumour microvessels. *J Pathol*. 1997. 183(3):p. 325-9.

199. Iwaoki Y, Matsuda H, Mutter GL, Watrin F, Wolgemuth DJ. Differential expression of the proto-oncogenes c-abl and c-mos in developing mouse germ cells. *Exp Cell Res*. 1993. 206(2):p. 212-9.

200. Naz RK. c-Abl proto-oncoprotein is expressed and tyrosine phosphorylated in human sperm cell. *Mol Reprod Dev*. 1998. 51(2):p. 210-7.

201. Kharbanda S, Pandey P, Morris PL, et al. Functional role for the c-Abl tyrosine kinase in meiosis I. *Oncogene*. 1998. 16(14):p. 1773-7.

202. Tybulewicz VL, Crawford CE, Jackson PK, Bronson RT, Mulligan RC. Neonatal lethality and lymphopenia in mice with a homozygous disruption of the c-abl proto-oncogene. *Cell*. 1991. 65(7):p. 1153-63.

203. Hardin JD, Boast S, Schwartzberg PL, et al. Abnormal peripheral lymphocyte function in c-abl mutant mice. *Cell Immunol*. 1996. 172(1):p. 100-7.

204. Yaba A, Agus S, Yıldırım E, Erdogan CS, Yılmaz B. Interaction of the mTERT telomerase catalytic subunit with the c-Abl tyrosine kinase in mouse granulosa cells. *J Recept Signal Transduct Res*. 2020. 40(4):p. 365-373.

205. Yildirim E, Yaba A. Determination of c-Abl tyrosine kinase and mTERT catalytic subunit of telomerase expression level during prenatal-postnatal mouse ovary-testis development. *Reprod Biol*. 2020. 20(4):p. 555-567.

206. Gonfloni S, Di Tella L, Caldarola S, et al. Inhibition of the c-Abl-TAp63 pathway protects mouse oocytes from chemotherapy-induced death. *Nat Med*. 2009. 15(10):p. 1179-85.

207. Mutluay D, Oner H. The Abelson tyrosine kinase (c-Abl) localization in preimplantation mouse development. *Rom J Morphol Embryol*. 2017. 58(4):p. 1385-1391.

208. Watanabe H, Ito H, Shintome A, Suzuki H. Effects of oxygen tension and humidity on the preimplantation development of mouse embryos produced by in vitro fertilization: analysis using a non-humidifying incubator with time-lapse cinematography. *Exp Anim*. 2022. 71(3):p. 338-346.

209. Morgan S, Lopes F, Gourley C, Anderson RA, Spears N. Cisplatin and doxorubicin induce distinct mechanisms of ovarian follicle loss; imatinib provides selective protection only against cisplatin. *PLoS One*. 2013. 8(7):p. e70117.

210. Yaba A, Agus S, Yildirim E, Erdogan CS, Yilmaz B. Interaction of the mTERT telomerase catalytic subunit with the c-Abl tyrosine kinase in mouse granulosa cells. *J Recept Signal Transduct Res*. 2020. 40(4):p. 365-373.

211. Young MA, Gonfloni S, Superti-Furga G, Roux B, Kuriyan J. Dynamic coupling between the SH2 and SH3 domains of c-Src and Hck underlies their inactivation by C-terminal tyrosine phosphorylation. *Cell*. 2001. 105(1):p. 115-26.

212. Weinerman R, Feng R, Ord TS, et al. Morphokinetic Evaluation of Embryo Development in a Mouse Model: Functional and Molecular Correlates. *Biol Reprod*. 2016. 94(4):p. 84.

213. Desai N, Ploskonka S, Goodman LR, Austin C, Goldberg J, Falcone T. Analysis of embryo morphokinetics, multinucleation and cleavage anomalies using continuous time-lapse monitoring in blastocyst transfer cycles. *Reprod Biol Endocrinol*. 2014. 12:p. 54.

214. Balakier H, Sojecki A, Motamedi G, Bashar S, Mandel R, Librach C. Is the zona pellucida thickness of human embryos influenced by women's age and hormonal levels? *Fertility and Sterility*. 2012. 98(1):p. 77-83.

215. Korotkevich E, Niwayama R, Courtois A, et al. The Apical Domain Is Required and Sufficient for the First Lineage Segregation in the Mouse Embryo. *Developmental Cell*. 2017. 40(3):p. 235-247.e7.

216. Hershko-Klement A, Raviv S, Nemerovsky L, et al. Standardization of Post-Vitrification Human Blastocyst Expansion as a Tool for Implantation Prediction. *J Clin Med*. 2022. 11(9):p.

217. Menchero S, Rollan I, Lopez-Izquierdo A, et al. Transitions in cell potency during early mouse development are driven by Notch. *Elife*. 2019. 8:p.

218. Ucar AY, Kayisli UA, Demir N. The c-Abl expression in uterine epithelium during the mouse estrus cycle. *J Mol Histol*. 2012. 43(1):p. 107-13.

219. Fierro-González JC, White MD, Silva JC, Plachta N. Cadherin-dependent filopodia control preimplantation embryo compaction. *Nat Cell Biol*. 2013. 15(12):p. 1424-33.

220. Bao M, Cornwall-Scoones J, Sanchez-Vasquez E, et al. Stem cell-derived synthetic embryos self-assemble by exploiting cadherin codes and cortical tension. *Nat Cell Biol*. 2022. 24(9):p. 1341-1349.

221. Kharbanda S, Yuan ZM, Weichselbaum R, Kufe D. Determination of cell fate by c-Abl activation in the response to DNA damage. *Oncogene*. 1998. 17(25):p. 3309-18.

222. Druker BJ, Talpaz M, Resta DJ, et al. Efficacy and safety of a specific inhibitor of the BCR-ABL tyrosine kinase in chronic myeloid leukemia. *The New England journal of medicine*. 2001. 344(14):p. 1031-7.

223. Hossain S, Dubielecka PM, Sikorski AF, Birge RB, Kotula L. Crk and ABI1: binary molecular switches that regulate abl tyrosine kinase and signaling to the cytoskeleton. *Genes Cancer*. 2012. 3(5-6):p. 402-13.

224. Rogers EM, Allred SC, Peifer M. Abelson kinase's intrinsically disordered region plays essential roles in protein function and protein stability. *Cell Commun Signal*. 2021. 19(1):p. 27.

225. Panjarian S, Iacob RE, Chen S, Engen JR, Smithgall TE. Structure and Dynamic Regulation of Abl Kinases*. *Journal of Biological Chemistry*. 2013. 288(8):p. 5443-5450.

226. Miething C, Mugler C, Grundler R, et al. Phosphorylation of tyrosine 393 in the kinase domain of Bcr-Abl influences the sensitivity towards imatinib in vivo. *Leukemia*. 2003. 17(9):p. 1695-1699.

227. Meng Z, Moroishi T, Guan KL. Mechanisms of Hippo pathway regulation. *Genes Dev*. 2016. 30(1):p. 1-17.

228. Aragona M, Panciera T, Manfrin A, et al. A mechanical checkpoint controls multicellular growth through YAP/TAZ regulation by actin-processing factors. *Cell*. 2013. 154(5):p. 1047-1059.

229. Nakajima H, Yamamoto K, Agarwala S, et al. Flow-Dependent Endothelial YAP Regulation Contributes to Vessel Maintenance. *Dev Cell*. 2017. 40(6):p. 523-536.e6.

230. Elosegui-Artola A, Oria R, Chen Y, et al. Mechanical regulation of a molecular clutch defines force transmission and transduction in response to matrix rigidity. *Nat Cell Biol*. 2016. 18(5):p. 540-8.

231. Dupont S, Morsut L, Aragona M, et al. Role of YAP/TAZ in mechanotransduction. *Nature*. 2011. 474(7350):p. 179-83.

232. Moon S, Kim W, Kim S, et al. Phosphorylation by NLK inhibits YAP-14-3-3-interactions and induces its nuclear localization. *EMBO Rep*. 2017. 18(1):p. 61-71.

233. Ege N, Dowbaj AM, Jiang M, et al. Quantitative Analysis Reveals that Actin and Src-Family Kinases Regulate Nuclear YAP1 and Its Export. *Cell Syst*. 2018. 6(6):p. 692-708.e13.

234. Aureille J, Buffière-Ribot V, Harvey BE, et al. Nuclear envelope deformation controls cell cycle progression in response to mechanical force. *EMBO Rep*. 2019. 20(9):p. e48084.

235. Owens DJ, Fischer M, Jabre S, et al. Lamin Mutations Cause Increased YAP Nuclear Entry in Muscle Stem Cells. *Cells*. 2020. 9(4):p.

236. Melino G, De Laurenzi V, Vousden KH. p73: Friend or foe in tumorigenesis. *Nat Rev Cancer*. 2002. 2(8):p. 605-15.

237. John K, Alla V, Meier C, Pützer BM. GRAMD4 mimics p53 and mediates the apoptotic function of p73 at mitochondria. *Cell Death Differ*. 2011. 18(5):p. 874-86.

238. Stamatiadis P, Cosemans G, Boel A, et al. TEAD4 regulates trophectoderm differentiation upstream of CDX2 in a GATA3-independent manner in the human preimplantation embryo. *Human Reproduction*. 2022. 37(8):p. 1760-1773.

239. Home P, Saha B, Ray S, et al. Altered subcellular localization of transcription factor TEAD4 regulates first mammalian cell lineage commitment. *Proc Natl Acad Sci U S A*. 2012. 109(19):p. 7362-7.

240. Lin KC, Moroishi T, Meng Z, et al. Regulation of Hippo pathway transcription factor TEAD by p38 MAPK-induced cytoplasmic translocation. *Nature Cell Biology*. 2017. 19(8):p. 996-1002.

241. Cheeks RJ, Canman JC, Gabriel WN, Meyer N, Strome S, Goldstein B. C. elegans PAR proteins function by mobilizing and stabilizing asymmetrically localized protein complexes. *Curr Biol*. 2004. 14(10):p. 851-62.

242. Goehring NW, Trong PK, Bois JS, et al. Polarization of PAR proteins by advective triggering of a pattern-forming system. *Science*. 2011. 334(6059):p. 1137-41.

243. Cline EG, Nelson WJ. Characterization of mammalian Par 6 as a dual-location protein. *Mol Cell Biol*. 2007. 27(12):p. 4431-43.

244. Baum B, Perrimon N. Spatial control of the actin cytoskeleton in Drosophila epithelial cells. *Nat Cell Biol*. 2001. 3(10):p. 883-90.

245. Lanier LM, Gertler FB. From Abl to actin: Abl tyrosine kinase and associated proteins in growth cone motility. *Curr Opin Neurobiol*. 2000. 10(1):p. 80-7.

246. Larue L, Ohsugi M, Hirchenhain J, Kemler R. E-cadherin null mutant embryos fail to form a trophectoderm epithelium. *Proc Natl Acad Sci U S A*. 1994. 91(17):p. 8263-7.

247. Ridley AJ. Life at the leading edge. *Cell*. 2011. 145(7):p. 1012-22.

248. Woodring PJ, Hunter T, Wang JY. Regulation of F-actin-dependent processes by the Abl family of tyrosine kinases. *J Cell Sci*. 2003. 116(Pt 13):p. 2613-26.

249. Sossey-Alaoui K, Li X, Ranalli TA, Cowell JK. WAVE3-mediated cell migration and lamellipodia formation are regulated downstream of phosphatidylinositol 3-kinase. *J Biol Chem*. 2005. 280(23):p. 21748-55.

250. Cui W, Marcho C, Wang Y, et al. MED20 is essential for early embryogenesis and regulates NANOG expression. *Reproduction*. 2019. 157(3):p. 215-222.

251. Gönczy P. Mechanisms of asymmetric cell division: flies and worms pave the way. *Nat Rev Mol Cell Biol*. 2008. 9(5):p. 355-66.

252. Zernicka-Goetz M. Cleavage pattern and emerging asymmetry of the mouse embryo. *Nat Rev Mol Cell Biol*. 2005. 6(12):p. 919-28.

253. Hubatsch L, Peglion F, Reich JD, et al. A cell size threshold limits cell polarity and asymmetric division potential. *Nat Phys*. 2019. 15(10):p. 1075-1085.

254. Cordes S, Frank CA, Garriga G. The C. elegans MELK ortholog PIG-1 regulates cell size asymmetry and daughter cell fate in asymmetric neuroblast divisions. *Development*. 2006. 133(14):p. 2747-56.

255. Chen H, Qian W, Good MC. Integrating cellular dimensions with cell differentiation during early development. *Curr Opin Cell Biol*. 2020. 67:p. 109-117.

256. Morais-de-Sá E, Sunkel C. Adherens junctions determine the apical position of the midbody during follicular epithelial cell division. *EMBO Rep*. 2013. 14(8):p. 696-703.

257. Guillot C, Lecuit T. Adhesion disengagement uncouples intrinsic and extrinsic forces to drive cytokinesis in epithelial tissues. *Dev Cell*. 2013. 24(3):p. 227-41.

258. Paim LMG, FitzHarris G. Cell size and polarization determine cytokinesis furrow ingression dynamics in mouse embryos. *Proc Natl Acad Sci U S A*. 2022. 119(12):p. e2119381119.

259. Hawdon A, Geoghegan ND, Mohenska M, et al. Apicobasal RNA asymmetries regulate cell fate in the early mouse embryo. *Nat Commun*. 2023. 14(1):p. 2909.

260. Hara Y, Kimura A. Cell-Size-Dependent Control of Organelle Sizes During Development. In: Kubiak JZ, ed. *Cell Cycle in Development*. Springer Berlin Heidelberg; 2011:93-108.

261. Margolis RL, Wilson L. Microtubule treadmills—possible molecular machinery. *Nature*. 1981. 293(5835):p. 705-711.

262. Hara Y, Merten Christoph A. Dynein-Based Accumulation of Membranes Regulates Nuclear Expansion in Xenopus laevis Egg Extracts. *Developmental Cell*. 2015. 33(5):p. 562-575.

263. Tsichlaki E, FitzHarris G. Nucleus downscaling in mouse embryos is regulated by cooperative developmental and geometric programs. *Scientific Reports*. 2016. 6(1):p. 28040.

264. Hao Y, Lai L, Mao J, Im G-S, Bonk A, Prather RS. Apoptosis and In Vitro Development of Preimplantation Porcine Embryos Derived In Vitro or by Nuclear Transfer1. *Biology of Reproduction*. 2003. 69(2):p. 501-507.

265. Mohr LR, Trounson AO. Comparative ultrastructure of hatched human, mouse and bovine blastocysts. *J Reprod Fertil*. 1982. 66(2):p. 499-504.

266. Hurst PR, Jefferies K, Eckstein P, Wheeler AG. An ultrastructural study of preimplantation uterine embryos of the rhesus monkey. *J Anat*. 1978. 126(Pt 1):p. 209-20.

267. Blander JM. The many ways tissue phagocytes respond to dying cells. *Immunol Rev*. 2017. 277(1):p. 158-173.

268. Li Y, Xu J, Zhou CQ, Zhang CL, Zhuang GL. Nonprofessional phagocytosis in trophectoderm cells of human preimplantation blastocysts. *Syst Biol Reprod Med*. 2016. 62(4):p. 243-8.

269. Hardy K, Warner A, Winston RM, Becker DL. Expression of intercellular junctions during preimplantation development of the human embryo. *Mol Hum Reprod*. 1996. 2(8):p. 621-32.

270. Dale B, Gualtieri R, Talevi R, Tosti E, Santella L, Elder K. Intercellular communication in the early human embryo. *Mol Reprod Dev*. 1991. 29(1):p. 22-8.

7. APPENDICES

7.1. Ethical Approval

T.C. YEDİTEPE ÜNİVERSİTESİ
Hayvan Deneyleri Yerel Etik Kurulu (HADYEK)

ETİK KURUL KARARI

Protokol No	Toplantı Tarihi	Toplantı Sayısı	Karar No	Proje Yürütücüsü
2020-859	27.08.2020	2020/08	2020/08-6	Doç. Dr. Aylin Yaba Uçar
'Farede Preimplantasyon Dönemi Embriyonal Gelişiminde Hücre Kaderinin Belirlenmesinde c-Abl Protein Tirozin Kinaz ile YAP Arasındaki İlişkinin Belirlenmesi' isimli proje oy birliğiyle etik açıdan uygun görülmüştür.				

Hayvan Türü / Irkı	Toplam Hayvan Sayısı	Hayvanın Cinsiyeti
Fare / C57BL6	64	Dişi

Görevi	Adı Soyadı	Katılım Durumu
Başkan	Prof. Dr. Bayram YILMAZ	
Başkan Vekili	Prof. Dr. Erdem YEŞİLADA	
Üye	Veteriner Hekim Engin SÜMER	
Üye	Prof. Dr. M. Ece GENÇ	
Üye	Prof. Dr. Rukset ATTAR	
Üye	Prof. Dr. Gamze TORUN KÖSE	
Üye	Doç. Dr. Ediz DENİZ	
Üye	Doç. Dr. Aylin YABA UÇAR	
Üye	Doç. Dr. Burcu GEMİCİ BAŞOL	
Üye	Hakan GÖKSEL	
Üye	Ahmet ŞENKARDEŞLER	

7.2. Curriculum Vitae

Personal Information

Name	Ecem	**Surname**	Yıldırım

Education

Degree	Department	The name of the Institution Graduated From	Graduation year
Master	Institute of Health Sciences/Department of Histology and Embryology	Yeditepe University	2018
University	Faculty of Science/Biology	Trakya Univesity	2014
High school	Science Branch	Cengizhan High School	2009

All the grades must be listed if there is more than one (KPDS, ÜDS, TOEFL; EELTS vs),

English (YÖKDİL)	70

Work Experience (Sort from present to past)

Position	Institute	Duration (Year - Year)
Technical Personnel	Yeditepe University	2016-
Research Assistant	Yeditepe University	2016-
Department of Histology and Embryology - Assistant	İstanbul Medipol University, Center for Restorative and Regenerative Medicine (REMER)	2014-2015

Computer Skills

Program	Level
Microsoft Office (Excel, Word, Powerpoint)	Good
GraphPad	Good
EndNote	Good
Image Lab	Good
Photoshop	Good

****Excellent, good, average or basic**

Scientific works

The articles published in the journals indexed by SCI, SSCI, AHCI

E. Yildirim*,* S. Aksoy, T. Onel, A. Yaba. Gonadal development and sex determination in mouse. Review Article. *Reproductive Biology*. 2020.
Yaba, S.Aguş, ***E. Yildirim****,* C.S. Erdogan*,* B Yilmaz. Interaction of the mTERT telomerase catalytic subunit with the c-Abl tyrosine kinase in mouse granulosa cells. Research Article. *Journal of Receptors and Signal Transduction*. 2020.
E. Yildirim and A. Yaba. Determination of c-Abl tyrosine kinase and mTERT catalytic subunit of telomerase expression level during prenatal-postnatal mouse ovary-testis development. Research Article. *Reproductive Biology*. 2020.
E. Yildirim, G. Bora, T. Onel, N. Talas, A. Yaba. Cell fate determination and Hippo signaling pathway in preimplantation mouse embryo. Review Article. *Cell Tissue Research.* 2021.
T. Onel, ***E. Yildirim,*** S. Doğan, A. Yaba. Determination of mTOR signal pathway in MMTV- TGFα mice ovary at different ages. Research Article. *Journal of Histotechnology.* 2022.
T. Onel, C.S. Erdogan, B. Aru, ***E. Yildirim,*** G. Yaikkaya Demirel, A. Yaba. Effect of rapamycin treatment in human seminoma TCam-2 cells through inhibition of G1-S transition. *Naunyn Schmiedebergs Arch Pharmacol.* 2023.
B. Uner, S. Ozdemir, ***E. Yildirim,*** A. Yaba, C. Tas, M. Uner, Y. Ozsoy. Loteprednol loaded nanoformulations for corneal delivery: Ex-vivo permeation study, ocular safety assessment and stability studies. *Journal of Drug Delivery Science and Technology.* 2023.

S. Ozdemir, B. Uner, J. Baranauskaite, E. Sumer, ***E. Yıldırım***, A. Yaba. Design and characterization of dexamethasone loaded microsponges for the management of ulcerative colitis. *European Journal of Pharmaceutics and Biopharmaceutics*. 2023.
F. Khoubbieh, C.S. Erdoğan, T. Onel, ***E. Yıldırım***, E. Sumer, A. Yaba, B. Yilmaz. Effect of methylphenidate on the onset of puberty and reproductive organ development in rats. *Physiology & Behavior.* 2023.
C. Canse, ***E. Yildirim***, A. Yaba. Overview of junctional complexes during mammalian early embryonic development. *Frontiers in Endocrinology*. 2023.
G. Bora, T. Önel, ***E. Yildirim***, A. Yaba. Circadian regulation of mTORC1 signaling via Per2 dependent mechanism disrupts folliculogenesis and oocyte maturation in female mice. *Journal of Molecular Histology*. 2023.

Proceedings presented in international scientific meetings and published in proceedings book.

Yaba Ucar, MS. Aydın, S. Agus, E. Günalan, ***E. Yıldırım***, B. Yılmaz. (2017). Role of mTOR (Mammalian Target of Rapamycin) Signal Mechanism in the Treatment of Polycystic Ovary Syndrome (PCOS). Poster Presentation. 64th Annual Meeting of the Society for Reproductive Investigation, Orlando FL- USA, March 15-18.
E. Yıldırım & A. Yaba Ucar. Determination of c-Abl Tyrosine Kinase and mTERT Catalytic Subunit of Telomerase Expression Level During Mouse Prenatal and Postnatal Gonadal Development, Poster Presentation, 34th Annual Meeting Of The European Society Of Human Reproduction And Embryology, 01 July 2018, 04 August 2018.
Yaba Ucar, M. Ş. Aydın, S. Agus, E. Günalan, ***E. Yıldırım***, B. Yılmaz. Impaired Follicular Development And Ovulation In PCOS Mouse Model Can Rescued By Rapamycin Treatment, Poster Presentation, 34th Annual Meeting Of The European Society Of Human Reproduction And Embryology, 01 July 2018, 04 August 2018.
T. Önel, ***E. Yıldırım***, S. Doğan & A. Yaba Ucar.The Acceleration Of Reproductive Aging In Mmtv-tgf-alpha Mice, Poster Presentation, 34th Annual Meeting Of The European Society Of Human Reproduction And Embryology, 01 July 2018, 04 August 2018.
H. K. Parlaktaş, ***E. Yıldırım***, T. Önem, H. Zortul, F. Arıcıoğlu & A. Yaba Uçar. Effect Of Maternal Separation Stress And Use Of Antidepressants On Rat Ovarian Reserve, Poster Presentation, 34th Annual Meeting Of The European Society Of Human Reproduction And Embryology, 01 July 2018, 04 August 2018.
T. Önel, ***E.Yıldırım***, H.K. Parlaktaş, S. Doğan, A. Yaba Ucar. Effect of TGF-α Activation on Follicle Development in Mice. Poster Presentation. Awakening of the genome: The maternal-to-zygotic transition. EMBO Workshop. Prague/Czech Republic. 15-18 May 2019.
A. Yaba Uçar, ***E.Yıldırım***. c-Abl and mTERT Expression in Mouse Oocyte and Preimplantation Embryos. Poster Presentation. Awakening of the genome: The maternal-to-zygotic transition. EMBO Workshop. Prague/Czech Republic. 15-18 May 2019.
E. Yıldırım, Ö. Başer, T. Önel, H.K. Parlaktaş, Y. Yavuz, N. Talaş, B. Yılmaz, A. Yaba. Kisspeptin is mediated mTOR Signal Pathway in Ovarian Follicular Development in Mouse. Poster Presentation. Awakening of the genome: The maternal-to-zygotic transition. EMBO Workshop. Prague/Czech Republic. 15-18 May 2019.
G. Bora, T. Önel, ***E.Yıldırım***, A. Yaba. The effect of circadian rhythm disruption due to constant light on ovarian and oocyte aging through possible relationship between PER2 and mTOR signaling pathway. Oral Presentation. European Society of Human Reproduction and Embryology (ESHRE). 2021
E.Yıldırım, T. Onel, A. Yaba. Determination of the Role of c-Abl Tyrosine Kinase During Mouse Compaction Stage Preimplantation Embryos. Oral Presentation. 4th East Mediterranean Congress of Laboratory Animal Science. 9-11 Dec 2021.
T. Onel, N. Talas, ***E.Yıldırım***, A. Yaba. Determination of the c-Abl Tyrosine Kinase in Response to DNA Damage in Mouse Granulosa Cells. Oral Presentation. 4th East Mediterranean Congress of Laboratory Animal Science. 9-11 Dec 2021.
E.Yıldırım, T. Onel, A. Yaba. The Role of c-Abl Tyrosine Kinase in Cell Fate Specification and Morphogenesis in Preimplantation Mouse Embryo. Oral Presentation. 15th National and 1st International Congress of Histology and Embryology. 26-28 May 2022.
Ecem Yıldırım, Yavuz Yavuz, Tuğçe Önel, Zehra Yağmur Erol, Aylin Yaba Uçar & Bayram Yılmaz. Effects Of Chemogenetic Modulation Of Hypothalamic Arcuate Nucleus Kisspeptin Neurons On Folliculogenesis in Kiss-Cre Polycystic Ovarian Syndrome Mouse Model. Poster Presentation. FENS. Paris/ France. 9-13 June 2022.
E. Yıldırım, B. Yılmaz, A. Yaba Uçar. Farede Oosit Maturasyonunda c-Abl Tirozin Kinaz ve mTERT Telomeraz Katalitik Alt Ünitesinin Ekspresyonunun İmmunofloresan Yöntem ile Gösterilmesi. Poster Sunumu, Cell and Tissue Biology Research. Volume 5, Supplement, 13. National Histology and Embryology Congress, 2016 IZMIR.
Aylin Yaba Uçar, Sami Aguş, ***Ecem Yıldırım***, Bayram Yılmaz, Necdet Demir. Fare Oositi ve Preimplantasyon Dönemi Embriyolarında mTERT Telomeraz Katalitik Alt ünitesinin c-Abl Protein Tirozin Kinaz Tarafından

Düzenlenmesi. Oral Sunum, Cell and Tissue Biology Research. Volume 5, Supplement, 13. National Histology and Embryology Congress, 2016 IZMIR.
E. Yıldırım & A. Yaba Uçar. Farede Prenatal ve Postnatal Dönem Ovaryum Ve Testis Gelişiminde c-Abl Tirozin Kinaz Ve mTERT Telomeraz Katalitik Alt Ünitesinin Ekspresyonunun Gösterilmesi, Poster Sunumu, 14. Ulusal Histoloji Ve Embriyoloji Kongresi, 10 Mayıs 2018, 13 Mayıs 2018.
H. K. Parlaktaş, ***E. Yıldırım***, T. Önel, H. Zortul. F. Arıcıoğlu & A. Yaba Uçar, Anneden Ayrılma Stresinin ve Antidepresan Kullanımının Sıçan Ovaryumları Üzerindeki Etkisinin Gösterilmesi, Poster Sunumu, 14. Ulusal Histoloji ve Embriyoloji Kongresi, 10 Mayıs 2018, 13 Mayıs 2018.
A. Yaba Uçar, ***E. Yıldırım***, T. Önel & H. K. Parlaktaş. Farede DMBA ile Indüklenmiş Ovotoksisitede c-Abl Ve mTERT Ekspresyonlarının Belirlenmesi, Poster Sunumu, 14. Ulusal Histoloji Ve Embriyoloji Kongresi, 10 Mayıs 2018, 13 Mayıs 2018.
T. Önel, ***E. Yıldırım***, S. Doğan & A. Yaba Uçar. Mmtv-TGF-a Farelerde Ovariyal Yaşlanma Sürecinde mTOR Ekspresyonunun Belirlenmesi, Poster Presentation, 14. Ulusal Histoloji Ve Embriyoloji Kongresi, 10 Mayıs 2018, 13 Mayıs 2018.
E. Yıldırım, Ö. Başer, T. Önel, H.K. Parlaktaş, Y. Yavuz, N. Talaş, B. Yılmaz, A. Yaba. Farede Kisspeptin Aktivasyonu ile Ovaryumlarda Foliküler Gelişimin, mTOR ve p-mTOR Seviyelerinin Değerlendirilmesi, Sözlü sunum, 24. Ulusal Elektron Mikroskobi Kongresi, 24-26 Nisan 2019.
G. Bora, ***E.Yıldırım***, T. Önel, E. Günalan, H.K. Parlaktaş, N. Talaş, B. Gemici Başol, A. Yaba Uçar. Yüksek yağlı diyetin sıçan ovaryumlarında foliküler gelişim ve mTOR sinyal yolağı üzerindeki etkisi. Poster sunumu. 24. Ulusal Elektron Mikroskobi Kongresi, 24-26 Nisan 2019.
H.K. Parlaktaş, ***E.Yıldırım***, T. Önel, H. Zortul, F. Arıcıoğlu, A. Yaba Uçar. Anneden ayrılma stresinin sıçan ovaryumları üzerindeki etkisinin mTOR yolağı üzerinden değerlendirilmesi. Poster sunumu. 24. Ulusal Elektron Mikroskobi Kongresi, 24-26 Nisan 2019.
A. Yaba Uçar, ***E.Yıldırım***, T. Önel, H.K. Parlaktaş, N. Demir. Farede DMBA maruziyeti ile oluşturulan prematüre over yetmezliğinde foliküllerin ultrastrüktürel olarak incelenmesi. Poster sunumu. 24. Ulusal Elektron Mikroskobi Kongresi, 24-26 Nisan 2019.
T. Önel, ***E.Yıldırım***, H.K. Parlaktaş, S. Doğan, A. Yaba Uçar. TGF-α aktivasyonunun farelerde folikül gelişimi üzerindeki etkisinin gösterilmesi. Sözlü sunum. 24. Ulusal Elektron Mikroskobi Kongresi, 24-26 Nisan 2019.
E. Yıldırım, B. Yılmaz, A. Yaba Uçar. Farede Oosit Maturasyonunda c-Abl Tirozin Kinaz ve mTERT Telomeraz Katalitik Alt Ünitesinin Ekspresyonunun İmmunofloresan Yöntem ile Gösterilmesi. Poster Sunumu, Cell and Tissue Biology Research. Volume 5, Supplement, 13. National Histology and Embryology Congress, 2016 IZMIR.
Aylin Yaba Uçar, Sami Aguş, ***Ecem Yıldırım***, Bayram Yılmaz, Necdet Demir. Fare Oositi ve Preimplantasyon Dönemi Embriyolarında mTERT Telomeraz Katalitik Alt ünitesinin c-Abl Protein Tirozin Kinaz Tarafından Düzenlenmesi. Oral Sunum, Cell and Tissue Biology Research. Volume 5, Supplement, 13. National Histology and Embryology Congress, 2016 IZMIR.
E. Yıldırım & A. Yaba Uçar. Farede Prenatal ve Postnatal Dönem Ovaryum Ve Testis Gelişiminde c-Abl Tirozin Kinaz Ve mTERT Telomeraz Katalitik Alt Ünitesinin Ekspresyonunun Gösterilmesi, Poster Sunumu, 14. Ulusal Histoloji Ve Embriyoloji Kongresi, 10 Mayıs 2018, 13 Mayıs 2018.
H. K. Parlaktaş, ***E. Yıldırım***, T. Önel, H. Zortul. F. Arıcıoğlu & A. Yaba Uçar, Anneden Ayrılma Stresinin ve Antidepresan Kullanımının Sıçan Ovaryumları Üzerindeki Etkisinin Gösterilmesi, Poster Sunumu, 14. Ulusal Histoloji ve Embriyoloji Kongresi, 10 Mayıs 2018, 13 Mayıs 2018.
A. Yaba Uçar, ***E. Yıldırım***, T. Önel & H. K. Parlaktaş. Farede DMBA ile Indüklenmiş Ovotoksisitede c-Abl Ve mTERT Ekspresyonlarının Belirlenmesi, Poster Sunumu, 14. Ulusal Histoloji Ve Embriyoloji Kongresi, 10 Mayıs 2018, 13 Mayıs 2018.
T. Önel, ***E. Yıldırım***, S. Doğan & A. Yaba Uçar. Mmtv-TGF-a Farelerde Ovariyal Yaşlanma Sürecinde mTOR Ekspresyonunun Belirlenmesi, Poster Presentation, 14. Ulusal Histoloji Ve Embriyoloji Kongresi, 10 Mayıs 2018, 13 Mayıs 2018.
E. Yıldırım, Ö. Başer, T. Önel, H.K. Parlaktaş, Y. Yavuz, N. Talaş, B. Yılmaz, A. Yaba. Farede Kisspeptin Aktivasyonu ile Ovaryumlarda Foliküler Gelişimin, mTOR ve p-mTOR Seviyelerinin Değerlendirilmesi, Sözlü sunum, 24. Ulusal Elektron Mikroskobi Kongresi, 24-26 Nisan 2019.
G. Bora, ***E.Yıldırım***, T. Önel, E. Günalan, H.K. Parlaktaş, N. Talaş, B. Gemici Başol, A. Yaba Uçar. Yüksek yağlı diyetin sıçan ovaryumlarında foliküler gelişim ve mTOR sinyal yolağı üzerindeki etkisi. Poster sunumu. 24. Ulusal Elektron Mikroskobi Kongresi, 24-26 Nisan 2019.
H.K. Parlaktaş, ***E.Yıldırım***, T. Önel, H. Zortul, F. Arıcıoğlu, A. Yaba Uçar. Anneden ayrılma stresinin sıçan ovaryumları üzerindeki etkisinin mTOR yolağı üzerinden değerlendirilmesi. Poster sunumu. 24. Ulusal Elektron Mikroskobi Kongresi, 24-26 Nisan 2019.

A. Yaba Uçar, ***E.Yıldırım***, T. Önel, H.K. Parlaktaş, N. Demir. Farede DMBA maruziyeti ile oluşturulan prematüre over yetmezliğinde foliküllerin ultrastrüktürel olarak incelenmesi. Poster sunumu. 24. Ulusal Elektron Mikroskobi Kongresi, 24-26 Nisan 2019.
T. Önel, ***E.Yıldırım***, H.K. Parlaktaş, S. Doğan, A. Yaba Uçar. TGF-α aktivasyonunun farelerde folikül gelişimi üzerindeki etkisinin gösterilmesi. Sözlü sunum. 24. Ulusal Elektron Mikroskobi Kongresi, 24-26 Nisan 2019.

Others (Projects / Certificates / Rewards)

Polikistik Over Sendromu (PKOS)'nun Tedavisinde mTOR (Mammalian Target of Rapamycin) Sinyal Mekanizmasının Rolü, **TUBİTAK** #214S328, Bursiyer
Farede Prematüre Over Yetmezliğinde mTERT Telomeraz Katalitik Alt Ünitesinin Rolünün Belirlenmesi, **TUBİTAK** #215S867, Bursiyer
Polikistik Over Sendromu Oluşturulan Transgenik Kisspeptin-Cre Farelerde Optogenetik ve Farmakogenetik Yöntemlerle Ovaryum Fonksiyonlarının Santral Düzenlenmesinin ve Mekanizmalarının Araştırılması, **TUBİTAK** #219S554, Bursiyer
14. National Histology and Embryology Congress Poster Second Award. ***Yıldırım E***, Yaba Uçar A. Determination of c-Abl Tyrosine Kinase and mTERT Catalytic Subunit of Telomerase Expression Level During Prenatal and Postnatal Mouse Ovary and Testis Development, May 10-13, 2018, Antalya/ Turkey.
Certificate of Honour from Master Degree, 2018.
Scholarship for workshop participation. Awakening of the genome: The maternal-to-zygotic transition. EMBO Workshop. Prague/Czech Republic. 15-18 May 2019.
Yeditepe University 2018-2019 Academic Year Evaluation Award, School of Medicine, Young Researcher Awards.
4th East Mediterranean Congress of Laboratory Animal Science Oral Presentation 1st Award. **E. Yıldırım,** T. Onel, A. Yaba. Determination of the Role of c-Abl Tyrosine Kinase During Mouse Compaction Stage Preimplantation Embryos. 9-11 Dec 2021.
Yeditepe University 2021-2022 Academic Year Evaluation Award, School of Medicine, Young Researcher Awards.